THE EFECT OF SILICONE GEL BREAST PROSTHESIS ON THE ELECTRON BEAM DOSE DISTRIBUTION

BY

Ndeshihafela Vera Uushona

A dissertation submitted in partial fulfillment of the requirement for the degree of

Masters of Science in Medicine

in the

Faculty of Health Sciences

at the

University of Limpopo, South Africa

Supervisor: Mr DPA Maboe

Co- Supervisor: Dr AC Chamberlain

August 2009

ACKNOWLEDGEMENTS

Firstly, I would like to thank Almighty God for His kindness and constant love, which He has shown me in numerous ways.

This work was produced with the assistance and guidance of the following people, to whom I would like to express my sincere gratitude.

- Mr DPA, my supervisor for highlighting the basic Monte Carlo geometries, his support and guidance. Dr AC Chamberlain, my co supervisor for his guidance, advice and support throughout this study, for his ever readiness and assistance.
- My colleagues in the department of medical physics, for their assistance in compiling this work, especially Ntlamele Sehloho, Petro van der Westhuizen and Kgomotso Tlhapi. The Medical physics team of Polokwane General Hospital, who spent their time to assist me in measurements and data acquisition.
- Mr E Sithole from the department of Physics, for the lively discussion of the data and Dr S Inyang for his assistance and advice.
- My Sponsor, the DAAD which granted me a scholarship, to enable me to conduct this study.
- My family and friends for their support and bearing with me while I was away during my studies and friends at Medunsa who made my stay away from home pleasant and the BLW family.

DECLARATION

I, *Ndeshihafela Vera Uushona*, hereby declare that the work on which this dissertation is based, is original (except where acknowledgements indicate otherwise) and that neither the whole work nor any part of it has been, is being, or shall be submitted for another degree at this or any other university, institution for tertiary education or examining body.

Dedication

To my husband Michael, my daughter Victoria, my Siblings Violine, Betty and Oiva. Not forgetting my late parents for inspiring me to succeed in all that I do.

ABSTRACT

Introduction

The primary role of breast cancer treatment with radiation is to deliver a sufficient radiation dose to the cancer cells without unduly causing biological damage to the healthy tissues. For over 50 years, electron beam therapy has been an important modality for providing an accurate dose of radiation to superficial cancers and disease and for limiting the dose to underlying normal tissues and structures in particular to boost the dose to the tumour bed and surgical scars after mastectomy. The Monte Carlo code MCNP5 was used to determine the effect of silicone gel breast prosthesis on the electron beam dose distribution.

Materials and Method

Percentage depth dose curves (PDD) for 6, 9, 12, and 15 MeV electron energies along the electron central axis depth dose distributions in a water phantom and with silicone prosthesis immersed in a water phantom were simulated using MCNP5.

In order to establish the accuracy of the MCNP5 code, the depth dose curves obtained using MCNP5 were compared against the measured depth dose curves obtained from the Varian 2100C linear accelerator. The simulated depth dose curves with silicone prosthesis immersed in water were compared to the measured depth dose curves with the

silicone prosthesis in water. The dose at the interface of the prosthesis with water was measured using thermoluminiscent dosimeters.

Results

The simulated and measured depth dose curve and the investigated dosimetric parameters are within 2%. Simulations in the presence of silicone showed a decrease in dose as the at the interface as the beam passes from the prosthesis to water for most energies however, for 15 MeV beam there is an increase in dose at the interface between the prosthesis and water and this was verified by physical measurements.

Conclusion

There were good correlations between the measured and MCNP simulated depth dose curve. Differences were in order of 2%. Small deviations occurred due to the fact that the simulations assumed a monoenergetic beam that exits the accelerator head, while in the measured results the beam exiting from the accelerator head includes scatted radiation from the collimators and the applicator. The presence of the prosthesis does not perturb the electron beam central axis depth dose curve however, the 15 MeV beam enhanced the dose in front of the interface between the prosthesis and water. Despite the limitations mentioned above MCNP5 results agree reasonably with the measured results. Hence, MCNP5 can be very useful in simulating electron percentage depth dose data.

Key Words

MCNP5, Silicone gel prosthesis, Electron beam therapy, Depth dose, Dose distribution.

TABLE OF CONTENT

TABLE OF FIGURES

LIST OF TABLES

Table

CHAPTER 1

INTRODUCTION

1.1 Overview

The primary aim of breast cancer treatment is to cause biological damage to the tumour without harming other healthy tissues surrounding the breast. Over the past 40 years, approximately two million women have undergone breast augmentation for cosmetic and tissue replacement following mastectomy (breast reconstruction). Irradiation of breast cancer in the presence of breast prosthesis is sometimes necessary in the event of the development or recurrence of breast cancer.

There is great concern among radiation therapists and oncologists as to whether the presence of the prosthetic implant will interfere with the delivery of the prescribed radiation dose. Electron beams, with their finite penetration and rapid dose fall-off, offer a mode of adequately treating the tumour and minimizing the radiation to the underlying normal structures such as the lungs and heart.

The dose distribution from an electron beam can be greatly affected by the presence of inhomogeneities such as lungs, bones, prosthesis etc [Podgorsak 2003]. The dose within the inhomogeneities is difficult to calculate or measure, but several techniques such as the boltzmann integral-differential equation, convolution methods and Monte Carlo techniques can be used to predict the dose in any inhomogeneous medium. Ma et al

[1997] maintained that of all the possible available methods for obtaining the dose distribution due to a radiation beam. The Monte Carlo method is one of the most powerful tools for studying the complex behaviour of the interaction of radiation beams with matter. Several authors such as Rogers et al [1988], Andreo [1998, 1991], Simpkin and Mackie [1990] and Mackie [1985] have proved that Monte Carlo simulation can accurately determine the distribution of absorbed dose within the patient. Deng J et al [2001] and Chow [2007] demonstrated that the Monte Carlo method is able to handle multiple electron scattering in the presence of inhomogeneities much more accurately than existing analytical dose models.

1.2 Aims and Objectives

The primary purpose of this study was to determine the effect of silicone gel breast prosthesis/implants on the electron beam dose distribution, by simulating the central electron beam depth dose distribution along the central axis of the beam in water and the prosthesis and simulating the dose distribution with the silicone prosthesis immersed in water. This was done using the general purpose Monte Carlo code MCNP5. In order to establish the accuracy of the MCNP5 code, the depth dose curves obtained from MCNP5 were compared against the measured depth dose curves obtained from the linear accelerator using a water phantom and the published central axis depth dose distributions. To obtain a better understanding of the dose perturbations produced by the prosthesis, the dose enhancement factor which is the ratio of the dose in water with the prosthesis to the dose in water without the prosthesis at the same depth was calculated.

1.3 Scope

In consideration of the major parameters influencing electron beam therapy, a review of interaction of electrons with matter will be introduced in Chapter 2. Furthermore a description of interaction of photons with matter will be given. Some dosimetric quantities used to define the radiation beam will also be discussed.

Since the focus of this work is to consider the effect of silicone gel breast prosthesis on the electron beam dose distribution, it is equally important to consider the basic silicone implant generations, chemistry, the effect of prosthesis on radiation and imaging. This will be discussed in Chapter 3. The MCNP code used in this study is reviewed in Chapter 4, as well as various applications in Medical Physics.

The Materials and Methodology used to conduct this research is discussed in Chapter 5, while the depth dose distribution obtained with the Monte Carlo simulation will be compared with the measured results obtained from the linear accelerator in Chapter 6.
Chapter 7 will deal with the discussion and conclusion derived from the results obtained in Chapter 6. Input, output data files and simulated geometry are presented in Appendices.

CHAPTER 2

BASIC RADIATION PHYSICS

2.1 Overview

The aim of this chapter is to introduce the basic interaction process which may occur when ionization radiation interacts with matter. The factors influencing such interaction processes and some dosimetric quantities used to define radiation beams are discussed.

2.2 Photon interactions

When a photon beam passes through matter, some of the photons interact with the atoms of the material and they are absorbed, scattered or transmitted. The attenuation of photons in a material is described by the following equation in a homogenous medium.

$$I = I_0 e^{\mu x} \qquad 2.1$$

Where I is the intensity of photons transmitted across a thickness x, I_0 is the initial intensity of photons, and μ is the linear attenuation coefficient. Khan [2003], states that the linear attenuation coefficient depends on the energy of the photon, the density and atomic number of the material being transversed. When the linear attenuation coefficient is divided by the density of the material, a more fundamental attenuation coefficient, the mass attenuation coefficient, is obtained and represented as (μ/ρ). The mass attenuation coefficient is independent of the material's density [Johns and Cunningham 1983]. Other

corresponding coefficients are the *electronic attenuation coefficient* ($_e\mu$) and *atomic attenuation coefficient* ($_a\mu$), respectively [Khan 2003]:

$$_e\mu = \frac{\mu}{\rho}.\frac{1}{N_o} cm^2 / electron \qquad 2.2$$

$$_a\mu = \frac{\mu}{\rho}.\frac{Z}{N_o} cm^2 / atom \qquad 2.3$$

Where Z is the atomic number and N_o is the number of electrons per gram. The thickness of any given material where 50% of the incident fluence has been attenuated is known as the half-value layer (HVL). Like the attenuation coefficient, the HVL is dependent on the photon energy and is inversely proportional to the attenuation coefficient. It is expressed as:

$$HVL = \frac{0.693}{\mu} \qquad 2.4$$

2.2.1 Interaction of photons with matter

There are five basic ways in which a photon interacts with matter [Thomas et al 1990]. These are the Photoelectric effect, Compton Scattering, Pair production, Coherent Scattering and Photo-disintegration. They are presented in the following sections.

2.2.2 Photoelectric effect

In the photoelectric (photon-electron) interaction (Figure 2.1), a photon interacts with an atom and ejects one of the bound electrons from the K, L, M, or N shells. In this process, the photon transfers its entire energy to the atom. The ejected electron is called a photoelectron and appears with an energy given by equation 2.5 [Khan 2003]:

$$E_e = h\nu - E_b \qquad 2.5$$

Where E_b represents the binding energy of the photoelectron in its original shell and $h\nu$ is the energy of the photon.

The interaction leaves an ionized atom with a vacancy in one of its bound shells. This vacancy is quickly filled through the capture of a free electron from other outer shells of the atom with the emission of characteristic x-ray photon. In some cases, there is a possibility of emission of the Auger electrons, which are monoenergetic electrons produced by the absorption of characteristic x-rays internally by the atom.

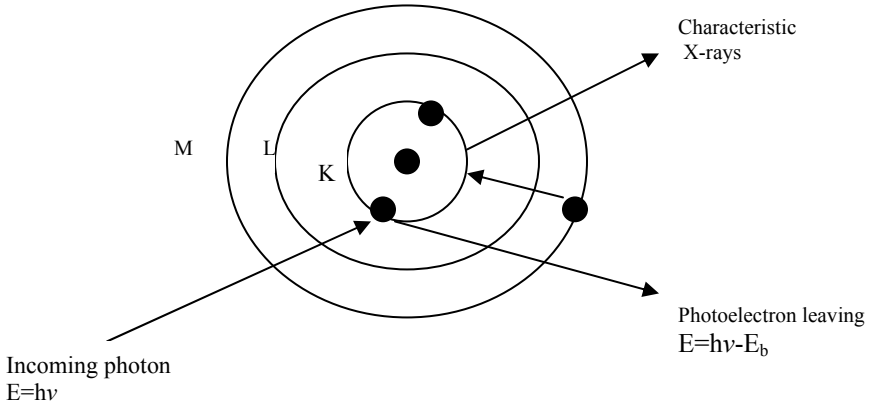

Figure 2.1 Diagram illustrating the photoelectric effect

The photoelectric interaction will only occur if the energy of the incident photon is greater than the binding energy of the electron with which it interacts [Thomas et al 1990].

2.2.3 Compton scattering

In the Compton interaction, an incident photon with relatively high energy strikes a free outer shell electron, ejecting it from its orbit. The photon is deflected through an angle ϕ with respect to its original direction. The reaction produces an ion pair, a positive atom and an electron, which is called the recoil electron (*E*) as shown in Figure 2.2. The photon transfers a portion of its energy to the recoil electron and the rest is retained by the deflected (scattered) photon.

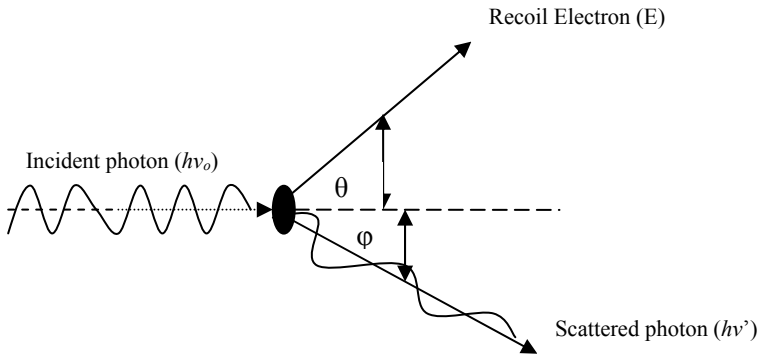

Figure 2.2: Diagram illustrating the Compton scattering

The amount of energy the photon retains is determined by its initial energy and the angle of deflection (θ) of the recoil electron [Thomas et al 1990].

The expressions that relate the energy transfer and the scattering angle for any given interaction can be derived by writing simultaneous equation for the conservation of energy and momentum and the relativistic relationship between energy and momentum. The final expression is given below by equations 2.7 to 2.9 [Khan 2003]:

$$E = hv_0 \frac{\alpha(1-\cos\phi)}{1+\alpha(1-\cos\phi)} \qquad 2.7$$

$$hv' = hv_o \frac{1}{1+\alpha(1-\cos\phi)} \qquad 2.8$$

$$Cos\theta = (1+\alpha)\ tan\,\phi/2 \qquad 2.9$$

Where hv_o, hv' and E are the energies of the incident photon, scattered photon, and electron, respectively and, $\alpha = hv_o/m_oc^2$, where m_oc^2 is the rest energy of the electron (0.511 MeV).

2.2.4 Pair production

When a photon with energy greater than 1.022 MeV passes near the nucleus of the atom, it interacts strongly with the electromagnetic field of an atomic nucleus in such a manner that its energy is converted into matter [Thomas et al 1990]. The interaction produces a pair of particles, an electron and a positively charged positron as illustrated in Figure 2.3 below. These two particles have the same mass, each equivalent to the rest mass energy of the electron 0.511 MeV.

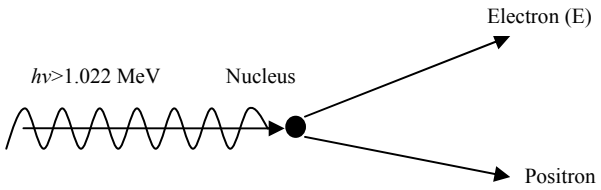

Figure 2.3: Diagram illustrating the pair production

2.2.5 Coherent Scattering

These are the interactions in which radiation undergoes a change in direction without a change in wavelength (λ) [Thomas et al 1990]. Coherent scattering does not cause ionization when a photon interacts with matter as no energy is transferred to the electron. There are two types of Coherent scattering, Thomson scattering and Rayleigh scattering. In Thomson scattering, a single electron is involved in the interaction, while Rayleigh scattering results from a cooperative interaction with all the electrons of the atom.

2.2.6 Photo disintegration

Photo-disintegration occurs when a high energy photon is absorbed by the nucleus of an atom. This interaction results in an emission of a neutron, a proton, an alpha particle, or a cluster of particles. The photon must have sufficient energy to overcome nuclear binding energies of the order 7 to 15 MeV.

Podgorsak [2003] states that photo-disintegration reaction does not play an active role in photon attenuation, it is rather of concern in high energy radiotherapy treatment rooms because of the neutron production reactions.

2.3 Dosimetric Quantities

A number of quantities and units have been defined for describing a monoenergetic ionizing radiation beam and the amount of energy it may deposit in some medium. In this section, dosimetric quantities and their units are defined according to ICRU [1980] report 33 on radiation quantities and units.

2.3.1 Particle fluence and energy fluence

(a) Fluence or particle fluence Φ is defined as the number of particles *dN* that would cross a sphere of cross section area *dA*.

$$\Phi = \frac{dN}{dA} \qquad 2.14$$

The unit for fluence is *particles/m*^{2}. The rate at which the particles pass through unit area per unit time is defined as the fluence rate.

$$\phi = \frac{d\Phi}{dt} \qquad 2.15$$

The unit for fluence rate is *particles/m*^{2}*s*.

(b) The quantity used to describe the amount of energy crossing a unit area is energy fluence.

$$\Psi = \frac{dN}{dA} h\nu \qquad 2.16$$

The unit for energy fluence is J/m^2 for photons or MeV/m^2 for electrons. The energy carried across unit area per unit time is called the energy fluence rate and is given by equation 2.18.

$$\psi = \frac{d\Psi}{dt} \qquad 2.17$$

Energy fluence is also referred to as intensity.

2.3.2 Exposure and absorbed dose

When a photon beam passes through air, it produces excitation and ionization [Graham 1996]. The measure of the amount of ionization that occurs in air is called exposure *(X)*. Exposure is thus defined as quotient of *dQ* by *dm*, where *dQ* is the absolute value of the total charge of the ions of one sign produced in air when all the electrons liberated by photons in air of mass *dm* are completely stopped in air.

$$X = \frac{dQ}{dm} \qquad 2.18$$

The unit for exposure is coulomb per kg of air (Ckg^{-1}).

Khan [2003] states, exposure is a measure of ionization in air only, it cannot be used for photon energies above 3MeV. Podgorsak [2003] has thus defined a non- stochastic quantity absorbed dose for all types of ionizing radiation (indirectly and directly), which is defined as:

$$Absorbed\ dose = \frac{d\overline{E}}{dm} \qquad 2.19$$

Where $d\overline{E}$ is the mean energy imparted by ionizing radiation to material of mass *dm*. The units for absorbed dose is Joules per kilogram (J/kg) and the special name is gray (Gy).

2.3.3 Kerma

Kerma stands for Kinetic Energy Released per unit Mass of an absorber. Podgorsak [2003] described kerma as non-stochastic quantity applicable to indirectly ionizing radiation, such as photons and neutrons. It is defined as:

$$K = \frac{d\overline{E}_{tr}}{dm} \qquad 2.20$$

Where $d\overline{E}_{tr}$ is the sum of the initial kinetic energies of all the charged ionizing particles (electrons) liberated by uncharged particles (photons) in a material *dm*.

2.3.4 Relationship between absorbed dose and kerma

Due to the non-zero (finite) range of the secondary electrons released through photon interactions, the transfer of energy (Kerma) from the photon beam and the absorption of energy by the medium (absorbed dose) do not take place at the same location.

The relationship between absorbed dose and Kerma is best described by Figure 2.6 below.

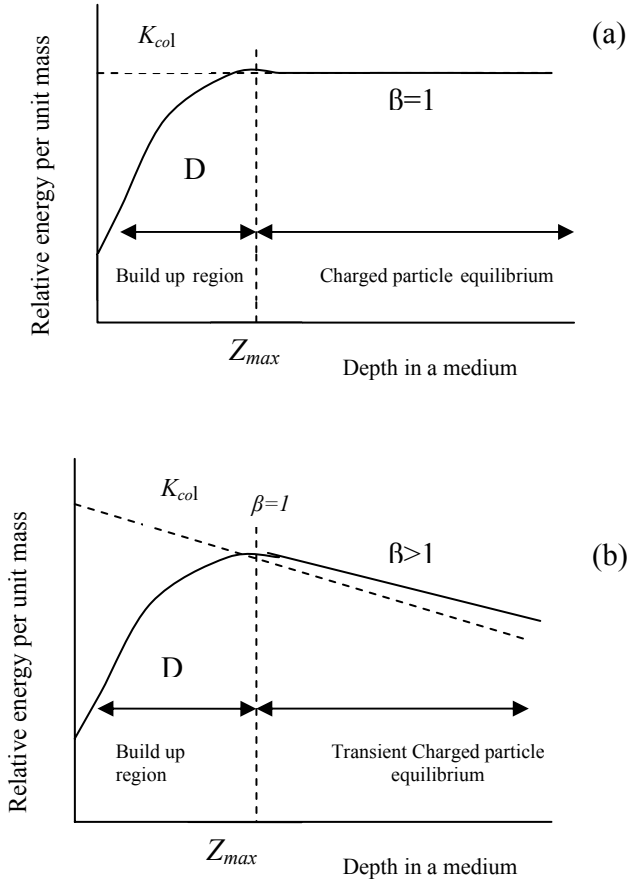

Figure 2.4: Relationship between collision kerma and absorbed dose

As the high energy beam penetrates the medium, Kerma is maximal at the surface of the irradiated material and this is because the particle fluence is greatest at the surface. Initially, the charged particle fluence and hence the absorbed dose increases as a function of depth until the depth of maximum dose (Z_{max}) is attained. If there was no attenuation or scattering, the situation in Figure 2.4 (a) would occur, and electronic equilibrium is achieved. Since a radiation beam does undergo attenuation and scattering the situation in Figure 2.4 (b) is achieved, when a constant relation between collision kerma and absorbed dose exists. Collision kerma and absorbed dose decreases constantly after the depth of maximum dose, but the absorbed dose curve is slightly above the kerma curve.
The build up region in the absorbed dose curve is responsible for the skin sparing effect when high-energy photon beams are used. The surface dose is due to electron contamination in the beam.

2.4 Electron interactions

As electrons travel through a medium, they interact with the medium by a variety of processes due to coulomb forces [Khan 2003]. However, because of their relatively small mass, the electrons suffer greater multiple scattering between the incident electron and the nuclei of the medium, and in the process lose energy.

The main types of processes are (a) inelastic collisions with atomic electrons resulting in ionization and excitation of atoms, (b) inelastic collisions with atomic nuclei resulting in

bremsstralung production, (c) elastic collisions with atomic nuclei, resulting in elastic scattering, and (d) elastic collisions with atomic electrons.

In elastic collisions, the kinetic energy is not lost but the electron‘s direction may be changed or the energy redistributed among the particles emerging from the collision. However, in inelastic collisions, kinetic energy is lost through interactions with the orbital electrons of the atoms in the material or with the electric field of the nuclei in which the bremsstrahlung photon is emitted. The energy lost to the atomic electrons is called collision energy, while the energy lost to the nucleus is called radiative energy [Metcalfe et al 1997].

The total distance an electron travels in a material before losing all its energy is referred to as its range and is determined by the initial energy of the electrons and the density of the material. Metcalfe et al [1997] observed that high initial electron energy and/or a slower rate of energy loss gives rise to a larger electron range. One important characteristic of electron interactions is that all electrons with the same energy have the same range in a specific material.

2.4.1 Electron stopping and scattering powers

The energy transferred from the electron to the medium by collision or radiative processes is quantified by the use of stopping powers. Johns and Cunningham [1983] defined stopping powers as the energy lost per unit thickness of medium, expressed as:

$$S = \frac{dE}{dX} \qquad 2.23$$

Similar to attenuation coefficients, stopping powers are expressed as density-independent quantities. Thus, the total mass stopping power is denoted as

$$\left(\frac{s}{\rho}\right)_{tot} = \left(\frac{s}{\rho}\right)_{col} + \left(\frac{s}{\rho}\right)_{rad} \qquad 2.24$$

Where $(s/\rho)_{col}$ is the mass collision stopping power and $(s/\rho)_{rad}$ is the mass radiative stopping power respectively.

Khan [2003] and Podgorsak [2003] observed that the rate of energy loss for collision interaction depends on the electron energy and on the electron density of the medium. They added that the mass stopping power is greater for low atomic number material than for high atomic number material and this is because high atomic number materials have fewer electrons per gram than lower atomic number materials. The rate of energy loss for radiative interactions (bremsstrahlung) is approximately proportional to the electron energy and the square of the atomic number (Z^2). The typical energy loss for a therapy electron beam averaged over its entire range is about 2 MeV/cm in water and water-like tissue.

In the domain of radiation dosimetry, another parameter closely related to the collision stopping power and called the restricted mass stopping power (L/ρ) has been introduced. Restricted stopping powers exclude the energy carried away by "delta rays" which is a recoil particle that causes secondary ionization. The units for linear and the mass stopping powers are MeV/cm and MeV.cm^2/g respectively.

Similarly to mass stopping powers, the mass scattering powers T are defined as the ratio of $d\,\overline{\theta}^2$ and ρl, where $\overline{\theta}^2$ is the mean square scattering angle .

$$T = \frac{d\overline{\theta}^2}{dl} \qquad 2.25$$

Scattering powers decrease with electron energy and increases with the atomic number of the medium.

2.4.2 Production of electron beams in a linear accelerator

The linear accelerator (LINAC) is based on the acceleration of energetic particles such as electrons to very high energies using high frequency electromagnetic waves through a linear tube. Figure 2.11 is a block diagram of a typical medical LINAC design [Khan 2003].

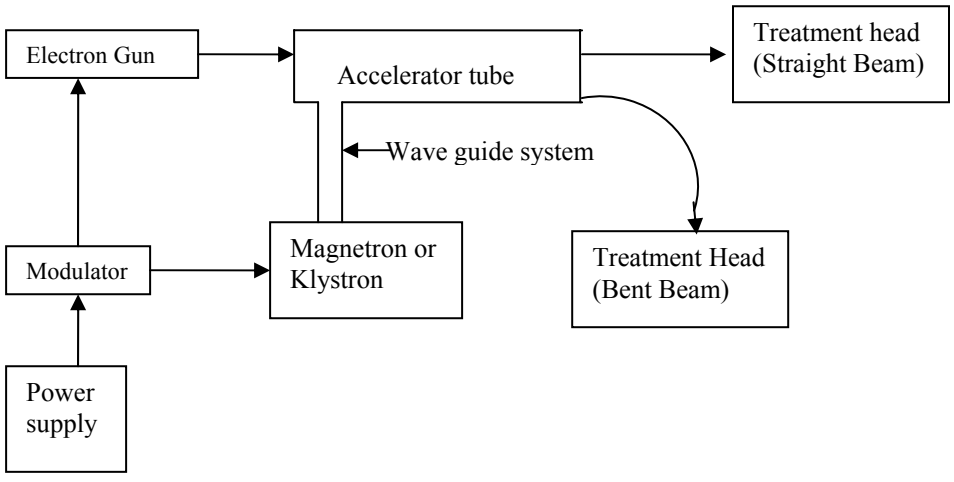

Figure 2.5: A Schematic block diagram of a Medical Linear Accelerator [Khan2003:43]

Accelerators used in radiotherapy accelerate electrons either by travelling or stationery electromagnetic waves of frequencies in the microwave region of ~ 3000 megacycles/sec. The power supply provides direct current (DC) to the modulator which forms high voltage pulses which are simultaneously delivered to the magnetron/klystron and the electron gun. The magnetron/klystron then produces pulsed microwaves which are injected into the accelerator tube via the wave guide system, at the same time electrons produced in the electron gun are injected into the accelerator tube. The electrons with an initial energy of about 50 keV interact with the electromagnetic field of the microwaves of the tube, which causes them to be accelerated to higher megavoltage energy regions. The high energy electrons emerge from the exit window of the accelerator tube in a form of a pencil beam ~ 3mm in diameter [Khan 2003] to the treatment head. Depending on the energy, it either emerges as a straight or bent beam using bending magnets, focusing coils and other components of the beam transport system.

After leaving the accelerator tube, the electron beam is made to strike the electron scattering foil which spreads the beam and gives uniform electron fluence across the treatment field. After the scattering foil, the beam is then incident on monitoring ion chambers whose primary functions are to monitor radiation dose produced by the beam. After passing the ion chambers, the beam is further collimated by continuously movable collimators. The electron beam is then further shaped by an external electron applicator attached to the treatment head. Collimation of the beam is necessary to limit its size and to protect surrounding healthy tissues.

2.4.3 Percent depth dose specification

In selecting the appropriate electron beam energy to be used for a specified clinical case, the first consideration is matching the central- axis depth- dose parameters to the clinical situation. ICRU 35 [1984] has defined several parameters to characterize the electron beam central-axis depth-dose curve as shown in Figure 2.6.

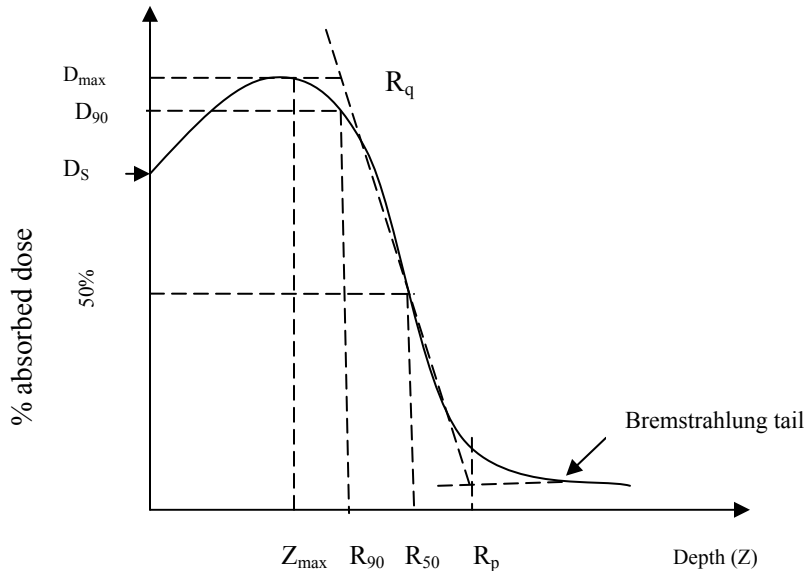

Figure 2.6 Typical Electron beam PDD Curve in water

Figure 2.6 shows a typical electron beam central axis depth dose curves. The electron beams exhibits a high surface dose, the dose then builds up to the maximum, at a depth referred to as depth of maximum dose (Z_{max}). The continuous energy loss and scattering of electrons are responsible for the sharp drop off beyond Z_{max}. The dose levels off at a small low level dose component referred to as bremsstrahlung tail which is a result of photon contamination. The depth of maximum dose and the gradient of the dose fall-off vary with the incident energy of the electron. At beam energies greater than

approximately 20 MeV, percentage depth-dose curves lose their sharp fall-off and begin taking on characteristics of photon beams due to bremsstrahlung energy loss, whereas their penumbrae broaden with depth, due to increased multiple coulomb scattering.

R_{90} and R_{50} in Figure 2.10 are the depths on the electron depth dose curve at which the percentage depth doses beyond Z_{max} attain value of 90% and 50%, R_q is the depth at which the tangent to the depth dose curve at the point of inflection intersects the maximum dose level and R_p known as the practical range is defined as the depth at which the tangent plotted through the steepest section of the depth dose curve intersects with extrapolation line of the background due to bremsstrahlung.

R_{90} is also known as the therapeutic range for electron beam therapy, and if possible, it should coincide with the treatment margin. R_{90} is approximately given by E/4 in centimeters of water, where E is the nominal energy of the beam.

Each of the parameters defined in Figure 2.6 is of clinical importance and can be affected by small differences in energy, scattering foils, collimation and source to surface distance (SSD). Thus, measurement of the central-axis depth-dose curve is therefore critical. The AAPM report of radiation therapy task group no 25 [Khan et al 1991] recommends the use of a small cylindrical ionization chamber to determine the percent depth dose in an electron beam taking into account the characteristics of the chamber, the electron beam energy and its variation with depth. The measured depth ionization distribution must be then converted to a depth dose distribution by using the appropriate stopping power ratios

to water to air at depths in the water as discussed in the IAEA TRS 398 protocol [IAEA 2001].

2.4.4 Electron energy specification

Electron energy specification for accurate dosimetry of clinical electrons is complicated by the large variation in the design of the beam shaping systems. The electron beam inside the accelerator tube just before hitting the accelerator window is the intrinsic beam with very small energy and angular spread [Khan et al 1991]. As the beam passes through the exit window, scattering foil, monitor chamber, collimator system, air and other materials in reaching the phantom surface, electron energy and angular spread are increased. The beam shaping system may generate a broader energy distribution of the initial electron beam and generate secondary and scattered electrons in collimators.

Due to the complexity of the electron beam, there is no single energy parameter that will fully define the electron beam. Khan [2003] and Podgorsak [2003] defined several parameters to describe the electron beam, (i) the most probable (kinetic) energy $E_{p,o}$ at the patient surface, (ii) the mean energy $\overline{E}_o$ on the patient surface, (iii) the mean energy $\overline{E}_z$ at the depth z, and (iv) the half value depth R_{50}.The most probable and the mean energy at depth z are related to the practical range as shown in equation 2.26 and 2.27 respectively, while the mean energy on the patient surface is related to the half value depth as shown in equation 2.28.

$$E_{p,o} = 0.22 + 1.98R_p + 0.0025R_p^{\ 2} \qquad 2.26$$

$$\overline{E}_z = \overline{E}_o(1 - z/R_p) \qquad 2.27$$

$$\overline{E}_o = CR_{50} \qquad 2.28$$

Where $E_{p,o}$ is in MeV, R_p in cm and C=2.33 MeV/cm of water. IAEA [2001] specified R_{50} as the beam quality index for electron beams.

2.4.5 Clinical use of electron beam therapy

The steep fall-off of the dose beyond the depth of maximum dose is one of the physical characteristics of the electron beam that makes it a unique therapeutic modality. Electron beams are usually used for the treatment of superficial or subcutaneous cancers within 6cm of the surface. A sterilization dose can be delivered to the tumour while the total volume of irradiated tissue is sharply limited. Electron beam energies in the range of 6-20 MeV are principally used in the treatment of (1) skin and lip cancer, (2) chest-wall and neck (elective post-surgery and recurrent disease) cancers, (3) upper respiratory and digestive-tract lesions for 1 to 5 cm in depth (using the electron beam alone , in combination with photon beams, in association with interstitial therapy or as a boost treatment to primary lesions), (4) Head and neck cancers, and (5) boost treatment to lymph nodes, operative scars and residual tumour.

2.4.6 Tissue inhomogeneity

The presence of inhomogeneities can greatly affect the electron beam dose distribution. The main effects are:

1. The different attenuation in the various tissues which depends on the densities of the tissues involved (changes in the attenuation of the primary beam).
2. The alterations in the electron scattering pattern, which depend on the atomic number of the tissue in the electron beam path (changes in secondary electron fluence). The scatter perturbations may effect the dose distribution in the neighbourhood of the inhomogeneity.

CHAPTER 3

SILICONE GEL DOSIMETRY

3.1 Overview

Breast reconstruction in patients who have undergone mastectomy for carcinoma of the breast is becoming more frequent with increasing emphasis on self-image and improved methods of cosmetic surgery. The prosthesis generally used consists of a silicone implant, characterized by a soft, thin envelope containing transparent silicone gel. In some patients, lesions occur, that had breast augumentation with silicone implants and is now reluctant to the remove the implant, and other patients develop local recurrences after the implant was inserted for breast reconstruction. In either case, the radiation oncologist is often faced with the task of satisfactorily treating the cases.

The flexibility, strength and texture of the silicone breast prosthesis make it similar to the natural breast. The chemical properties of silicone, the history (generation) of silicone implants is discussed in the following sections, as well as the effect of the prosthesis on radiation and imaging.

3.2 Silicone implant generations

Silicone- filled breast prosthesis were created by Cronin and Gerow in 1962. Since then very few other materials have been used for breast augmentation, and this is partly due to the success of silicone as a medical device.

The evolution in design and manufacturing of breast implants has focused on four major areas: characteristics of the shell, characteristic of the filler, shape, and surface configuration. Breast implants has been classified into generations based on the time period of their development. Table 3.1 below shows the generation of silicone gel filled implants.

Table 3.1: Generations of Silicone Gel Filled Breast Implants

Implant Generation	**Production period**	**Characteristics**
First generation	1960's	Thick Shell (0.25mm average) Thick, Viscous Gel Dacron Patch
Second generation	1970's	Thin shell (0.13mm average) Less Viscous Gel No Patch
Third generation	1980's-1992	Thick, Silica Reinforced, Barrier Coat Shells
Fourth generation	1992-present	Stricter manufacturing standards; Refined third generation devices
Fifth generation	1993-present	Cohesive Silicone gel filled Devices; forms stable devices

All the changes from the first to the fifth generation have been made with an aim to improve the safety and clinical performance of the implant.

Although silicone implants have been in use over two decades, in 1992 the Food and Drug Administration (FDA) passed a moratorium restricting the use of silicone breast implants to women seeking breast reconstruction, because of the increasing concerns regarding the relationship between silicone and connective tissue disorders as well as other illness due to silicone gel.

After 14 years of several reviews and investigations on the safety of silicone implants by the scientific community, the FDA re- approved the use of the implants on 17 November 2006 since every reputable study that has examined the safety of silicone implants, found no link between silicone implants and autoimmune disease [Muzaffar and Rohrich 2002].

3.3 Silicone Chemistry

Silicones are a family of polymers which are not found naturally. They comprise of an alternating silicon-oxygen atom backbone (Figure 3.1 below) and organic side groups [van Diest et al 1998]. Silicone's intrinsic properties: thermal and oxidative stability, chemical and biological inertness, hydrophobic nature, elasticity, non adhesiveness to tissue and sterilization have made it to be used widely as a medical device [van Noort and Blank 1981, Mcgrath and Burckhardt 1984]. The polymer utilized medically is poly-dimethylsiloxane (PDMS).

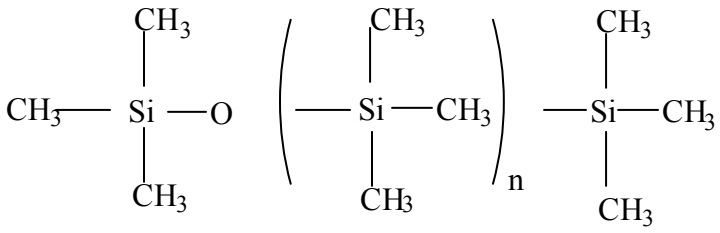

Figure 3.1: building block of silicone implant prosthesis

Silicone contained implants are divided into four main types: (1) Silicone rubber envelopes filled with saline; (2) Silicone rubber envelopes covered with a polyester polyurethane foam coating; (3) Silicone rubber envelopes filled with silicone gel; (4) dual silicone rubber envelopes, the inner envelope containing silicone gel and the outer envelope filled with saline, [Kossovsky and Freiman 1994]. The physical state of silicone gel filled implants is determined by the degree of chemical cross-linking which occurs between the vinyl and hydrogen groups on silicon atoms [Picha and Goldstein 1991, LeVier et al 1993].

Silicone oils are straight chains of PDMS without cross-linking and are insoluble in water. The gel consists of cross-linked (of various degrees) PDMS chains together with variable amounts of PDMS liquid. Elastomers of silicone have high degrees of cross-linking and contain little free PDMS oil. A special silicone elastomer with a barrier coating on the breast implant's shell is specially selected to minimize migration of PDMS from the implants. In an effort to reduce gel bleed from the silicone filled implants phenyl or triflouropropyl groups are bounded to the shell to decrease the shell permeability to the PDMS oil [Barker et al 1981, Caffee 1986].

A simplified description of breast implant construction is shown in Figure 3.2 below.

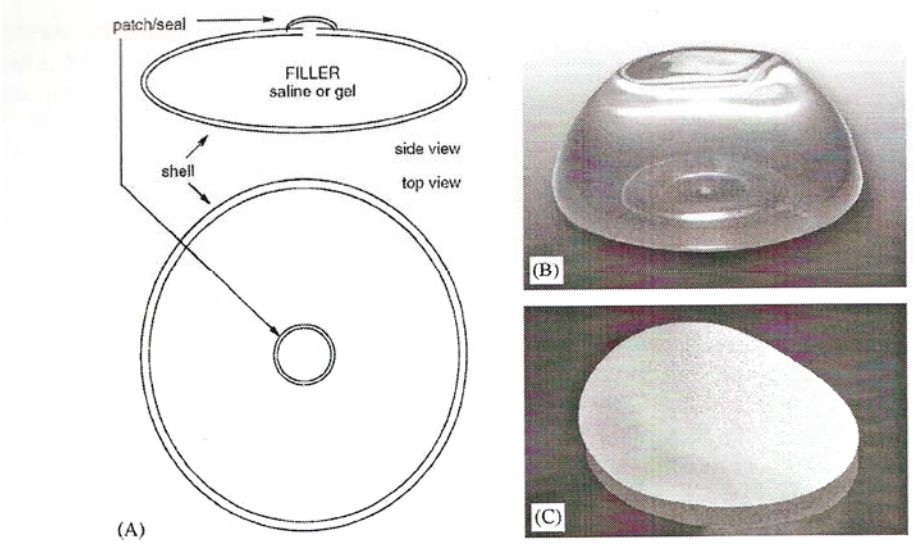

Figure 3.2: Structural features of breast implants. (A) General characteristics. (B) Round/ responsive implant (smooth surface). (C) Cohesive/contoured implant (textured surface). [Brook, 2006:3278].

Physical constants of silicone gel used for implants are tabulated in table 3.2 (Arthur et al 1991).

Table 3.2: Physical constants of silicone gel as a mammary filling material.

Physical	**Constants**
Density (g/cc)	0.97
Coefficient of friction	0.60
Viscosity (CP)	400.0

3.4 Implants and pathology

Silicone oils, gels and rubbers are potentially bioactive agents that may induce host reactions. There are many questions as to the exact biological activity of the different silicones and their long term significance [van Diest et al 1998].

The most common problem with breast implants is capsular contracture, which occurs if the scar or capsule around the implant begins to tighten and squeezes down on the soft implant, which makes the breast feel hard, this causes local discomfort and upward displacement of the implant. Capsular contractures are more common when the implants are placed behind the breast tissue and in front of chest muscles.

Commonly a fibrous capsule forms around silicone breast implants, which occurs when the silicone shell has a hole or a tear that allows the migration of the contents outside the shell. There is, however evidence that silicones may migrate into and through these capsules [Beekman et al 1997]. On the other hand, rupture of the capsules may occur by accident, mammography, or closed capsulotomy (squeezing until the capsule ruptures, a once accepted method of disrupting a hard tissue capsule) which may facilitate migration of silicones into the surrounding breast [van Diest et al 1998].

Leakage from silicone breast implants which occurs when silicone “bleeds” through the silicone shell, may lead to a variety of locoregional pathological processes with a more or less specific morphology. In general, the incident of these pathological processes will increase with implant age. As yet, there is insufficient evidence for systemic effects of silicone leakage such as autoimmune and connective tissue diseases, and there does not

seem to be an increased risk of breast cancer in patients with silicone breast implants [van Diest et al 1998].

Arthur et al [1991] reported that the presence of silicone gel in subcutaneous locations causes inflammatory foreign body reaction and occasionally requires extensive surgery for its removal.

Experimental models have demonstrated that, when radiotherapy is combined with surgery, it may lead to increased rate of infections resulting from impaired tolerance of irradiated tissue to bacterial contamination [Ariyan et al 1980].

3.5 Prosthesis and radiation

When breast carcinoma arises in the augmented or reconstructed breast, conservative management (i.e., limited surgery and definitive irradiation) is feasible without compromising the therapy or the cosmetic results. Thus, conservative management should be offered as an option to patients who are interested in breast prosthesis conservation [Rvu et al 1990].

Typically, prostheses used for breast reconstruction or augumentation contain a material of higher atomic number (Z) than human tissue and this may effect the radiation dose distribution within the breast.

The dosimetry at the interface between tissue and a high Z-medium is a well known problem. Cheng et al [2005] demonstrated that dose perturbations exist between two dissimilar media with different atomic composition or in the presence of a contrast medium.

For breast irradiation, the dosimetric effect of breast implants has been studied previously. Early studies showed that the magnitude of dose perturbation at interface is dependent on the beam energy and the atomic number of the medium [Das and Chopra 1995, Das 1997].

Different authors have irradiated patients with prosthesis, their results follows:
Jacobson et al [1986] and Stabile et al [1990] treated patients with silicone gel prostheses with external radiation for recurrent disease or as a primary therapy. The majority of patients had excellent cosmetic results with minimal late skin changes and no fibrosis or contracture, they thus concluded that with proper surgical and radiotherapeutic treatment, good cosmetic results can be obtained in patients without comprising their therapy.

Shedbalkar et al [1980] studied the radiation effects on silicone gel, and the dose distribution of radiation through mammary prostheses and found that, silicone gel behaves like tissue and the half-value thickness for silicone gel and water are almost the same (within experimental margin for error), the linear absorption coefficient for silicone gel and water are also comparable (within experimental margin for error).

Krishnan et al [1983] studied the effect of silicone gel breast prostheses on the absorbed dose distribution using, 9-20 MeV electron beams with the presence of breast prosthesis and without the prosthesis in a water phantom. Their results revealed no significant difference in the dose delivered due to the presence of the prosthesis. Clinical verification

of the dosimetry in the presence of the silicone gel implant does not compromise treatment by irradiation in the management of breast cancer [Krishnan et al 1986].
Klein and Kuske [1993] studied changes in photon dose distributions due to breast prostheses and maintain that prostheses do not effect the photon beam distribution but rather radiation affects the prostheses.

There are a number of concerns with regard to the technique used in radiotherapy with patients with a reconstructed breast. Some techniques are reported to significantly distort the chest wall anatomy, radiotherapy portals need to be modified adequately and this makes treatment more difficult and may increase the volume of irradiated heart or lung. Buchholz et al [2002] believes that a non uniform thickness of the chest wall across the electron field used for irradiation of internal mammary nodes may also cause significant dose inhomogeneities in this area.

3.6 Prosthesis and imaging

Silicone filled implants have an extremely low x-ray transmission, which is reported to interfere with the detection of small masses forming in the breast [Gumucio et al 1989], but Arthur et al [1991] reported that special mammography procedures using excessive radiation have been developed to detect tumors in the presence of the prosthesis. Effective mammography is dependent on many factors. These include radiologic materials and techniques, the position of the patient, location of the implant, and adequate flattening of the breast tissues.

Noone et al [1994] and Senkus- Konefka et al [2004] found that the diagnosis of breast cancer recurrence should not be affected by the presence of the prosthesis, as most prostheses are usually placed under the pectoralis muscles (i.e. under the tissue layer most frequently affected by local recurrences (skin and subcutaneous tissue)).

Calcifications (deposit of calcium containing salts) are known to occur in tissue around implants. These are believed to increase with time and may remain once the implant has been removed. These calcifications are not considered harmful, but they can be seen on mammograms, and thus interfere with mammographic findings and interpretation of results. Stevanovic and Jakovljevic [2001] compared magnetic resonance imaging (MRI) and mammography imaging and found MRI to be superior in revealing recurrence with micro calcifications, in revealing recurrences near the chest wall, and it is also more sensitive in detection of multi focal tumours. However, MRI, mammography and ultrasound are not standards.

Madsen et al [2000], studied the effects of silicone breast prostheses on measurements of body composition by dual energy x-ray absorptiomentry, and found that the silicone prostheses had only a minor impact on the assessment of soft tissue composition.

CHAPTER 4

MONTE CARLO TECHNIQUES

4.1 Overview

Although the physics of photons and electron interactions in matter is well understood, in general it is impossible to develop an analytic expression to describe particle transport in a medium. One widely used technique for solving this problem involves Monte Carlo simulation of radiation in which one uses knowledge of the probability distributions governing the individual interactions of electrons and photons in matter to simulate the random trajectories or histories of individual particles.

Monte Carlo is a common tool in areas of research and clinical development where interactions of radiation with matter are important, namely diagnostic radiology, nuclear medicine, radiation shielding, radiation protection and dosimetry [Abdullah et al 2005, Andreo 1998]. With the development of computer technology and variance reduction techniques the Monte Carlo method is becoming an accurate and practical approach in the calculation for electron and photon doses.

Several codes have been developed for particle transport; this includes MCNP, EGS, ETRAN and BEAM which are more applicable in Medical physics. The new versions in place now are MCNP5, EGSnrcMp and BEAMnrcMp. This work used MCNP5, because of its relative simplicity, rich physics and because it can also handle complex geometries.

4.2 The Monte Carlo Method

Monte Carlo simulation is a stochastic technique which is based on random numbers and probability statistics. In Monte Carlo calculations, the particle tracks or histories are generated by simulating the random nature of the particles interaction with the medium. To do this one requires mathematical expressions for the probability relationships which govern the track length of an individual particle between interaction points, the choice of an interaction type at each such point, the choice of a new energy and a new direction if the interaction is of a scattering type, and the possible production of additional particles. One needs a complete understanding of the physics of the various processes a particle undergoes in its lifetime from the time it is born in the source until it is absorbed or leaves the system under consideration, in order to make selections of the specific values for these variables. The statistical uncertainty of the calculation depends on the N, the number of particle histories simulated, which usually decreases as $N^{-1/2}$ [Kawrakow and Rogers 2000].

The other approach to numerical modeling is the deterministic technique (numerical solutions to the Boltzmann transport equation. The fundamental advantage of Monte Carlo techniques over deterministic techniques is that Monte Carlo techniques represent more accurately the geometry and the nuclear data than deterministic techniques. Deterministic techniques require reasonably simple geometries for the numerical technique to work, and use the multi-group approximation to cross-section data. Monte Carlo techniques can handle complex geometries and continuous cross section data (as

well as simple geometry and multi group data). Monte Carlo techniques can also handle back scatter from high density materials such as bone and scatter perturbations by air cavities more accurately than deterministic techniques.

The disadvantage of the Monte Carlo techniques is that they are statistical in nature and do not provide an exact solution to the problem. All results represent estimates with associated uncertainties. In addition, Monte Carlo techniques can be quite time-consuming on a computer, as small uncertainties are required. The deterministic method solves the integro-differential transport equation for the average particle behavior, while Monte Carlo solves the integral transport equation [X-5 Monte Carlo team 2003]. Siebers et al [2000] observed that Monte Carlo techniques always yield the absorbed dose in any medium, where as all current analytical methods effectively yield equivalent water dose.

The relationship between Monte Carlo techniques and deterministic techniques is that deterministic techniques provide a highly exact solution to a significantly simplified approximation of the problem, while Monte Carlo techniques provide an approximate solution to a highly exact representation of the problem.
Recurring problems in Monte Carlo codes are numerical round off problems as particles cross boundaries [Rogers et al 1995].

4.3 Electron transport simulation

Electron Monte Carlo transport calculations play an increasingly significant role in electron beam therapy. Although the simulation of electron transport is of particular interest in radiotherapy, there are some difficulties in the simulation of electron transport. Firstly electrons undergo hundreds of thousands of interactions with matter before slowing down, thus an event by event simulation of an electron is often not possible. Secondly, the cross section for electrons is five to six orders of magnitude higher than those of neutron or photons of the same energy [Svatos 1997]. Thirdly, the fractional energy loss per collisions is frequently five orders of magnitude smaller for electrons than for photons, thus the number of interactions required for an electron to give up all its energy is very large.

Berger [1963] developed the condensed history (CH) technique (macroscopic techniques). In the CH technique, large numbers of transport and collision process are condensed to a single electron step. The cumulative effect of the individual interactions is taken into account by sampling the change of the particles energy and direction of motion at the end of the step from appropriate multiple scattering distributions [Kawrakow 2000]. Physical interactions of electrons are classified into groups which provide detailed "macroscopic pictures" of the physical process: The electron energy E, direction u, position r and the distance S_n [Andreo 1991].

According to Berger [1963], the condensed history can be classified into two schemes:

1. Class I scheme, groups all the interactions, and particles on a predetermined energy loss grid. The scheme has the potential for a more accurate treatment of multiple elastic scattering, although there are some disadvantages associated with the lack of correlation between energy loss and secondary particle production, as well as the necessity for difficult interpolations when the particle steps do not conform to the predetermined grid because of interfaces and/or energy loss straggling.

2. Class II scheme also known as mixed procedures, groups only minor collisions where energy losses or deflections are small, but considers the individual sampling of major events or "catastrophic collisions", where a large energy loss or deviation occurs. Andreo and Brahme [1984] has introduced procedures to account for energy-losses and deflection below the threshold of major collisions, using restricted energy-loss straggling and restricted multiple scattering during the classification between major and minor events.

4.4 Electron energy spectrum

The electron energy spectrum is an important component of any dose calculation code used for electron beam radiotherapy.

Several authors such as Ma et al [1993], Ma and Jiang [1999] have shown that there exists a difference between the dose distribution of electron beams of a clinical accelerator in a water phantom and the dose distribution of monoenergetic electrons of nominal energy of the clinical accelerator in water, and this is because the electron beams

which reaches the water surface travelling through the collimation system of the accelerator are no longer monoenergetic. Ma et al [1997] also showed that this is because when the beam passes through the treatment head and undergoes some discrete energy loss event such as bremsstrahlung and delta ray production, the sharp peak of the electron energy spectrum is broadened and the resultant energy spectrum is thus a broadened peak located at the most probable energy E_p with a low energy tail.

While calculating precisely the dose distribution of any incident electron beams, the energy spectrum of the incident electron beam should be taken into consideration. Great effort has been made to study and derive the electron and photon energy spectra in clinical electron beams.

Zhengming and Jette [1999] studied a regularization method to determine an effective energy spectrum for electrons in clinical electron beams from percentage depth dose (PDD) data. Jiang et al [2000] used a hybrid approach to tune the Monte Carlo calculated energy spectra of electron beams according to the R_{50} variation between the measured central axis PDD and the Monte Carlo simulated axis PDD.

Faddegon and Blevis [2000] used a public domain code FERDO to unfold the electron energy spectra from the measured depth dose distributions with the photon background subtracted. Their approach yielded smooth but wide spectra with an average resolution of 16 ±3 % of the mean peak energy for all beams studied.

Deasy and Almond [1994] carried out Monte Carlo simulations to study the spectral dependence of electron central axis depth dose curves and found that the energy spread has only a small effect on the shape of the central axis depth dose curves.

Deng et al [2001] employed a random "creep" algorithm to determine the energy spectra of electrons and in a clinical electron beam. They compared the fitted energy spectra with the spectra obtained from the Monte Carlo full phase space simulations. The fitted energy spectra are in good agreement with the Monte Carlo simulated spectra in terms of peak location, peak width, amplitude and smoothness of the spectrum.

4.5 MCNP CODE

MCNP is a general-purpose Monte Carlo n-particle transport code that has many applications outside medical physics. It was originally a neutron transport code used for reactor calculations [Rogers 2006], but over the years has been regularly updated and can now be used for single or coupled photon/ electron transport. The electron transport in this code has been adapted from the Integrated Tiger Series (ITS) code which is based on electron transport code (ETRAN code) [Rogers 2006, Hableid and van Devender 1976, Berger and Seltzer 1968].

The code treats an arbitrary three-dimensional configuration of materials in geometric cells bounded by first and second degree surfaces and fourth- degree elliptical tori.

For photons, the code accounts for incoherent and coherent scattering, the possibility of fluorescent emission after photoelectric absorption, absorption in pair production with

local emission of annihilation radiation and bremsstrahlung. A continuous-slowing down model is used for electron transport that includes positrons k x-rays, and bremsstrahlung but does not include external or self-induced fields. The neutron energy covers the range from 10 MeV to 20 MeV for all isotopes and up to 150 MeV for some isotope. The photon energy regime is from 1keV to 100 GeV, while the electron energy regime is from 1 keV to 1000 MeV [X-5 Monte Carlo team 2003].

There are a number of important standard features that make MCNP very versatile and easy to use. These include a powerful general source, criticality source, and surface source; both geometry and output tally plotters; a rich collection of variance reduction techniques; a flexible tally structure; and an extensive collection of cross-section data (X-5 Monte Carlo team 2003) and are as follows:

4.5.1. Tally specifications

The tally cards are used to specify what type of information the user wants to gain from the Monte Carlo calculation. The latest version, MCNP5 contains numerous flexible tallies: surface current and flux, volume flux (track length), point or ring detectors, particle heating, fission heating, pulse height tally for energy or charge deposition, mesh tallies and radiography tallies.

Tallies are normalized to be per starting particle except for a few special cases with criticality source. In fact, MCNP can tally any quantity of the form

$$C = \int \phi(E) f(E) dE$$

Where $\phi(E)$ is energy-dependent fluence, and *f (E)* is any product or summation of the quantities in the cross- section libraries or a response function provided by the user.

4.5.2. Variance reduction

Variance reduction is one of the features that are crucial to the MCNP success of solving problem. Variance reduction is the modification of the faithful analogue simulation of particle histories in order to obtain an increase in the precision of the result per unit central processing unit time.

Two basic approaches can be applied to reduce the computational effort for a particular problem: (1) simplify the MCNP model, and (2) use non-analog simulations [Shultis and Faw 2006]. In the first approach, the model geometry and physics used to simulate particle transport can often be simplified or truncated.

The second basic approach is to reduce the variance of a tally by modifying the simulation process itself, making certain events more or less probable than they actually occur in nature. Shultis and Faw [2006] referred to such modification as *nonanalog* Monte Carlo. The MCNP has four classes of variance reduction techniques that range from the trivial to the esoteric [X-5 Monte Carlo team].

(i) *Truncation Method* speeds up calculations by truncating parts of phase space that do not contribute significantly to the solution. Energy cutoff and time cutoff are the specific truncation method available in MCNP.

(ii) *Population control*, the number of particles in regions of high/low importance can be artificially increased or reduced.

(iii) *Modified Sampling method*, certain events can be altered from their natural frequencies.

(iv) *Partially-deterministic calculations*, part of the random-walk simulation can be replaced by a deterministic point-kernel type of calculation.

4.5.3. Material specification

Specification of the material filling the various cells in MCNP calculations involves the following elements [Shultis and Faw 2006]: (a) defining a unique material number, (b) the element composition, and (c) the cross section composition.

4.5.4. Source specification

MCNP source specification card allows the user to specify a wide variety of source conditions without having to modify the code. Source variables of energy, time, position, direction and other parameters such as starting cell(s) or surface(s) are specified. Information about the geometrical extent of the source can also be given in the source specification card. Various analytic functions for fission and fusion energy spectra such as, Watt, Maxwellian, and Gaussian spectra; Gaussian for time and isotropic, cosine, and monodirectional for direction are available.

4.6 APPLICATION OF MONTE CARLO TECHNIQUES IN MEDICAL PHYSICS

Applications of the Monte Carlo method have been used in various fields of medical physics, namely nuclear medicine, x-ray diagnostics, radiotherapy physics and dosimetry,

radiation protection calculations and transport simulation using microscopic Monte Carlo codes.

Nuclear Medicine is the area where most of the early Monte Carlo calculations in the field were performed. The designs of positron emission tomography (PET) system using the Monte Carlo method have received considerable attention and a large number of applications have been developed [Del Guerra et al 1983, Andreo 1991]. Monte Carlo calculations have been found to be a powerful tool to quantify and correct for photon scattering, which usually produces blurring of the image and loss of contrast in nuclear medicine procedures [Dahlbom et al 1989]. Derenzo [1981] has simulated arrays of detectors of different materials and sizes, as well as other parameters of influence such as the effect of inter-crystal septa.

In Diagnostic radiology, the main goal of the application of Monte Carlo techniques is the optimization of diagnostic procedures to improve the image quality to patient dose ratio. Monte Carlo techniques have also been used in the determination of physical quantities in diagnostic radiology as well as in radiation aspects [Dance and Day 1984].

Radiotherapy is today the application with the largest impact on the considerable maturity reached by Monte Carlo techniques, and this is mainly due to the increasing need for improving the accuracy of absorbed dose determination, both in absolute (calibration of radiation sources) and relative (planning of patient treatment) calculations.

Monte Carlo can accurately model the physics of particle interactions by accounting for the geometry of individual linear accelerators, beam shaping devices such as blocks and

multileaf collimators (MLC's) and patient surface and density irregularities [Podgorsak 2003].

In Brachytherapy (use of encapsulated radioactive sources to treat cancer), Monte Carlo has mainly focused on the simulation of dose distributions around radiation sources and evaluation of dose conversion factors [Williamson 1995]. Monte Carlo calculations have been used to calculate the relationship between the air kerma (or exposure) measured in air on the transverse axis and the absorbed dose in water or tissue phantom surrounding the source, it has also been used to identify and explain the effect of ignoring the existence of fluorescent x-rays created in the material used to encapsulate Iodine-125 source [Rogers 2002].

One of the earliest and most critical applications of Monte Carlo techniques in medical physics has been in the calculation of medium-to-air stopping power ratios [Nahum 1983, Andreo 1988], which are used in various national and international dosimetry protocols on the dosimetry of megavoltage photons and electron beams. Monte Carlo technique obtain the electron fluence in the undisturbed medium at the point of the ion chamber and from this, the stopping power is then averaged over the fluence spectrum.

CHAPTER 5

MATERIALS AND METHODOLOGY

5.1 Overview

The basic radiation physics governing particle interactions, silicone dosimetry and Monte Carlo code used in this work has been well reviewed in the previous chapters. In this chapter, the methods used for Monte Carlo dose simulations and physical measurements are discussed.

5.2 MCNP Simulations

The simulations were carried on a Linux based Pentium IV operating system. The input file that contained the geometry specification, the description of the materials, location and characteristics of the electron source and the tally used was created. An example can be found in Appendix A. The source was located at 100 cm source to surface distance (SSD) and tally *F8 for energy deposition was used (Figure 5.1). For geometry specification, repeated structures were used, this make geometries with identical structures to be defined once and reproduced in as many positions as desired.

The first simulation was to obtain the electron central axis depth dose data in water and in a silicone phantom with density of 0.98g/cm^3 and 0.96/cm^3 respectively for nominal energies 6, 9, 12 and 15 MeV. The geometry is shown in Appendix B. Each water and

silicone cell was 0.2 cm thick, the input file is shown is Appendix A. The output file that contain the cell number, the energies deposited in the cells and the relative errors from the tally are shown in Appendix C. From the depth dose curves depth of maximum dose (D_{max}) and depth of 50% dose (R_{50}) were determined.

The second simulation was to obtain the electron central axis depth dose data with the silicone prosthesis immersed in water. A geometry that consists of silicone prosthesis immersed in water was then defined as shown in Appendix B. The thickness of the prosthesis used was 4 cm thick. The water and prosthesis cells were 0.2 cm thick. The input and output files, for silicone prosthesis immersed in water are shown in Appendix A and C respectively. From the depth dose curves, depth of maximum dose (D_{max}), and the percentage dose deposited immediately after the prostheses were determined. The density of the prostheses used was 0.96 and 0.98 g/cm^3.

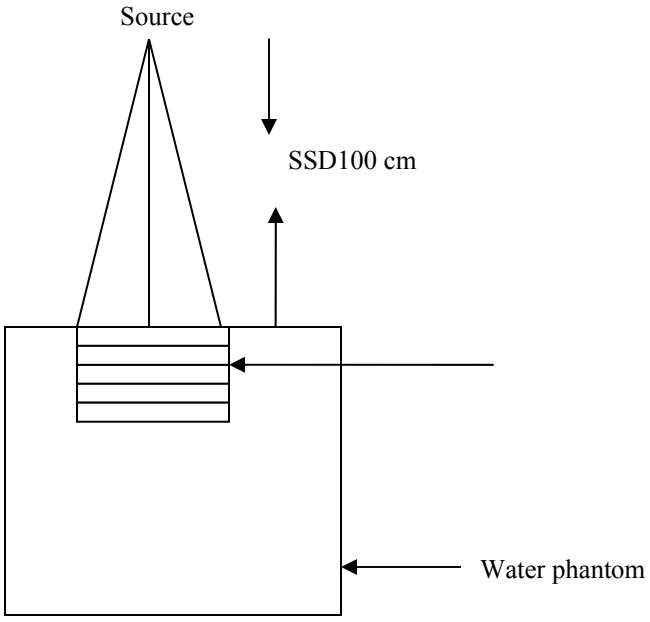

Figure 5.1: Simulation setup

The energy depositions in each cell at the respective depth, for all simulations are tabulated in Appendix D. All energy results were normalized to maximum energy which is 100% for all simulations. 100000 particles were run for each simulation. The simulations were performed for 6, 9, 12 and 15 MeV electron beams.

5.3 Physical Measurements

Measurements took place in two parts 1: to obtain the percentage depth dose measurements and 2: to obtain the dose enhancement factor.

5.3.1 Percentage depth dose (PDD) measurements

The equipment used to obtain the PDD measurements were: a Varian 2100C linear accelerator (LINAC) in electron mode, 10×10 cm^2 applicator, $50\times50\times50$ cm^3 Scanditronix Wellhofer medical scanning water phantom and its accessories, reference diode (RFA 300) and electron field diode (EFG-3G), OmniPro- Accept computer software for depth doses and profiles and silicone prosthesis of density 0.96 and 0.98 g/cm^3. The silicone prosthesis with density 0.96 and 0.98 g/cm^3 were used because of their availability. The diodes were preferred because they measure the dose directly without the need for ionization corrections [IAEA 2001, Khan et al 1991 and Haken et al 1987].

The procedure started by placing the gantry and collimator to 0^o. The water phantom was then filled with water up to 10 cm from its top, it was then positioned directly under the LINAC head and adjusted until its cross hair are aligned with the collimators cross hair.
The alignment of the water phantom with the central axis of the beam was confirmed using positioning lasers on the walls of the treatment room. The applicator was then inserted on the gantry and a 10×10 cm^2 field size was selected on the collimator setting. The water phantom was then adjusted until the water surface was at 100 cm SSD.

The electron field detector was arranged in such a way that its surface corresponds with the water surface, and this made it easier to sample the dose at various depths, whereas the reference detector was fixed at the same point in the field to monitor the beam intensity. Both detectors are water proof.

The movement of the detectors in the water phantom is controlled by the omniPro-Accept computer software. The detectors were connected to the water phantom from where a connection was made to the computer.

Using the omniPro-Accept dose measurement system, the electron field detector was instructed to move from the original position which is the surface down to 25 cm along the central axis of the beam, to obtain the depth dose measurements. All the data is recorded and stored on the system. All the obtained dose distribution results were normalized to the maximum dose which is 100%. Measurements were performed for 6, 9, 12 and 15 MeV electron beams. From the depth dose curves, surface doses (D_s), depth of maximum dose (D_{max}), depth of 50% dose (R_{50}) were determined.

Using the same set up as above silicone prosthesis, 4cm thick, with density of 0.96g/cm^3 was immersed below the water surface. Since the electron field detector cannot measure the dose in the prosthesis, it was commanded to move below the prosthesis from 4 cm to 25 cm downwards along the central axis of the beam. The obtained data was stored by the computer. The above was repeated with prosthesis of density 0.98g/cm^3 MeV. The measured PDD curves were compared to those obtained without the prosthesis immersed in water. Due to the short range of electrons, this setup could not be conducted for 6

MeV. Data obtained from the omniPro-Accept dose measurement system is shown in Appendix E. All curves are normalized at 100% at D_{max}.

5.3.2 Radiation dose enhancement factor

Radiation dose enhancement factor is defined as the ratio of the dose in the sample adjacent to the interface with substrate to that without the substrate. It was calculated using the following apparatus: 30× 40× 38 cm^3 CNMC water phantom and thermoluminiscent dosimeters (TLD).

The water phantom was filled with water until 5cm from the top and aligned in the central axis of the beam using its cross hairs, collimator cross hairs and the positioning lasers. The height of the treatment table was then adjusted so that the lateral lasers coincide with the isocenter mark on the phantom at an SSD of 100cm.The 10x10 cm^2 field was then set by inserting a 10x10 cm^2 applicator, on the LINAC head.

A TLD was placed at a depth of 4 cm below the water surface in the central axis of the beam and was irradiated with a 9 MeV beams. The same was done for 12 and 15 MeV beam, placing a different TLD for each energy.

The silicone prosthesis was then immersed in the water phantom and a TLD was positioned at the interface on the prosthesis (Figure 5.2). This was done for 9, 12 and 15 MeV beams.

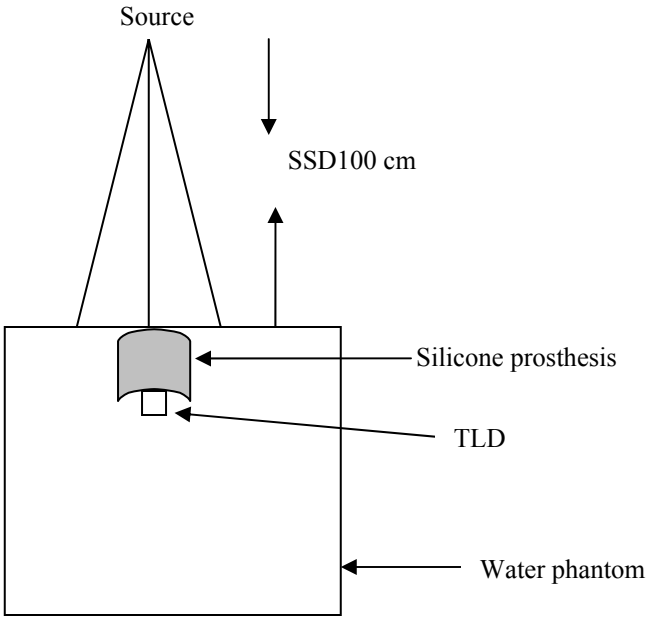

Figure 5.2: Dose enhancement physical measurement

5.4 The Gamma dose (Γ) comparison method

The simulated and measured PDD curves in particular R_{50} and D_{max} compared using the gamma dose comparison method (gamma index) [Low et al 1998, Low and Dempsey 2003]. They defined the gamma index as:

$$\Gamma(r_r, r_e) = \sqrt{\frac{(r_e - r_r)^2}{\Delta d^2} + \frac{(D_e - D_r)^2}{\Delta D^2}} \qquad 5.1$$

Where D_r and D_e are the reference and evaluated dose levels respectively and Δd^2 and ΔD^2 are the distance to agreement (DTA) and dose difference criteria. For this work, the DTA and dose criteria were selected as 2mm and 2% following recommendations by Fraass et al [1998] for the electron beams dose comparisons. The Γ comparison test passes if $\Gamma \leq 1$ [Jiang et al 2006 and Ju et al 2008].

CHAPTER 6

RESULTS

6.1 Overview

The methods used for simulations of the depth dose curves in a water and silicone phantom, silicone prosthesis immersed in water with MCNP and physical measurements were presented in chapter 5. In this chapter the results that were obtained are presented. The results are presented in terms of percentage depth dose (PDD) curves.

6.2 Monte Carlo Simulations results

6.2.1. Simulated Electron beam percentage depth doses curves for 6, 9, 12, and 15 MeV energies along the central axis in a water phantom, silicone phantom with densities 0.98 and 0.96 g/cm^3 are shown in Figures 6.1 to 6.3. The data obtained from the simulation is shown in Appendix D. All curves are normalized at 100% depth dose.

From the percentage depth dose curves depth of maximum dose (D_{max}) and depth of 50% (R_{50}) were determined and are tabulated in table 6.1 (a) and (b) below.

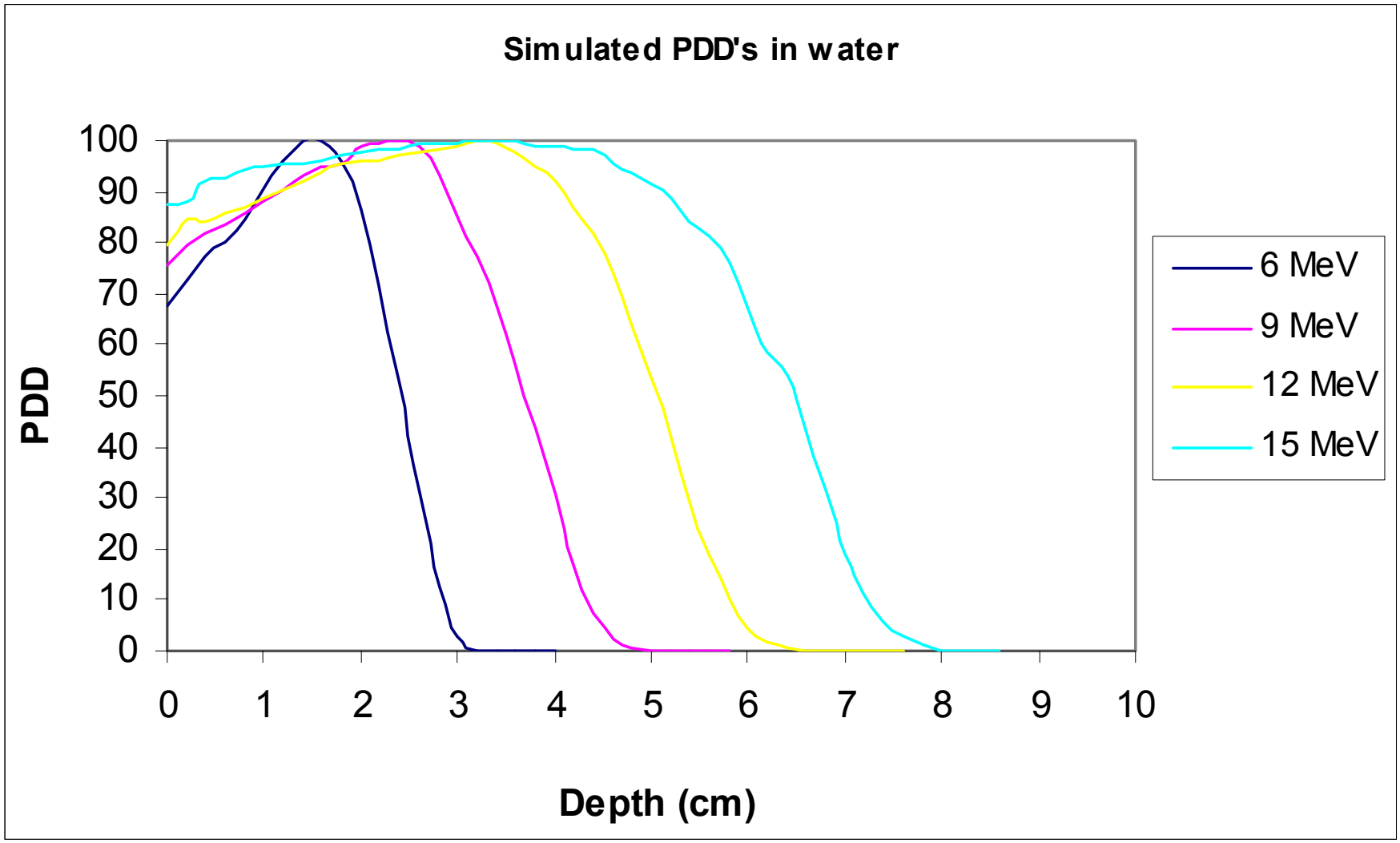

Figure 6.1: Simulated PDD curves for 6, 9, 12, and 15 MeV beams obtained in water phantom with uncertainty within ±2%.

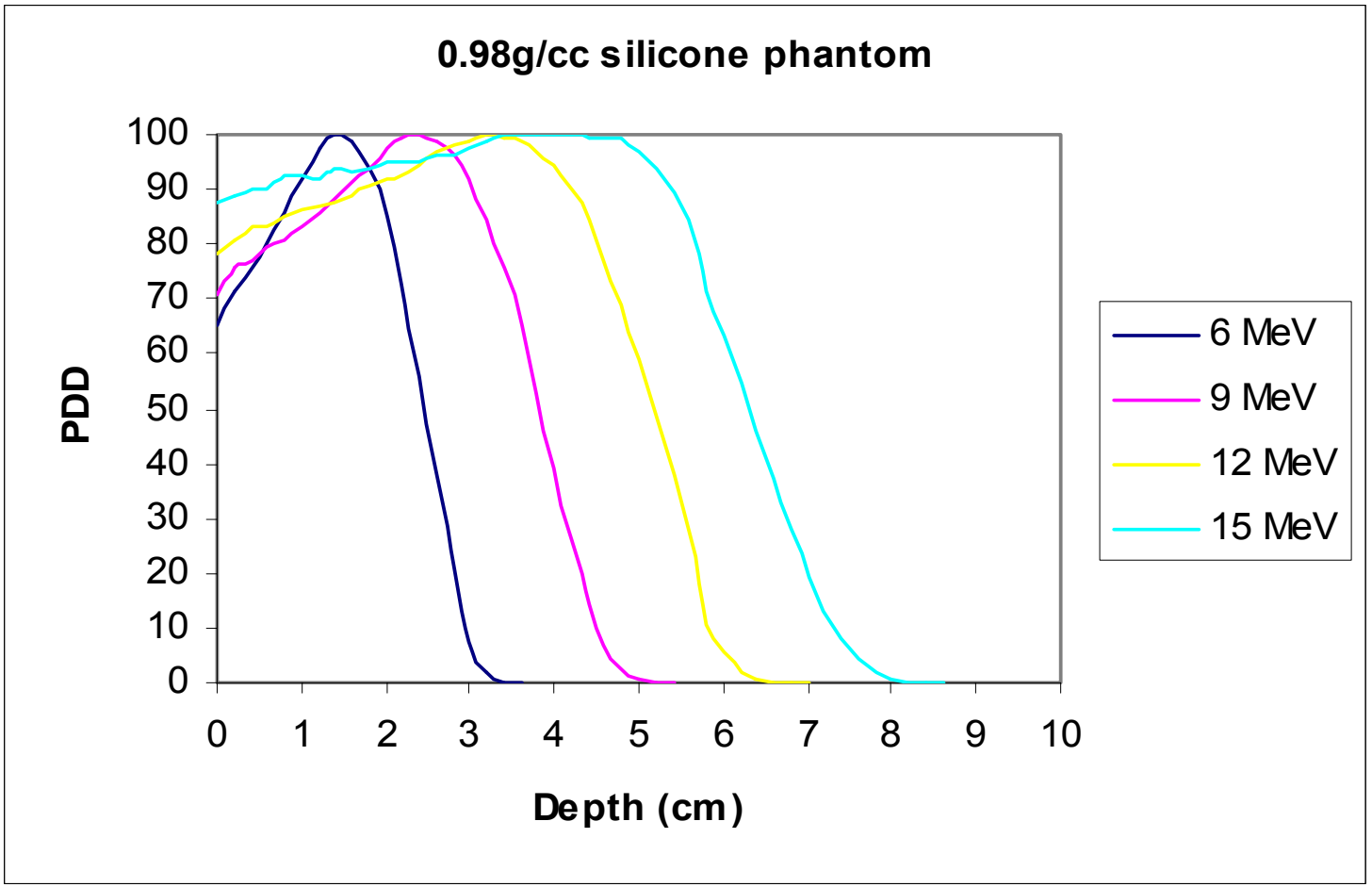

Figure 6.2: Simulated PDD curves for 6, 9, 12, and 15 MeV beams obtained in silicone phantom (0.98 g/cm^3) with uncertainty within ±2%.

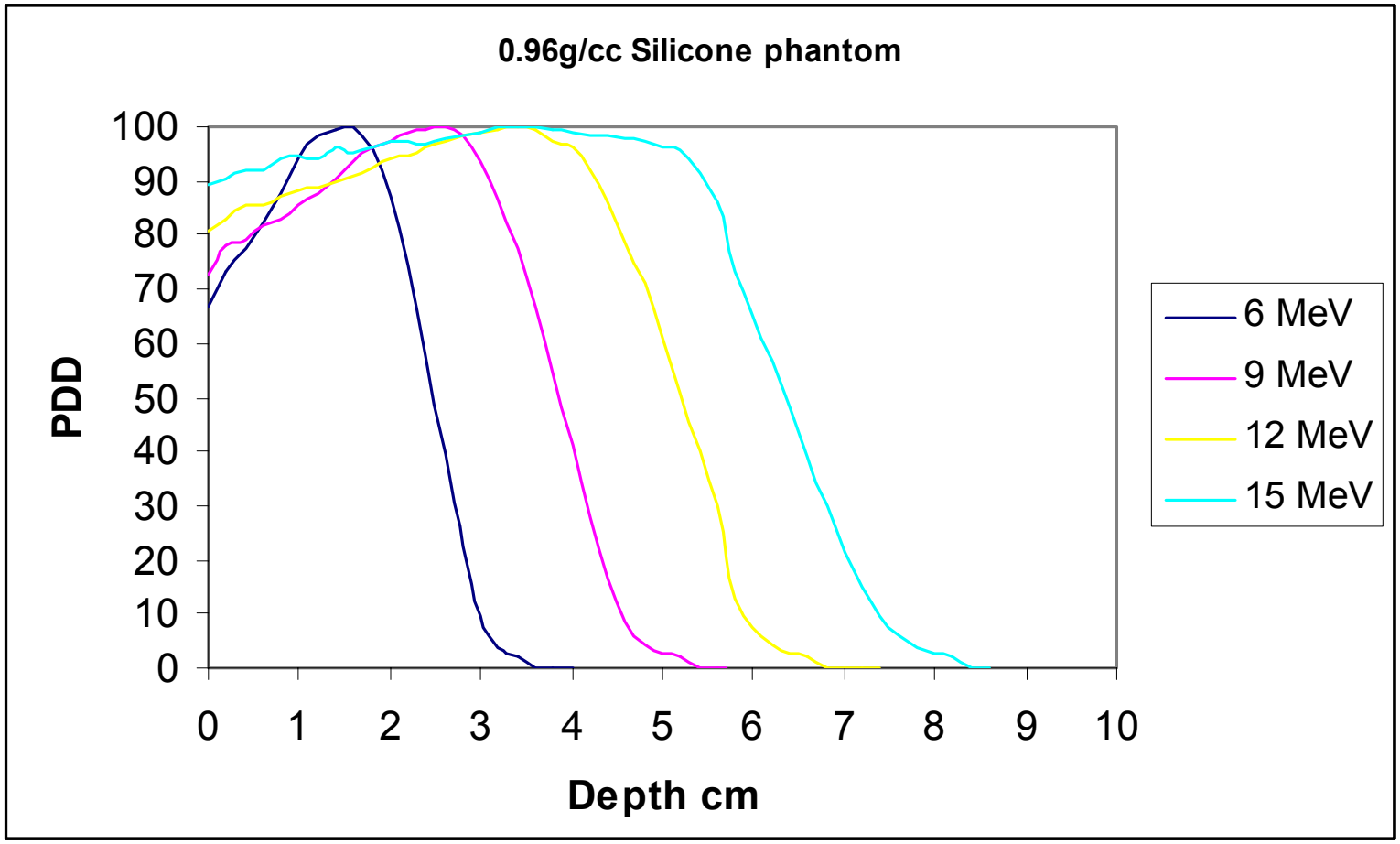

Figure 6.3: PDD curves for 6, 9, 12, and 15 MeV beams in silicone phantom (0.96g/cm^3) with uncertainty within ±2%.

Table 6.1(a) D_{max} (±0.1cm) for simulated PDD's in water and silicone phantoms.

Energy(MeV)	6	9	12	15
Water	1.4	2.4	3.2	3.6
Silicone (0.98g/cc)	1.4	2.4	3.2	3.6
Silicone (0.96g/cc)	1.6	2.6	3.4	3.6

Table 6.1(b) R_{50} (±0.1cm) for simulated PDD's in water and silicone phantoms.

Energy(MeV)	6	9	12	15
Water	2.5	3.8	5.1	6.5
Silicone (0.98g/cc)	2.5	3.8	5.2	6.5
Silicone (0.96g/cc)	2.6	3.7	5.2	6.3

Table 6.1 (a) shows that the D_{max} increases as the energy increases in both the water and silicone phantoms. Similarly, the R_{50} and increases with increase in energy as shown in Table 6.1 (b). ± 0.1cm is error obtained from the simulation.

6.2.2 Simulated PDD curves for 6, 9, 12 and 15 MeV beams with silicone prosthesis immersed in water are shown in Figure 6.4 and 6.5 respectively. The beam passed through 4cm thickness prosthesis then water.

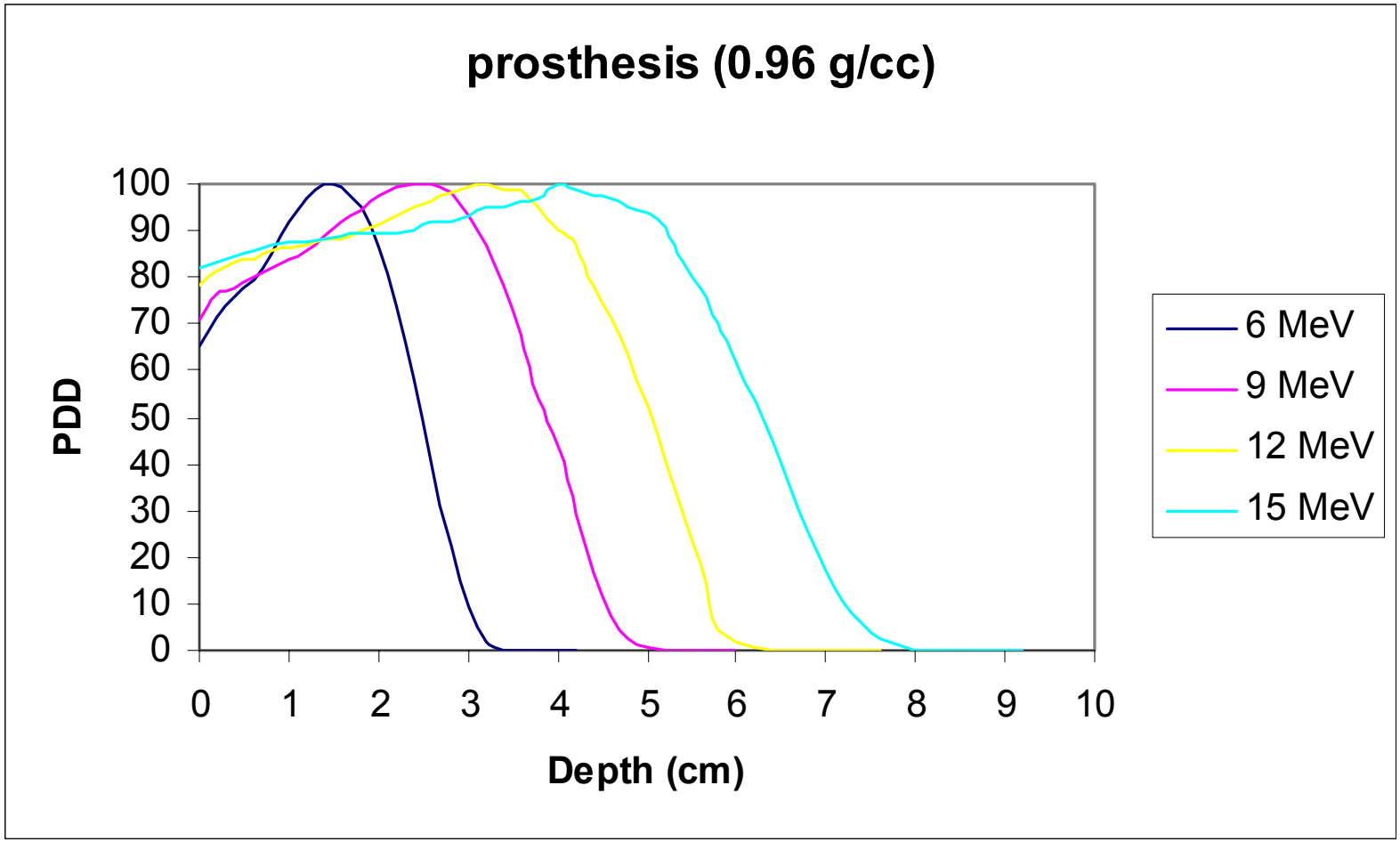

Figure 6:4 Simulated PDD curves obtained with silicone prosthesis (0.96g/cm^3) immersed in water with uncertainty within ±2%.

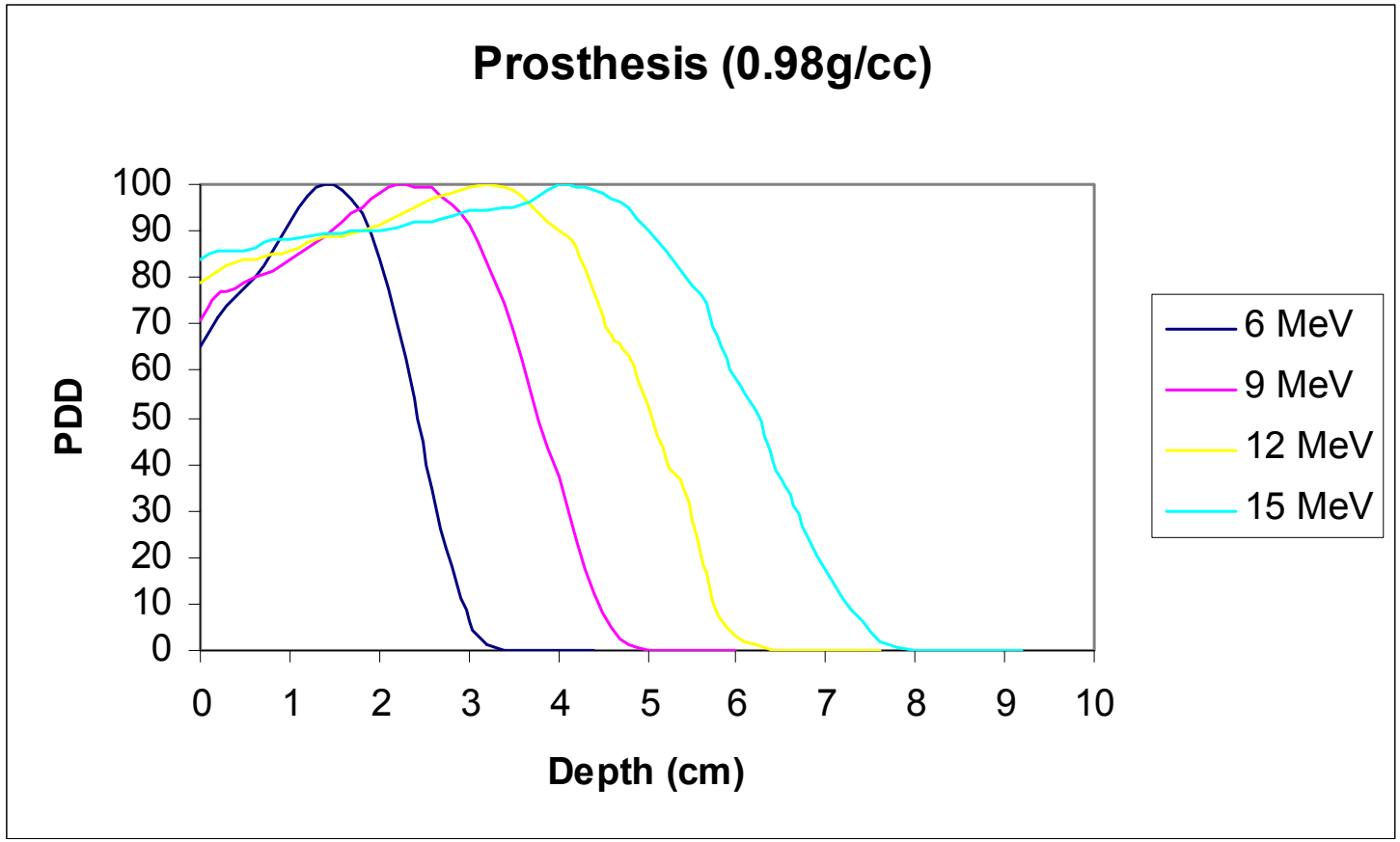

Figure 6:5 simulated PDD curves obtained with silicone prosthesis (0.98g/cm^3) immersed in water with uncertainty within ± 2%.

There is a build up in dose as the beam goes through the prosthesis until the depth of maximum dose. For 6, 9 and 12 MeV energies, a decrease in dose is observed when the beam reaches the silicone - water interface, but for 15 MeV energy beam, an increase in dose is observed. The 6 MeV energy beam is absorbed by the prosthesis. Data obtained from MCNP is in appendix D. R_{50} value is shown in Table 6.2 below and the percentage dose obtained beyond the prosthesis is shown in table 6.3 for both prosthesis and with out the prosthesis.

Table 6.2: R_{50} value for simulated PDD curves with silicone prosthesis

	R_{50} ± 0.1cm	
Energy (MeV)	0.96g/cc	0.98g/cc
6	2.3	2.5
9	3.7	3.8
12	5.0	5.1
15	6.3	6.3

Table 6.3: Percentage dose obtained beyond the prostheses (Simulated)

	Water			**0.96g/cc**			**0.98g/cc**		
Depth (cm)	9 MeV	12 MeV	15 MeV	9 MeV	12 MeV	15 MeV	9 Mev	12 MeV	15 MeV
4	30.5	92.07	98.73	24.3	89.7	100	37.38	20.81	100
4.2	17	87.07	98.533	19	86.75	98.7	23.83	86.33	99.45
4.4	7.2	82.015	98.2	9.8	78.19	97.4	12.62	76.8	98.72
4.6	2.1	73.799	95.72	5.6	71.3	97	5.7	67.8	97.19
4.8	0.3	64.19	93.92	0.7	63.3	95.4	1.3	63.1	95.19
5	0.02	53.3	91.58	0.4	52.3	93.65	0.18	52.03	89.88

6.3. Physical Measurement Results

6.3.1. Figure 6.6 shows the measured electron beam percentage depth dose (PDD) curves for 6, 9, 12 and 15 MeV nominal energies obtained from Varian 2100C linear accelerator obtained in a water phantom with an SSD of 100 cm. From the PDD curves the depth of maximum dose (D_{max}) and the depth of (R_{50}) were determined and are tabulated in Table 3 below. Results from the omni-Pro System are shown in Appendix E. All curves are normalized to the maximum depth dose 100%.

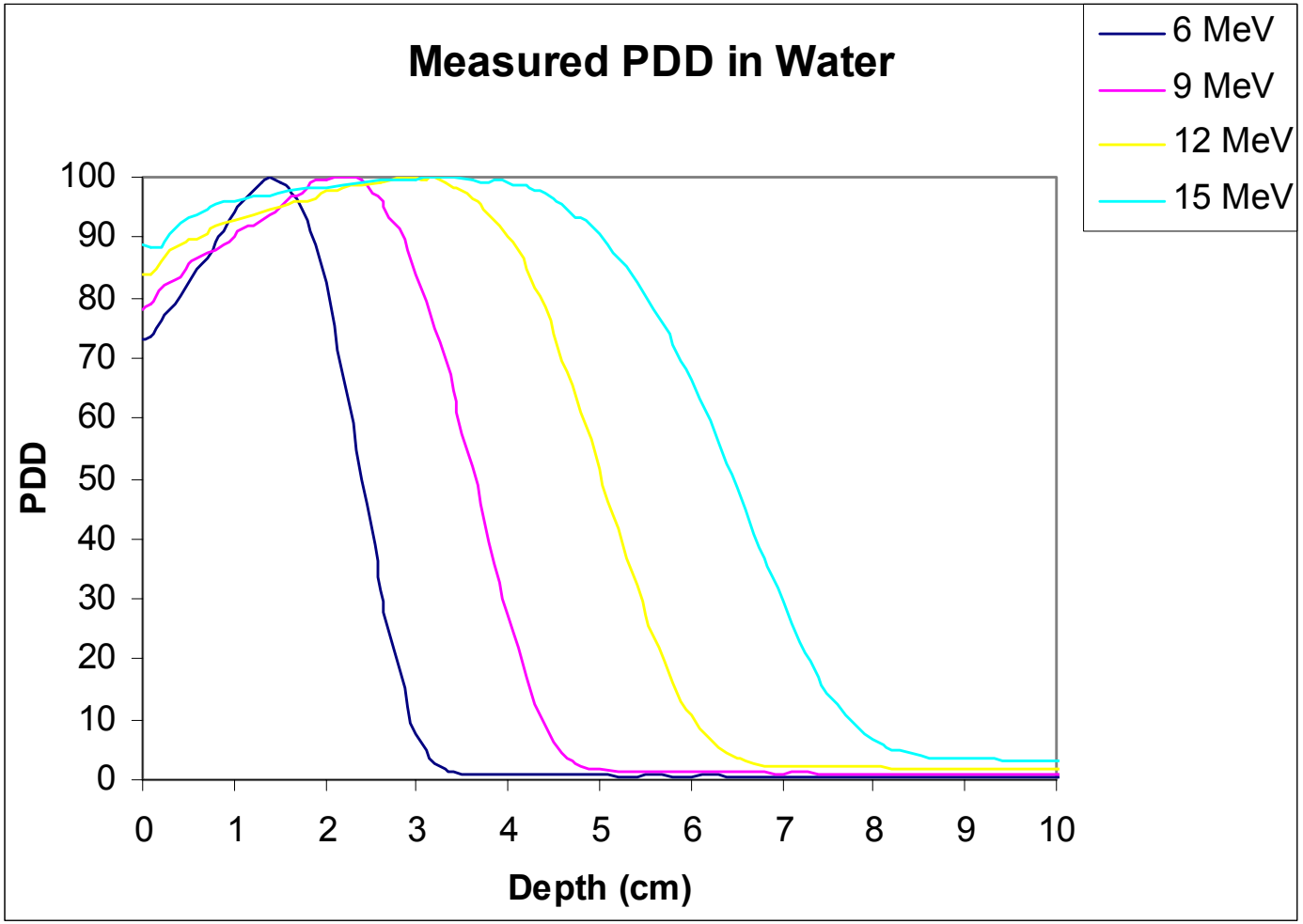

Figure 6:6 Measured PDD curves obtained in water with uncertainty within ± 0.5%

Table 6.4: Dosimetric parameters for measured electron beams in water (100 cm SSD)

Energy (MeV)	D_{max} ±0.1cm	R_{50} ±0.1cm
6	1.4	2.3
9	2.3	3.6
12	3.0	5.0
15	3.4	6.4

6.3.2. Figure 6.7 and 6.8 shows percentage depth dose curves obtained with the prosthesis immersed in water. Measurements were obtained from 4 to 25 cm below the water surface along the central axis of the beam. As mentioned in chapter 5, obtained PDD curves were only for 9, 12 and 15 MeV nominal energies.

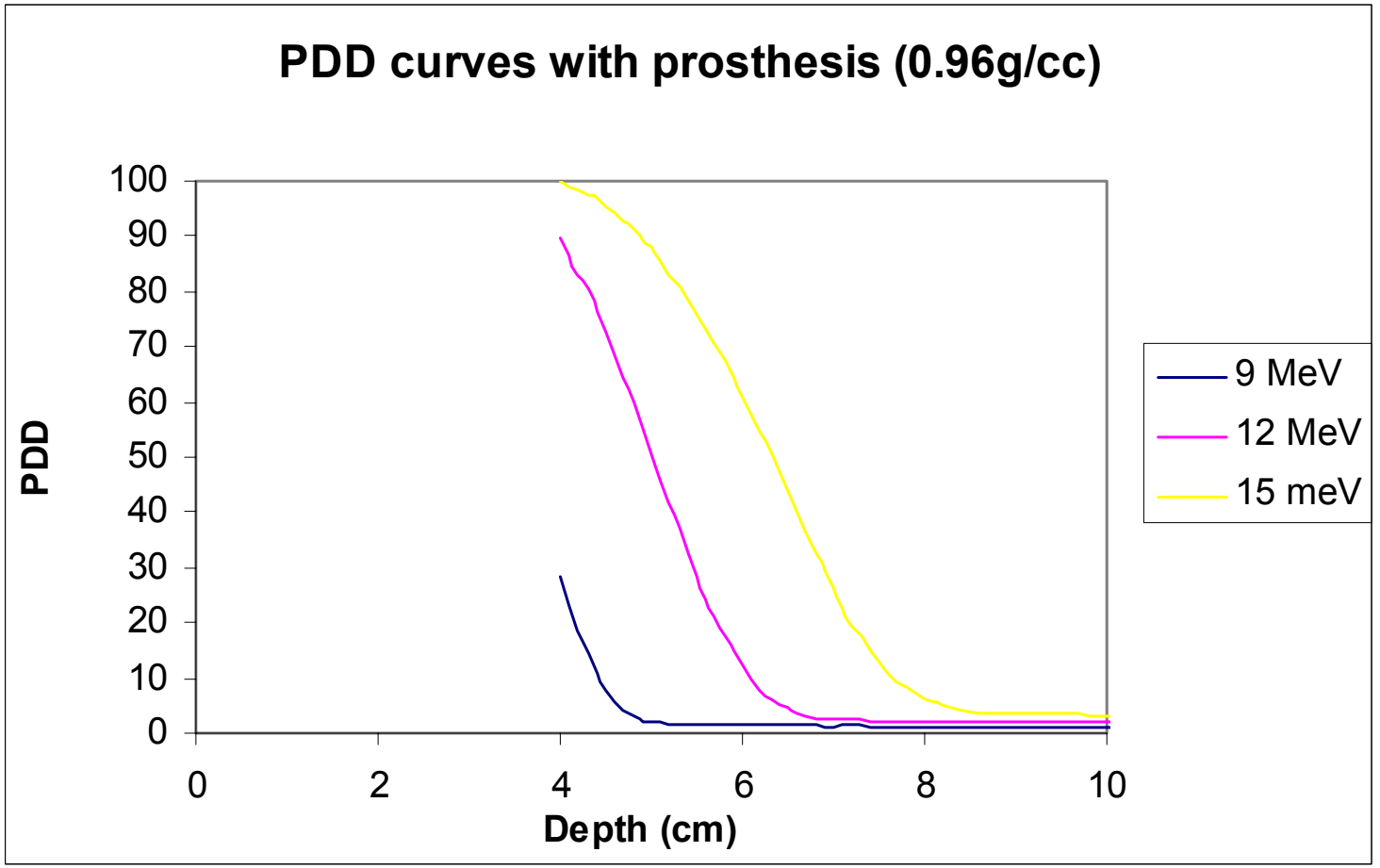

Figure 6.7: Measured PDD curves obtained with silicone prosthesis (0.96g/cm^3) immersed in water with uncertainty within ± 0.5%

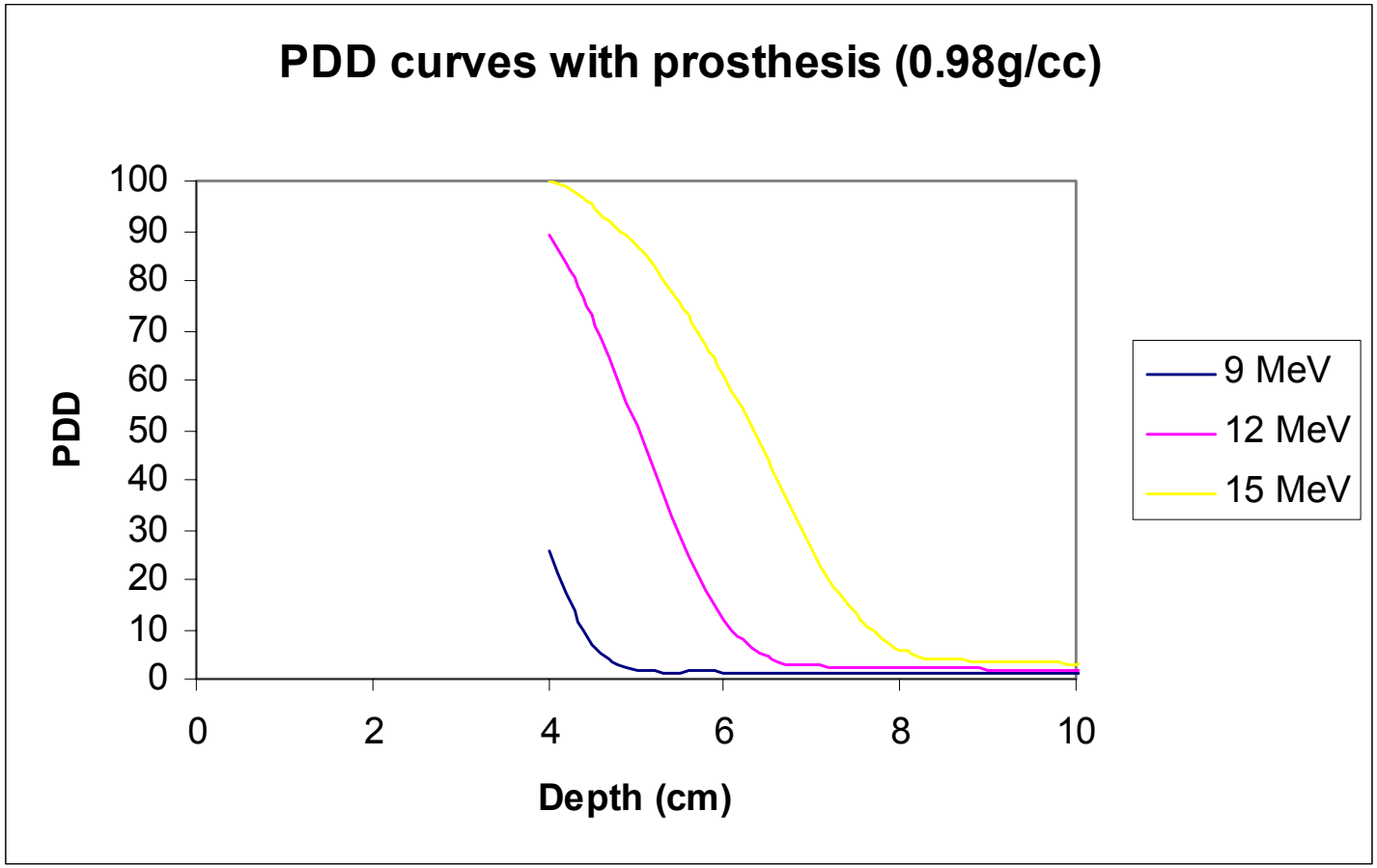

Figure 6.8: PDD curves obtained with silicone prosthesis (0.98g/cm^3) immersed in water with uncertainty within ± 0.5%.

The depth from 0 to 4 cm in figure 6.7 and 6.8 is the depth occupied by the prosthesis in the water phantom. The R50 Value for 9, 12 and 15 MeV beams obtained from Figure 6.7 and 6.8 is given in table 6.5 below. The Percentage dose obtained beyond the prostheses is shown in table 6.6. It is noted that for 9 MeV almost 80% of the beam is absorbed by the prosthesis.

Table 6.5: Dosimetric parameters obtained with the prosthesis immersed in water.

Energy (MeV)	R_{50} ± 0.1cm	
	0.96g/cc	0.98g/cc
9	NA	NA
12	4.9	4.7
15	6.3	6.3

NA in table 6.5 means that the R_{50} is within the prosthesis.

Table 6.6: Percentage dose beyond the prosthesis (Measured)

	Water			0.96g/cc			0.98g/cc		
Depth	9 MeV	12 MeV	15 MeV	9 MeV	12 MeV	15 MeV	9 MeV	12 MeV	15 MeV
4	27.2	90	99.1	28.1	89.5	100	26	89.4	100
4.2	16.9	84.7	98.6	18.7	83.2	98.6	17.4	83.7	98.6
4.4	9	78.4	97.2	10.9	76.3	96.7	9.7	76.5	96.56
4.6	4.3	69.7	95.4	5.7	68.7	94	5.2	68.6	93.23
4.8	2.2	61	93.22	3	59.6	91	2.7	60.2	90.39
5	1.6	51.6	90.5	1.9	50.2	87.8	1.8	51	87.058

6.4. Table 6.7 give the dose in Gray, obtained using thermoluminiscent dosimeters (TLD) placed at a distance of 4cm below the water surface in a water phantom with the prosthesis and without the prosthesis.

Table 6.7: TLD dose (Gy) readings

Energy (MeV)	Water	0.96g/cm^3 prosthesis	0.98 g/cm^3 prosthesis
9	0.13	0.102	0.08
12	0.30	0.28	0.11
15	0.81	0.83	0.82

The table shows that there is a decrease in dose when the beam goes through the prosthesis for 9 and 12 MeV, while for 15 MeV there is a slight increase in dose between the prosthesis and the water interface.

CHAPTER 7

DISCUSSION

7.1 Overview

In chapter 6, the results obtained using Monte Carlo simulation and the actual physical measurements were presented in terms of percentage depth doses and dosimetric parameters. The dose enhancement factor was also calculated. In this chapter, the simulated results will be compared against the measured results.

7.2 Benchmarking the MCNP code

7.2.1 The simulated and measured percentage depth dose measurements were compared as shown in Figure 7.1. Both graphs shows a build up of dose from the surface until the depth of maximum dose, followed by a steep fall off as explained in Khan [2003]. The major difference of more than 5% occurred below R_{50} towards the practical range and this is because of the simulation geometry which assumed a monoenergetic beam striking the surface. While in the measurement the beam striking the surface is comprised of the scatter radiation from the ion chamber, scatter foil, collimators and the applicators and this results in the bremstrahlung tail which is seen on the measured data but not on the simulated data.

Dosimetric parameters for measured and simulated results are compared in Figure 7.2 and 7.3 below. The simulated and measured PDD curves were compared using the gamma dose distribution comparison method explained in section 5.4.

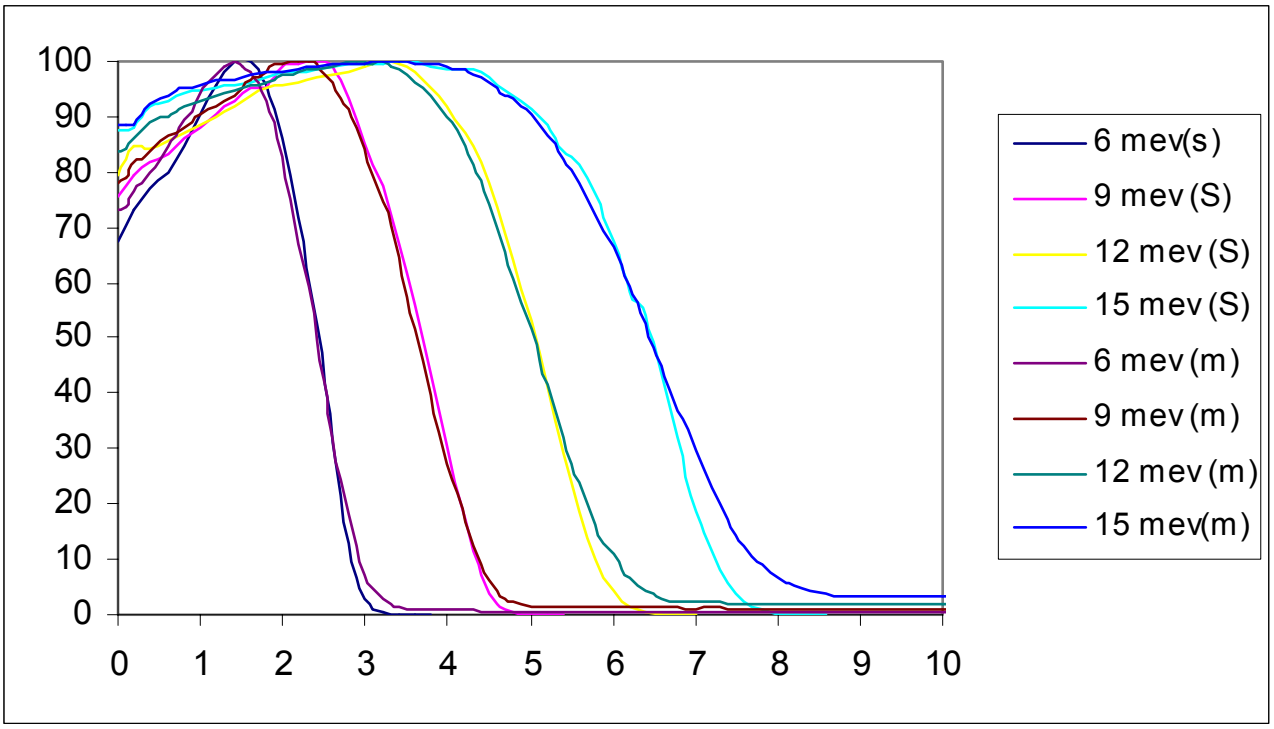

Figure 7.1: Comparison between the Measured (M) and the Simulated (S) PDD curves with uncertainty within ±2%.

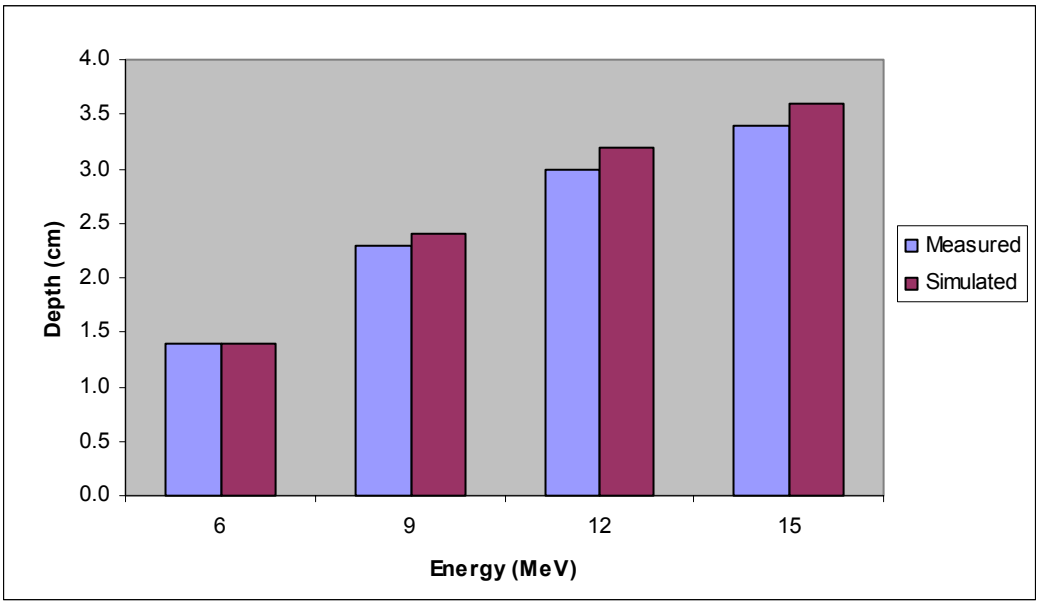

Figure 7.2: Comparing the D_{max} for the measured and simulated PDD curves in water.

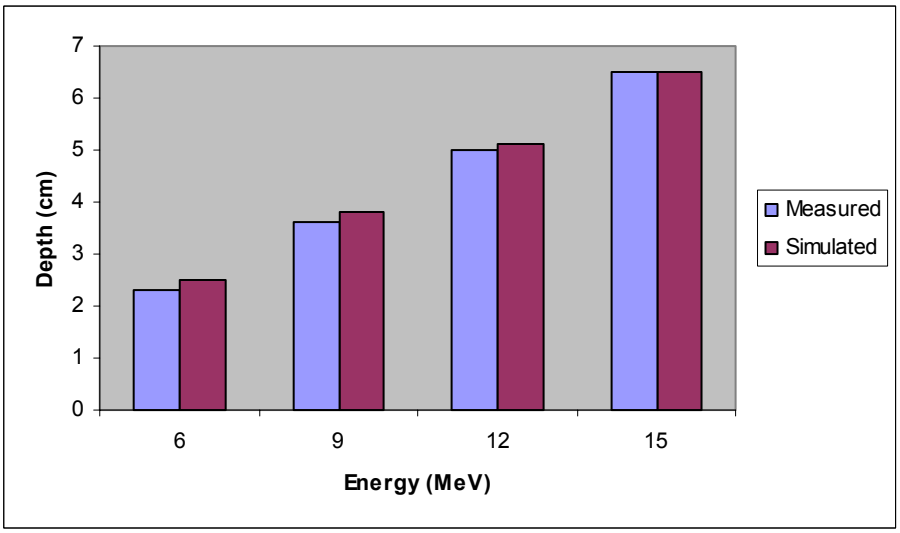

Figure 7.3 Comparing R_{50} values of measured and simulated PDD curves in water

Figures 7.2 and 7.3 shows that there is good agreement between the measured and simulated D_{max} and R_{50} . Although the simulated D_{max} and R_{50} value for 6, 9 and 12 MeV is higher than that of the measured, the calculated gamma index is less than 1. Thus, the

D_{max} and R_{50} values for the measured and simulated PDD curves are within 2mm as recommend by Fraass et al [1998].

Differences in percentage dose that occurred in the simulated and measured PDD's are shown in Figure 7.4. The difference is shown in terms of the gamma index.

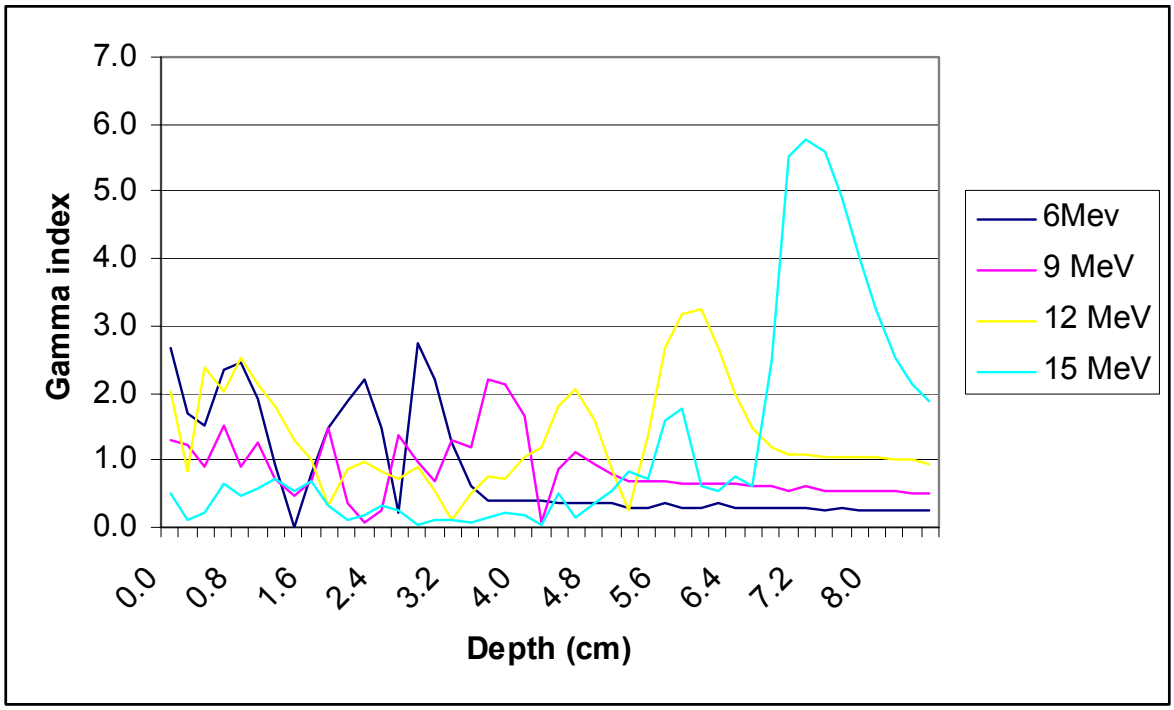

Figure 7.4: Gamma index between the measured and simulated PDD curves in water

There is a good relationship between the measured and simulated PDD for the 15 MeV because at most depths the gamma index is less then 1, axcept towards the bremstrahlung tail, where the gamma index is above 5. This big variation is due to the absence of the bremsstrahlung tail in the simulated PDDs. There is a variation greater then 1 for the 6, 9 and 12 MeV beam in the build up region, which is mostly attributed to the difference in the measured and simulation voxel and the statistical noise on the PDD's. Krishnan et al [1983], found a difference of about 33% towards the electron practical range and ststed that it is of no clinical significant.

7.2.2 The measured percentage depth dose curves with silicone immersed in water were compared with the percentage depth dose curve without the prosthesis is shown in Figure 7.5 below.

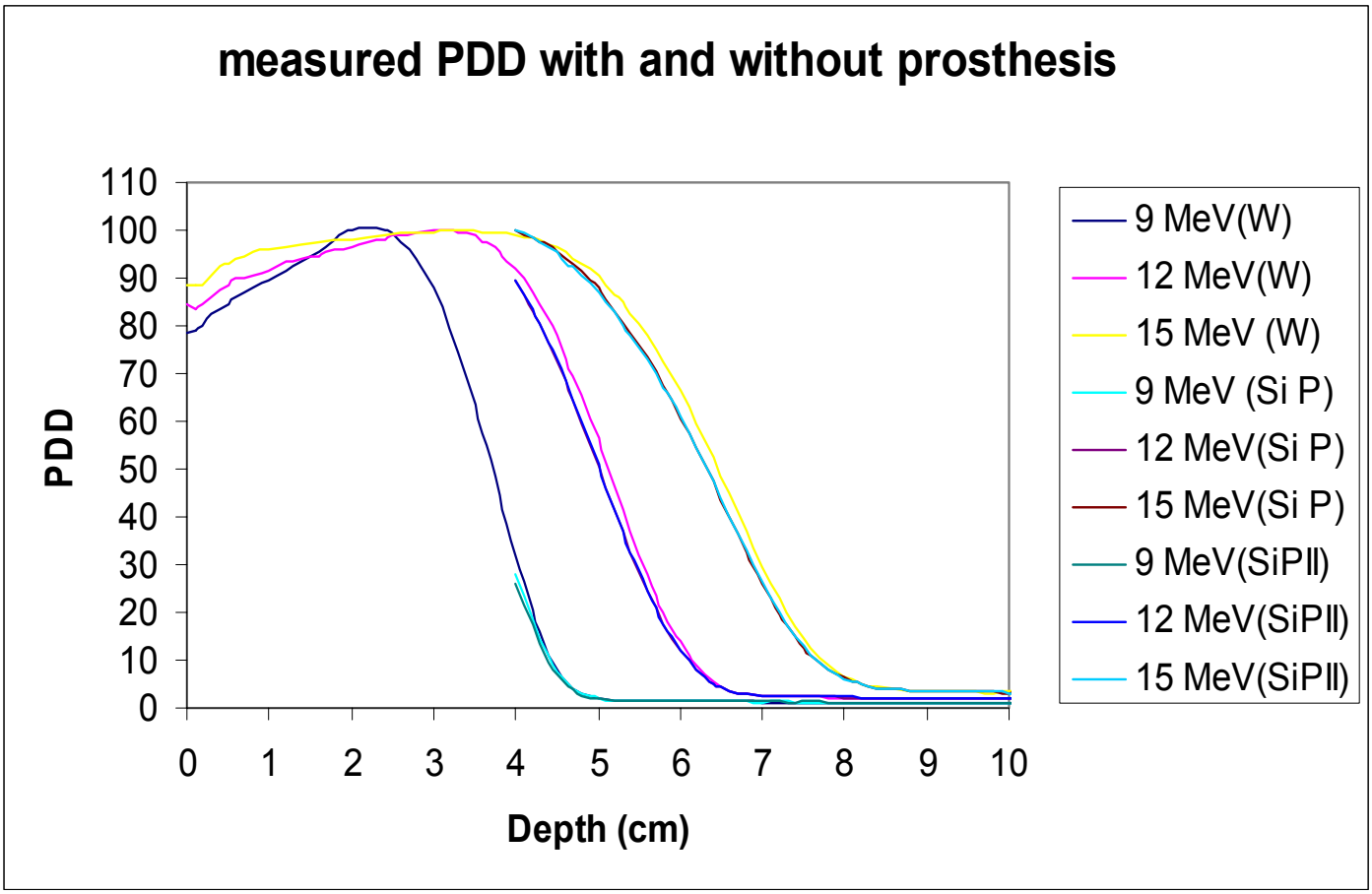

Figure 7.5: Comparison of measured PDD in water with and without the prosthesis of 0.96 g/cm^3 (SiP) and 0.98 g/cm^3 (SiPII) in water with uncertainty within ±2%.

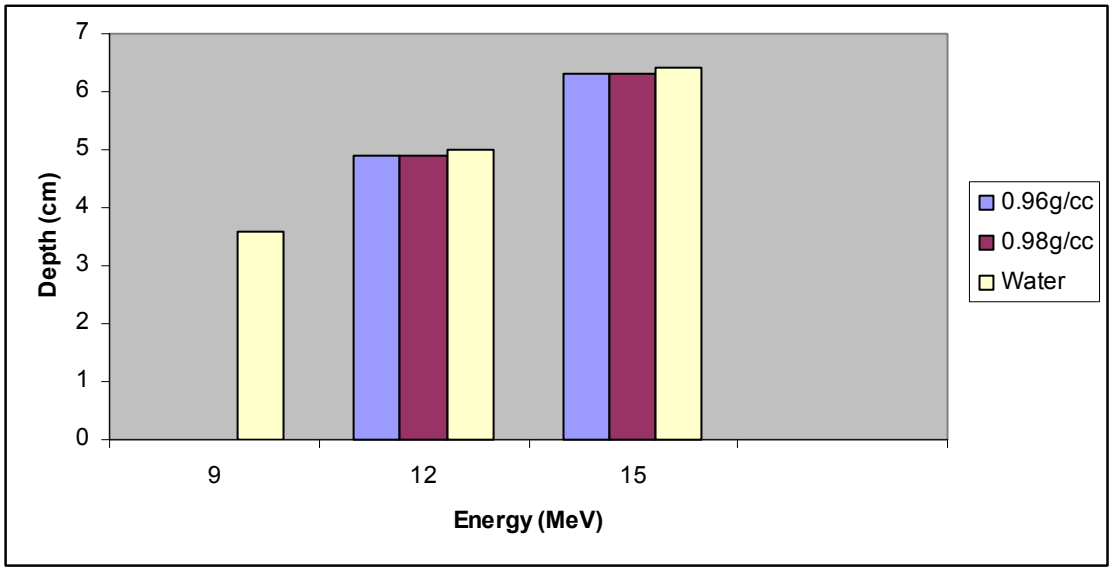

Figure 7.6: Comparing R_{50} for measured PDD with and without the prosthesis.

Figure 7.5 indicates a good agreement between the measured depth dose curves with and without the prosthesis in water because the gamma index for R_{50} was found to be less than 1. This is very much as expected according to Piontek and Kase [1980], the transmission of electrons of energies of 2 -20 MeV in silicone prosthesis is similar to that of water thus the presence of the prosthesis should not perturb the electron beam dose distribution. Figure 7.5 shows that there is a slight increase in percentage depth dose below the prosthesis for the 15 MeV beam compared to water and this was also observed from the simulation and this is due to the backscatter perturbation that exists between at the interface of two materials with different densities as was discussed by Das and Khan [1989]. Due to the short range of electrons about 80% of the 9 MeV beam is absorbed by the prosthesis, but the percentage dose difference for the 12 MeV in water and below the prosthesis is within the 2%.

7.2.4 The measured percentage depth doses with silicone immersed in water were compared with the simulated percentage depth dose as shown in Figure 7.7 and 7.8 below.

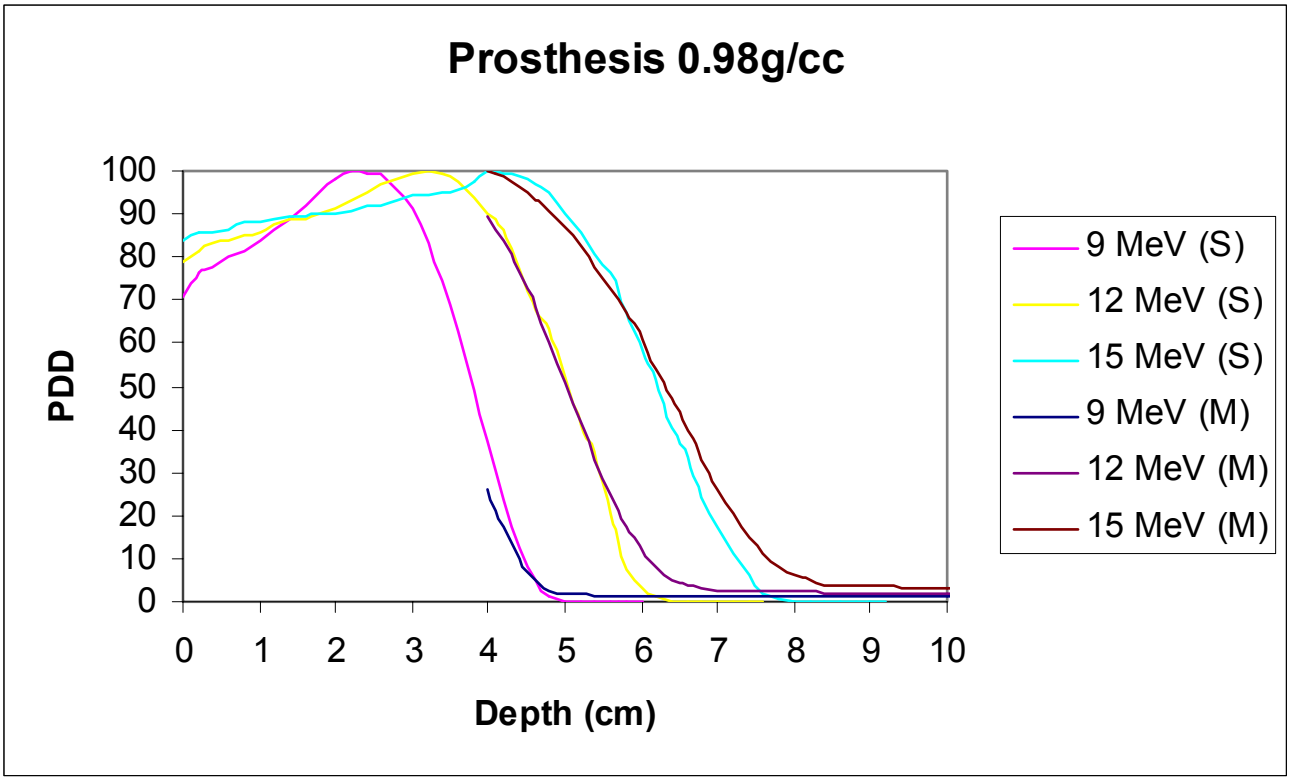

Figure 7.7 Comparison of simulated and measured PDD curves with prosthesis of 0.98 g/cm^3.

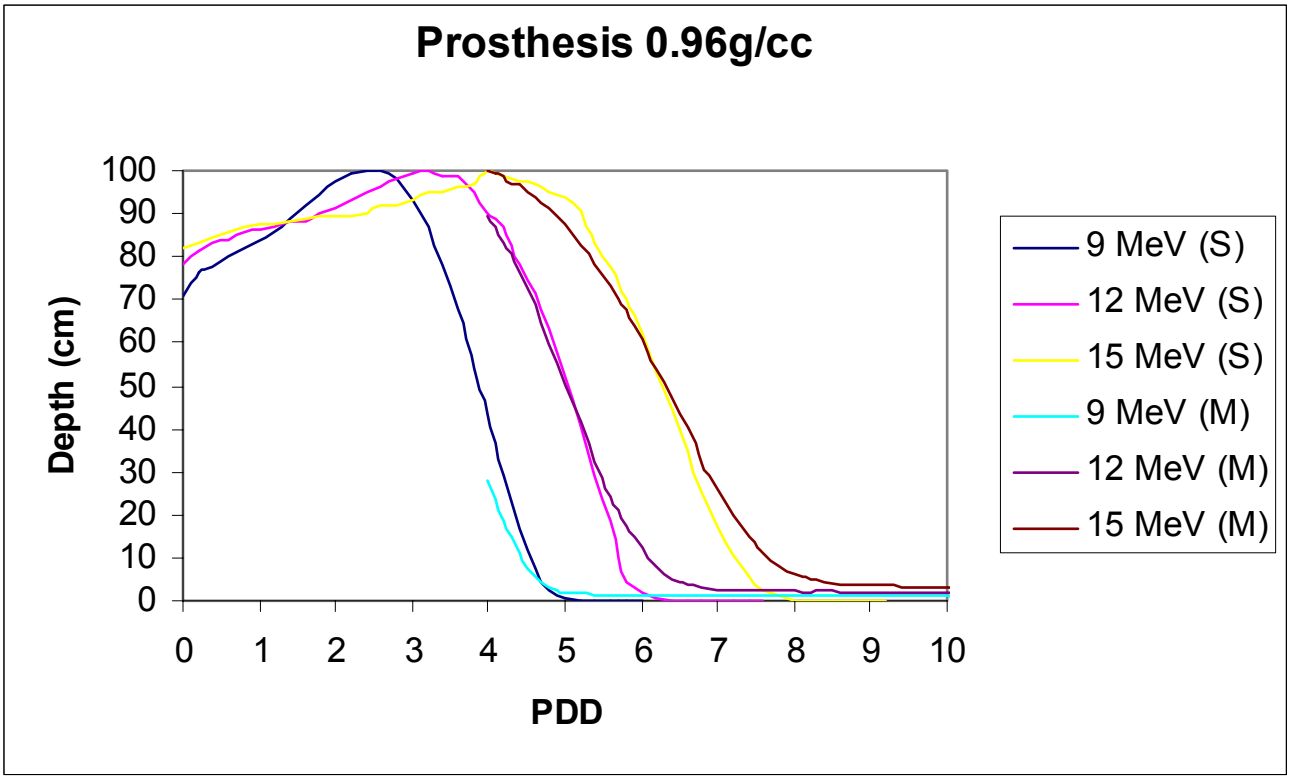

Figure 7.8 Comparison of simulated and measured PDD curves with prosthesis of 0.96 g/cm^3 with uncertainty of ±2%.

Figures 7.7 and 7.8 are showing the same situation that was observed in Figure 7.5, where there is a fluctuation of the dose observed in the interface between water and the prosthesis and an increase in percentage dose for 15 MeV. Below the depth of 50%, the measured and simulated PDD was found to be greater than 5% from the simulated PDD curve for all prosthesis, but this depth is not clinically significant as it happens near the electron practical range. These differences also in the dose fall off region are mostly attributed to the fact that a monoenergetic beam was used for the simulation. The R_{50} for the simulated and measured PDD curves in Table 7.1 below.

Table 7.1: Comparing R_{50} for measured and simulated PDD with and without the prosthesis

Energy (MeV)	Simulated R_{50} ±0.1cm		Measured R_{50} ±0.1cm	
	0.96g/cm^3	0.98g/cm^3	0.96g/cm^3	0.98g/cm^3
9	3.6	3.5	#	#
12	5	5	4.97	4.97
15	6.3	6.2	6.3	6.3

Good agreement exists between the measured and simulated R_{50} value in the presence of the prosthesis, as the gamma index was found to be less than 1. Just below the prosthesis the simulated PDD curve for the 15 MeV is slightly higher then the measured PDD. This is mostly attributed to bremsstralung radiation from secondary electrons and the re-build at the interface between the prosthesis and water.

7.3 The dose enhancement factor

Table 7.2 below shows the calculated dose enhancement factor for 9, 12 and 15 MeV energies using thermoluminscent dosimeters.

Table 7.2: The dose enhancement factor

Energy (MeV)	0.96g/cm^3	0.98g/cm^3
9	0.78	0.62
12	0.93	0.36
15	1.02	1.01

Table 7.2 shows that the dose enhancement factor for the prosthesis of 0.96g/cm^3 is high then that of the prosthesis with 0.98g/cm^3. For the 15 MeV beam table 7.5 shows that the prosthesis has enhanced the dose at the interface. Hsiao et al [2001] and Podgorsak [2003] observed that the dose enhancement factor at the interface depends on the beam energy, width of the inhomogeneity and the atomic number of the substrate.

Figure 7.9 to 7.12 below shows the dose enhancement factor calculated from the measured and simulated PDD curves from the interface (4 cm) to 5 cm depth. For the measured data the 12 MeV beam maintained a dose enhancement of less than 1. The DEF for 15 MeV was slightly higher than 1 with greatest being 1.01. The 9 MeV enhanced the dose from the depth of 4.4 cm and this is nearling to the practical range, which is of no clinical significant.

The simulated data also shows the same as the measured data, where the 9 meV enhanced the dose. The 12 MeV maintained a dose enhancement of less then 1 while the DEF for 15 MeV was slightly higher than 1 with greatest being 1.01.

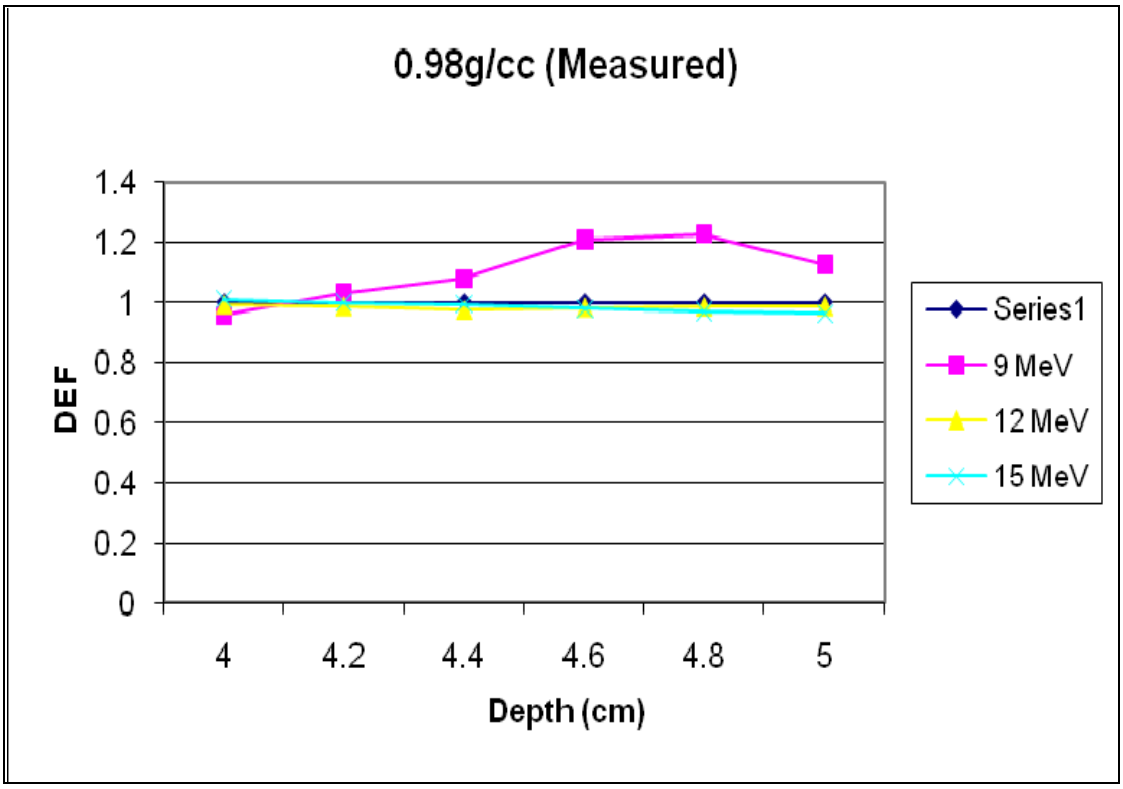

Figure 7.9: Calculated DEF for 0.98g/cc prosthesis (measured)

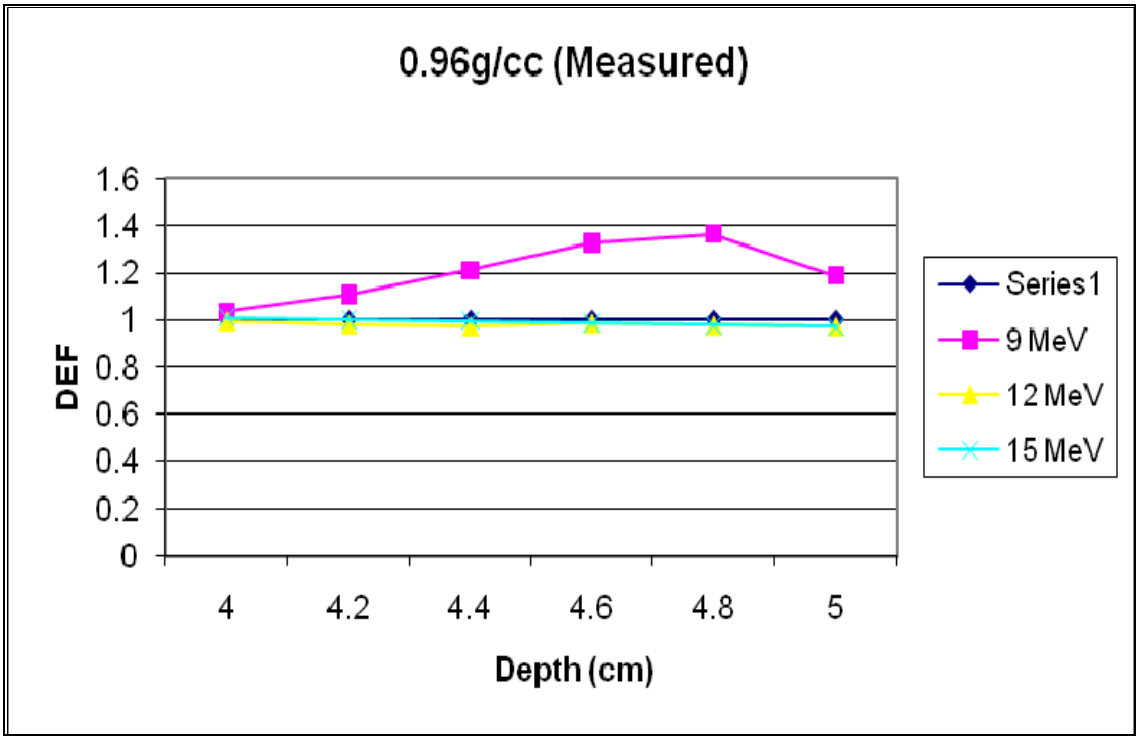

Figure 7.10: Calculated DEF for 0.96g/cc prosthesis (measured)

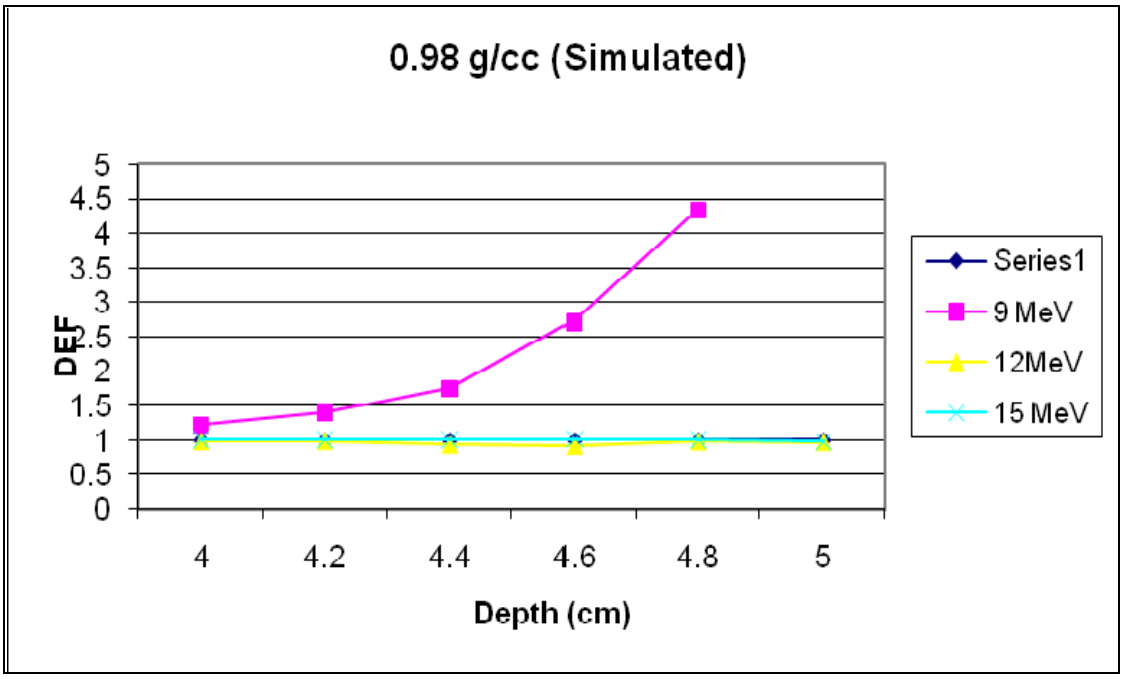

Figure 7.11: Calculated DEF for 0.98g/cc prosthesis (simulated)

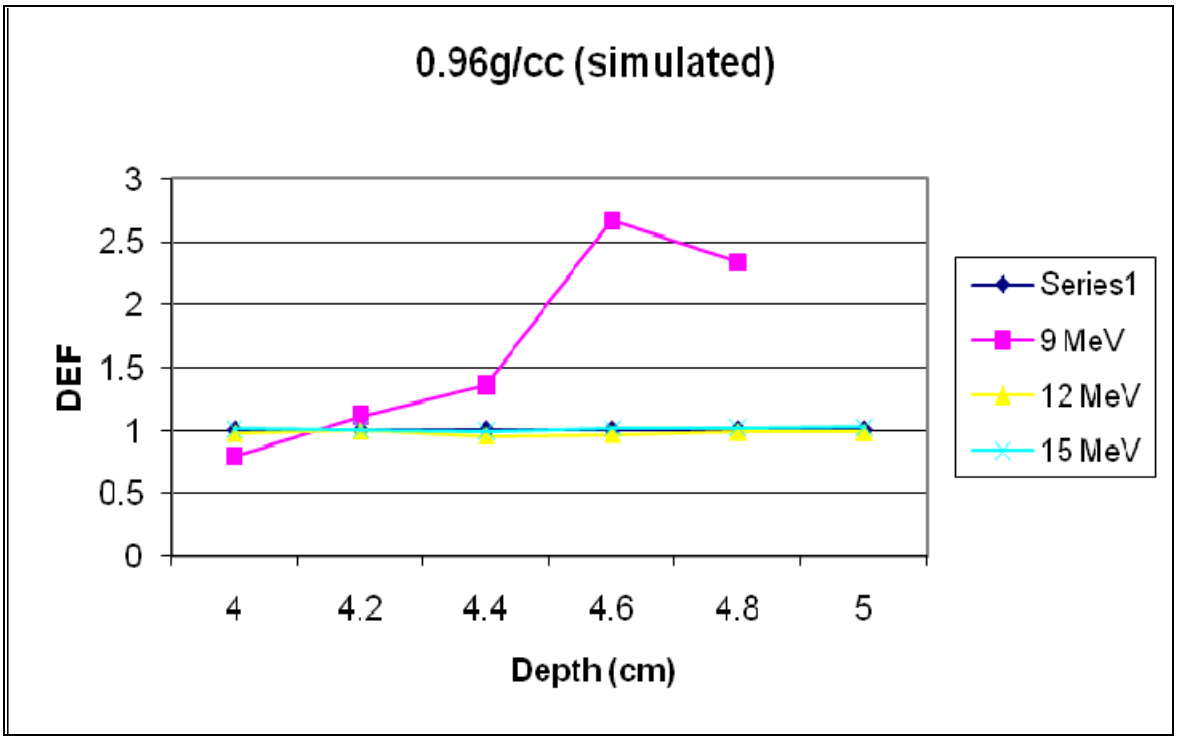

Figure 7.12: Calculated DEF for 0.96g/cc prosthesis (simulated)

7.4 Simulation and Measured errors

Each MCNP output file gives the relative errors that occurred during the simulation. Simulation time ranged from 1 hour to 5 hours depending on the energy. The statistical uncertainty of the simulation was between 0.2% - 1%. However, when comparing simulation and measured PDD curves the uncertainty towards the electron practical range and the bremsstrahlung tail was above 10%. The measured PDD with and with out the prosthesis uncertainty was 1%, but when comparing the two set of data the error was below 5% nearing the electron practical range. Krishnan et al [1983], observed a difference of about 33% near the practical range when compared the measured PDD with and without the prosthesis.

CHAPTER 8

CONCLUSION AND RECOMMENDATIONS

8.1 Overview

The main purpose of this study was to determine the effect of silicone gel breast prosthesis/implants on the electron beam dose distribution, by simulating the central electron beam depth dose distribution in water and in the prosthesis and simulating the dose distribution with silicone immersed in water, using the general purpose Monte Carlo code MCNP5.

8.2 MCNP5 transport code

This study has shown that MCNP5 can be used to simulate accurately the electron beam depth dose curves up to 2%. The code has also shown that low energy beams are absorbed by the prosthesis because of the electrons energy range.

The presence of the prosthesis does not perturb the dose distribution further in tissue, but when treating recurrence of breast cancer in the presence of prosthesis, this study recommends that 12 MeV beams be used, because the therapeutic range (R_{90}) is still attained and the dose is not enhanced. While at low energies, the therapeutic range is within the prosthesis due to the electron short range and at high energies the dose is slightly enhanced.

8.3 The future

This work used 6, 9, 12 and 15 MeV electron beams, silicone prosthesis of 4cm thickness and a monoenergetic electron beams along the central axis. Further focus could be on using higher electron beams and different sizes of the prosthesis and different angles. This work could also be benchmarked with the other Monte codes used in radiotherapy, in particular the Electron gamma shower code (EGS), where modeling of the Linear accelerator is possible and this could validate the results of this study.

Rogers [2002] maintained that as computing power continues to increase it is likely that research emphasis will change from studying dose deposition and other physical processes using Monte Carlo simulations of the passage of radiation through matter to studying biological process induced by the same radiation.

GLOSSARY

Breast Augmentation: Is a surgical procedure that increases the size of the breast by insertion of an implant.

Breast implant/ Prosthesis: Is a sac made of a rubber like silicone shell that is filled with saline or silicone gel.

Breast reconstruction: Surgery to restore the normal appearance of the breast following mastectomy or injury.

Calcification: Process in which tissue becomes hardened as a result of calcium deposits, usually detected by mammography.

Capsule: The name for the pocket the surgeon creates within the breast to insert an implant.

Capsular contracture: A complication following breast augumentation in which the scar tissue that normally forms in the capsule around the implants begins to contract and squeeze the implants.

Mastectomy: Complete surgical removal of the breast.

Silicone gel: A gelatinous substance made of silicone that is sometimes used to fill the breast implants.

Thermoluminiscent dosimeters (TLD): Are based on the inorganic materials which store a fraction of the energy deposited by the external source. The stored energy may be released by heating the TLD with thermal source or source.

REFERENCES

Abdullah AK, Nabil M and Akhtar AN (2005). The use of MCNP code for radiation transport and dosimetry calculations in training medical physics student. *Int J Sci Res* 15, X-Y.

Andreo P (1998). Monte Carlo applications in radiotherapy. *Radiation Physics and Chemistry* 53, 345-352.

Andreo P (1991). Monte Carlo techniques in medical radiation physics. *Phys Med Biol* 36, 861-920.

Andreo P (1988). Stopping power ratios for dosimetry, in *Monte Carlo Transport of Electrons and Photons*, edited by TM Jenkins, WR Nelson and A Rindi. New york: Plenum Publishing Corporation.

Andreo P and Brahme A (1984). Restricted energy loss straggling and multiple scattering of electrons in mixed Monte Carlo procedures. *Radiat Res* 100, 16-29.

Ariyan S, Marfuggi RA, Harder G and Goodie MM (1980). An experimental model to determine the effect of adjuvant therapy on the incidence of postoperative wound infection: 1, evaluating preoperative radiation therapy. *Plast reconstr Surg* 65, 328-337.

Arthur AB II, Richard AG and Robert AE (1991). Radiolucent prosthetic gel. *Plast Reconstr Surg* 87, 885-892.

Barker DE, Retsky MI, Schultz SL (1981). The new low bleed mammary prosthesis: An experimental study in mice. *Aesth Plast Surg* 5, 85.

Beekman WH, Feitz R, van Diest PJ (1997). Migration of silicone through the fibrous capsule around silicone mammary prosthesis following intracapsular failure. *Ann Plast Surg* 38, 441-445.

Berger MJ (1963). Monte Carlo calculations of the penetration and diffusion of fast particles. *Methods in Computational Physics* 1, 135-215.

Berger MJ and Seltzer SM (1968). ETRAN Monte Carlo Code system for electron and photon transport through extended media, Radiation shielding information center, computer code collection publication ccc-107.

Brook MA (2006). Platinum in silicone implants. *Biomaterials* 27, 3274-3286.

Buchholz TA, Strom EA, Perkins GH and McNeese MD (2002). Controversies regarding the use of radiation after mastectomy in breast cancer. *Oncologist* 7, 539-46.

Caffee HH (1986). The influence of silicone bleed on capsular contracture. *Ann Plastic Surgery* 17, 284.

Cheng C-W, Mitra R, LI XA and Das IJ (2005). Dose perturbations due to contrast medium and air in MammoSite treatment:An experimental and Monte Carlo study. *Med Phys* 37, 2279-2287.

Chow JCL (2007). Calculation of lateral buildup ratio using Monte Carlo simulation for electron radiotherapy. *Med Phys* 34, 175-182.

Dahlbom M, Eriksson L, Rosenqvist G and Bohm C (1989). A study of the possibility of using multi-slice PET systems for 3D imaging. *IEEE Trans Nucl Science 36*, 1066-1071.

Dance DR and Day GJ (1984). The computation of scatter in mammography by Monte Carlo methods. *Phys Med Biol* 35, 237-247.

Das IJ and Chopra KL (1995). Back Scatter dose perturbation in kilovoltage photon beams at high atomic number interfaces. *Med Phys* 22, 767-773.

Das IJ (1997). Forward dose perturbation at high atomic number interfaces in kilovoltage X-ray beams. *Med Phys* 24, 1781-1787.

Das I and Kahn F (1989). Backscatter dose perturbation at high atomic number interfaces in megavoltage photon beams. *Med phys* 16, 367-375.

Deasy JO and Almond PR (1994). The spectral dependence of electron central-axis depth dose curves. *Med Phys* 21, 1369-1376.

Del Guerra A, Peretz-Mendez V, Schwarts G and Nelson WR (1983). Design considerations for a high spatial resolution positron camera with dense drift space MWPCs. *IEEE Trans Nucl Science* **NS-30**, 646-652.

Deng J, Jiang SB, Pawlicki T, Li J and Ma CM (2001). Derivation of electron and photon energy spectra from electron beam central axis depth dose curves. *Phys Med Biol* 46, 1429-1449.

Derenzo SE (1981). Monte Carlo calculations of the detection efficiency of arrays of NaI(TI), BGO, CsF, Ge, and plastic detectors for 511 keV photons. *IEEE Trans Nucl Science* **NS-28**, 131-136.

Faddegon BA and Blevis I (2000). Electron spectra derived from depth dose distributions. *Med Phys* 27, 514-526.

Fraass B, Doppke K, Hunt M, Kutcher G, Starkschall G, Stern R, Van Dyke (1998). Quality assurance for clinical radiotherapy treatment planning, AAPM task group 53. *Med phys* 25, 1773-1829.

Graham DT (1996). Principles of radiological physics, third edition, Churchill Livingstone.

Gumucio CA, Pin P, Young VL, Destouet J, Monsees B and Eichling J (1989). The effect of breast implants on the radiographic detection of microcalcification and soft-tissue masses. *Plast Reconstr Surg* 84, 772-778.

Hableid JA and Vanderbender WH (1976). Computer Code. *Nucl Sci Eng* 57, 288-289.

Haken RKT, Fraass BA and Donald JJ (1987). The practical methods of electron depth-dose measurement compared to use of NACP design chamber in water. *Med Phys* 14, 1060-1066.

Hsiao HH, Jing C and Dennis V (2001). Photon radiation dose enhancement at material interface. *Applied radiation and isotope* 55, 323-326.

IAEA (2001). Absorbed Dose Determination in External Beam Radiotherapy. An international Code of practice for Dosimetry Based on Standards of Absorbed Dose to Water (TRS 398). International Atomic Energy Agency (IAEA), Vienna, Austria.

ICRU (1980). Radiation quantities and units. International Commission on Radiation Units and Measurements, Report no 33, Washington DC.

ICRU (1984). Radiation Dosimetry: Electron beams with energies Between Between 1 and 50 MeV. International Commission on Radiation Units and measurements, Report no 35, Bethesda.

Jacobson GM, Sause WT, Thomson JW and Plenk HP (1986). Breast irradiation following silicone gel implants. *Int J Radiat Oncl Biol Phys* 121, 835-838.

Jiang SB, Kapur A and Ma C-M (2000). Electron beam modeling and commissioning for Monte Carlo treatment planning. *Med Phys* 27, 180-191.

Jiang SB, Sharp GC, Neicu T, Berbeco SI, Flampouri S and Bortfeld T (2006). On dose distribution comparison. *Phys Med Bio* 51, 759-776.

Johns HE and Cunningham JR (1983). The Physics of Radiology, Fourth edition. Springfield, Illinois, USA.

Ju T, Simpson T, Deasy JO and Low A (2008). Geometrical γ interpretation of the doe distribution comparison technique: Interpolation-free calculation. *Med phys* 35, 879-887.

Kawrakow I and Rogers DWO (2000). The EGSnrc Code System: Monte Carlo simulation of electron and photon transport, Technical Report **PIRS-701**, National Research Council of Canada, Ottawa, Canada.

Kawrakow I (2000). Accurate condensed history Monte Carlo simulation of electron transport I: EGSnrc the new EGS4 version. *Med Phys* 27, 485-496.

Khan FM (2003). The Physics of Radiation Therapy, Third edition. Lippincott Williams and Wilkins, Philadelphia.

Khan FM, Doppke K P, Hogstrom KR, Kutcher GJ, Nath R, Prasad SC, Purdy JA, Rozenfeld M and Werner BL (1991). Clinical electron-beam dosimetry, report of AAPM Radiation Therapy Committee task Group No 25. *Med Phys* 18, 73-109.

Klein EE and Kuske RR (1993). Changes in photon dose distributions due to breast prosthesis. *Int J Radiat Oncl Biol Phys* 25, 541-549.

Kossovsky N, Freiman CJ (1994). Silicone breast implant pathology. Clinical data and immunologic consequences. *Arch pathol Lab Med* 118, 686-93.

Krishnan L, St George FJ, Mansfield CM and Krishnan EC (1983). Effect of silicone gel breast prosthesis on electron and photon dose distributions. *Med Phys* 10, 96-99.

Krishnan L and Krishnan EC (1986). Electron beam irradiation after irradiation reconstruction with silicone gel implant in breast cancer, *Am J Clinical Onc* 9, 223-226.

LeVier RR, Harrison Mc, Cook RR, and Lane TH (1993). What is Silicone? *Plast Reconstr Surg* 92, 163-167.

Low DA, Harms WB, Mutic S and Purdy JA (1998). A technique for the quantitative evaluation of dose distributions. *Med Phys* 25, 656-661.

Low DA and Dempsey JF (2003). Evaluation of the gamma dose distribution comparison method. *Med Phy* 30, 2455-2464.

Ma CM and Jiang SB (1999). Monte Carlo Modelling of Electron Beams from Medical Accelerators. *Phys Med Biol* 44, R157 – R189.

Ma CM, Rogers DWO, Faddegon BA, Ding GX, Wei JS, Bieljew AF and Mackie TR (1993). Simplified models of electron beams from a Clinac 2100C accelerator. *Med Phys* 20, 1295.

Ma CM, Faddegon BA, Rogers DWO and Mackie TR (1997). Accurate characterization of Monte Carlo Calculated electron beams for radiotherapy. *Med Phys* 24, 401-416.

Mackie TR, Scrimger, and Battista JJ (1985). A Convolution method of calculating dose for 15 MV x-rays. *Med Phys*12, 188-196.

Madsen OR, Lorentzen JS, Lauriden, Egsmose C and Sorensen (2000). Effects of silicone breast prostheses on the assessment of body composition by dual-energy x-ray absorptiometry. *Clinical physiology* 20, 279-282.

Mcgrath MH and Burckhardt BR (1984). The safety and efficacy of breast implants for augumentation mammoplasty. *Plast Reconstr Surg* 974, 550-560.

Metcalfe P, Kron T and Hoban P (1997). The physics of radiotherapy x-rays from linear accelerator. Medical physics publishing Madison, Wisconsin.

Muzaffar AR and Rohrich RJ (2002). The silicone gel-filled breasts implant controversy, an update. *Plastic Reconstruction Surgery* 109, 742-747.

Nahum AE (1983). Stopping Powers and Dosimetry. *NRCC report* **PXNR-2653**, National Research Council, Ottawa.

Noone RB, Frazier TG, Noone GC, Blanchet NP, Murphy JB and Rose D (1994). Recurrence of Breast Carcinoma following immediate Reconstruction: a 13 year review. *Plastic Reconstr Surg* 93, 96-106.

Picha GJ and Goldstein JA (1991). Analysis of the soft tissue response to components used in the manufacture of breast implants: rat animal model. *Plast Reconstr Surg* 87, 490-500.

Piontek RW and Kase KR (1980). Radiation Transmission Study of Silicone Elastomer for Mammary prosthesis. *Radiology* 136, 505-507.

Podgorsak EB (2003).Review of Radiation Oncology Physics: A handbook for teachers and Students. International Atomic Energy Agency (IAEA), Vienna, Austria.

Rogers DWO (2002). Monte Carlo techniques in Radiotherapy. *Medical Physics special issue* 58, 63-70.

Rogers DWO (2006). Fiftry years of Monte Carlo simulations for medical physics. *Phys Med Biol*. 51, R287-R301.

Rogers DWO, Faddegon BA, Ding GX, Ma CM and We J (1995). BEAM: A Monte Carlo code to simulate radiotherapy treatment units *Med phys* 22, 503-524.

Rogers DWO, Ewart GM, Bielajew AF and van Dyk G (1988). Calculation of Contamination of the Co-60 therapy Beam, in Proceedings of the IAEA *International Symposium on Dosimetry in Radiotherapy*. IAEA, Vienna 1, 303-312.

Rvu J, Yahalom J, Shank B, Chaglassian TA and McCormick B (1990). Radiation therapy after breast augumentation or reconstruction in early or recurrent breast cancer. *Cancer 1* 66, 844-847.

Siebers JV, Keall PJ, Nahon AE and Mohan R (2000). Converting absorbed dose to medium to absorbed dose to water for Monte Carlo based beams dose calculations. *Phys Med Biol* 45, 983-995.

Senkus-Konefka E, Welnicka-Jaskiewicz M, Jaskiewicz J and Jassem J (2004). Radiotherapy for breast reconstruction or augumentation. *Cancer treatment reviews* 30, 671-682.

Shedbalkar AR, Devata A and Padanilam T (1980). A study of effects of radiation on silicone prostheses. *Plastic Reconstruction Surgery* 65, 805-810.

Shultis JK and Faw RE (2006). An MCNP Primer. Department of Mechanical and Nuclear Engineering, Kansas State University, Manhattan.

Simpkin DJ and Mackie TR (1990). EGS4 Monte Carlo determination of the beta dose kernel in water. *Med Phys* 17, 178-187.

Stabile RJ, Santoro E, Dispaltro F, and Sanfilipp LJ (1990). Reconstructive breast surgery following mastectomy and adjunctive radiation therapy. *Cancer* 45, 2738-2743.

Stevanovic O and Jakovljevic (2001). Imaging of the Breast-the efficiency for breast cancer follow-up after conserving therapy and breast implant following mastectomy, *Archive of Oncology* 9, 85.

Svatos MM (1997). Single Scatter Electron Monte Carlo. Lawrence Livermore National Laboratory, Livermore, CA.

Thomas SC III, James ED and Robert CM JR (1990). Christensen's physics of Diagnostic Radiology, Fourth edition. Lea and Febiger, Philadelphia.

van Diest PJ, Beekman WH and Hage JJ (1998). Pathology of silicone leakage from breast implants. *J Clin Pathol* 51, 493-497.

van Noort R and Blank MM (1981). Silicone rubbers for medical applications. In Williams, ed. *Bio Compatibility of clinical implants materials*, Boca Raton, Fla: CRR 79-98.

Williamson JF (1995). Recent developments in basic brachytherapy physics, in Radiation Therapy Physics, edited by A.R Smith. Springer-Verlag, Newyork, 247-302.

X-5 monte carlo team (2003). MCNP-A general Monte Carlo N-particle Transport code (version 5), Los Alamos National Lab.

Zhengming L and Jette D (1999). On the possibility of determining an effective energy spectrum of clinical electron beams from percentage depth dose (PDD). *Phys Med Biol* 44, N177-N182.

APPENDIX A-1

Input file for water phantom simulation

```
Title: wbath
c cell cards
1  1 -1.0 -1 2 -3 4 -5 6                    imp:e=1
2     like 1 but trcl=(0 0 -0.2)
3     like 1 but trcl=(0 0 -0.4)
4     like 1 but trcl=(0 0 -0.6)
5     like 1 but trcl=(0 0 -0.8)
6     like 1 but trcl=(0 0 -1.0)
7     like 1 but trcl=(0 0 -1.2)
8     like 1 but trcl=(0 0 -1.4)
9     like 1 but trcl=(0 0 -1.6)
10    like 1 but trcl=(0 0 -1.8)
11    like 1 but trcl=(0 0 -2.0)
12    like 1 but trcl=(0 0 -2.2)
13    like 1 but trcl=(0 0 -2.4)
14    like 1 but trcl=(0 0 -2.6)
15    like 1 but trcl=(0 0 -2.8)
16    like 1 but trcl=(0 0 -3.0)
17    like 1 but trcl=(0 0 -3.2)
18    like 1 but trcl=(0 0 -3.4)
19    like 1 but trcl=(0 0 -3.6)
20    like 1 but trcl=(0 0 -3.8)
21    like 1 but trcl=(0 0 -4.0)
22    like 1 but trcl=(0 0 -4.2)
23    like 1 but trcl=(0 0 -4.4)
24    like 1 but trcl=(0 0 -4.6)
25    like 1 but trcl=(0 0 -4.8)
26    like 1 but trcl=(0 0 -5.0)
27    like 1 but trcl=(0 0 -5.2)
28    like 1 but trcl=(0 0 -5.4)
29    like 1 but trcl=(0 0 -5.6)
30    like 1 but trcl=(0 0 -5.8)
31    like 1 but trcl=(0 0 -6.0)
32    like 1 but trcl=(0 0 -6.2)
33    like 1 but trcl=(0 0 -6.4)
34    like 1 but trcl=(0 0 -6.6)
35    like 1 but trcl=(0 0 -6.8)
36    like 1 but trcl=(0 0 -7.0)
37    like 1 but trcl=(0 0 -7.2)
38    like 1 but trcl=(0 0 -7.4)
39    like 1 but trcl=(0 0 -7.6)
40    like 1 but trcl=(0 0 -7.8)
41    like 1 but trcl=(0 0 -8.0)
42    like 1 but trcl=(0 0 -8.2)
43    like 1 but trcl=(0 0 -8.4)
44    like 1 but trcl=(0 0 -8.6)
45    like 1 but trcl=(0 0 -8.8)
46    like 1 but trcl=(0 0 -9.0)
47    like 1 but trcl=(0 0 -9.2)
48    like 1 but trcl=(0 0 -9.4)
49    like 1 but trcl=(0 0 -9.6)
50    like 1 but trcl=(0 0 -9.8)
51    like 1 but trcl=(0 0 -10.0)
```

```
52  1 -1.0 #1 #2 #3 #4 #5 #6 #7 #8 #9 #10 #11 #12 #13 #14 #15 #16 #17 #18 #19
        #20 #21 #22 #23 #24 #25 #26 #27 #28 #29 #30 #31 #32 #33 #34 #35 #36
        #37 #38 #39 #40 #41 #42 #43 #44 #45 #46 #47 #48 #49 #50 #51 -10 11
        -12 13 -14 15                          imp:e=1
53   0  (10:-11:12:-13:14:-15) -20                    imp:e=1
55   0     20                                imp:e=0

c surface cards
c water blocks
1 pz 15
2 pz 14.8
3 py 5
4 py -5
5 px 5
6 px -5
c inner wbath
10 pz 15
11 pz -15
12 py 15
13 py -15
14 px 15
15 px -15
c sphere surface
20 so 116

c Data card
mode e
c material card
m1 1000 2  8000 1         $ water
c source card
SDEF POS 0 0 115 ERG 15 PAR 3 VEC 0 0 -1 DIR=1
c
c Tally cards
*F8:E 1 2 3 4 5 6 7 8 9 10 11 12 13 14 15 16 17 18 19 20 21 22 23 24 25 26 27
     28 29 30 31 32 33 34 35 36 37 38 39 40 41 42 43 44 45 46 47 48 49 50 51
c
NPS 100000
print
mode e
```

APPENDIX A-2

Example input file for silicone phantom

```
Title: sbath
c cell cards
1  1 -1.16 -1 2 -3 4 -5 6                          imp:e=1
2     like 1 but trcl=(0 0 -0.2)
3     like 1 but trcl=(0 0 -0.4)
4     like 1 but trcl=(0 0 -0.6)
5     like 1 but trcl=(0 0 -0.8)
6     like 1 but trcl=(0 0 -1.0)
7     like 1 but trcl=(0 0 -1.2)
8     like 1 but trcl=(0 0 -1.4)
9     like 1 but trcl=(0 0 -1.6)
10    like 1 but trcl=(0 0 -1.8)
```

```
11    like 1 but trcl=(0 0 -2.0)
12    like 1 but trcl=(0 0 -2.2)
13    like 1 but trcl=(0 0 -2.4)
14    like 1 but trcl=(0 0 -2.6)
15    like 1 but trcl=(0 0 -2.8)
16    like 1 but trcl=(0 0 -3.0)
17    like 1 but trcl=(0 0 -3.2)
18    like 1 but trcl=(0 0 -3.4)
19    like 1 but trcl=(0 0 -3.6)
20    like 1 but trcl=(0 0 -3.8)
21    like 1 but trcl=(0 0 -4.0)
22    like 1 but trcl=(0 0 -4.2)
23    like 1 but trcl=(0 0 -4.4)
24    like 1 but trcl=(0 0 -4.6)
25    like 1 but trcl=(0 0 -4.8)
26    like 1 but trcl=(0 0 -5.0)
27    like 1 but trcl=(0 0 -5.2)
28    like 1 but trcl=(0 0 -5.4)
29    like 1 but trcl=(0 0 -5.6)
30    like 1 but trcl=(0 0 -5.8)
31    like 1 but trcl=(0 0 -6.0)
32    like 1 but trcl=(0 0 -6.2)
33    like 1 but trcl=(0 0 -6.4)
34    like 1 but trcl=(0 0 -6.6)
35    like 1 but trcl=(0 0 -6.8)
36    like 1 but trcl=(0 0 -7.0)
37    like 1 but trcl=(0 0 -7.2)
38    like 1 but trcl=(0 0 -7.4)
39    like 1 but trcl=(0 0 -7.6)
40    like 1 but trcl=(0 0 -7.8)
41    like 1 but trcl=(0 0 -8.0)
42    like 1 but trcl=(0 0 -8.2)
43    like 1 but trcl=(0 0 -8.4)
44    like 1 but trcl=(0 0 -8.6)
45    like 1 but trcl=(0 0 -8.8)
46    like 1 but trcl=(0 0 -9.0)
47    like 1 but trcl=(0 0 -9.2)
48    like 1 but trcl=(0 0 -9.4)
49    like 1 but trcl=(0 0 -9.6)
50    like 1 but trcl=(0 0 -9.8)
51    like 1 but trcl=(0 0 -10.0)
52  1 -1.0 #1 #2 #3 #4 #5 #6 #7 #8 #9 #10 #11 #12 #13 #14 #15 #16 #17 #18 #19
        #20 #21 #22 #23 #24 #25 #26 #27 #28 #29 #30 #31 #32 #33 #34 #35 #36
        #37 #38 #39 #40 #41 #42 #43 #44 #45 #46 #47 #48 #49 #50 #51 -10 11
        -12 13 -14 15                          imp:e=1
53    0  (10:-11:12:-13:14:-15) -20                    imp:e=1
55    0     20                                  imp:e=0

c surface cards
c water blocks
1 pz 15
2 pz 14.8
3 py 5
4 py -5
5 px 5
6 px -5
c inner wbath
```

```
10 pz 15
11 pz -15
12 py 15
13 py -15
14 px 15
15 px -15
c sphere surface
20 so 116

c Data card
mode e
c material card
m1 1000 6 6000 2 8000 1 14000 1        $ silicone prosthesis
c source card
SDEF POS 0 0 115 ERG 9 PAR 3 VEC 0 0 -1 DIR=1
c
c Tally cards
*F8:E 1 2 3 4 5 6 7 8 9 10 11 12 13 14 15 16 17 18 19 20 21 22 23 24 25 26 27
     28 29 30 31 32 33 34 35 36 37 38 39 40 41 42 43 44 45 46 47 48 49 50 51
c
NPS 100000
print
mode e
```

APPENDIX A-3

Example input file with silicone prosthesis immersed in water

```
Title:silicone-water interface
c cell card
1  1 -1.0 -1 2 -3 4 -5 6                    imp:e=1
2    like 1 but trcl=(0 0 -0.2)
3    like 1 but trcl=(0 0 -0.4)
4    like 1 but trcl=(0 0 -0.6)
5    like 1 but trcl=(0 0 -0.8)
6  2 -0.98 -10 11 -12 13 -14 15                imp:e=1
7    like 6 but trcl=(0 0 -0.2)
8    like 6 but trcl=(0 0 -0.4)
9    like 6 but trcl=(0 0 -0.6)
10   like 6 but trcl=(0 0 -0.8)
11   like 6 but trcl=(0 0 -1.0)
12   like 6 but trcl=(0 0 -1.2)
13   like 6 but trcl=(0 0 -1.4)
14   like 6 but trcl=(0 0 -1.6)
15   like 6 but trcl=(0 0 -1.8)
16   like 6 but trcl=(0 0 -2.0)
17   like 6 but trcl=(0 0 -2.2)
18   like 6 but trcl=(0 0 -2.4)
19   like 6 but trcl=(0 0 -2.6)
20   like 6 but trcl=(0 0 -2.8)
21   like 6 but trcl=(0 0 -3.0)
22   like 6 but trcl=(0 0 -3.2)
23   like 6 but trcl=(0 0 -3.4)
24   like 6 but trcl=(0 0 -3.6)
25   like 6 but trcl=(0 0 -3.8)
```

```
26   like 1 but trcl=(0 0 -5.0)
27   like 1 but trcl=(0 0 -5.2)
28   like 1 but trcl=(0 0 -5.4)
29   like 1 but trcl=(0 0 -5.6)
30   like 1 but trcl=(0 0 -5.8)
31   like 1 but trcl=(0 0 -6.0)
32   like 1 but trcl=(0 0 -6.2)
33   like 1 but trcl=(0 0 -6.4)
34   like 1 but trcl=(0 0 -6.6)
35   like 1 but trcl=(0 0 -6.8)
36   like 1 but trcl=(0 0 -7.0)
37   like 1 but trcl=(0 0 -7.2)
38   like 1 but trcl=(0 0 -7.4)
39   like 1 but trcl=(0 0 -7.6)
40   like 1 but trcl=(0 0 -7.8)
41   like 1 but trcl=(0 0 -8.0)
42   like 1 but trcl=(0 0 -8.2)
43   like 1 but trcl=(0 0 -8.4)
44   like 1 but trcl=(0 0 -8.6)
45   like 1 but trcl=(0 0 -8.8)
46   like 1 but trcl=(0 0 -9.0)
47  1 -1.0 #1 #2 #3 #4 #5 #6 #7 #8 #9 #10 #11 #12 #13 #14 #15 #16 #17
     #18 #19 #20 #21 #22 #23 #24 #25 #26 #27 #28 #29 #30
     #31 #32 #33 #34 #35 #36 #37 #38 #39 #40 #41 #42 #43 #44 #45
     #46  -30 31 -32 33 -34 35   imp:e=1
48 0   (30:-31:32:-33:34:-35) -40                  imp:e=1
49 0  40                                    imp:e=0

c surface card
c 1st water cell
1 pz 16
2 pz 15.8
3 py 5
4 py -5
5 px 5
6 px -5
c silicone cells
10 pz 15.0
11 pz 14.8
12 py 5
13 py -5
14 px 5
15 px -5
c wbath
30 pz 16
31 pz -16
32 py 16
33 py -16
34 px 16
35 px -16
c sphere surface
40 so 117

c data card
mode e
c material cards
m1 1000 2 8000 1   $ water
```

```
m2 1000 6 6000 2 8000 1 14000 1 $ silicone prosthesis
c source card
SDEF POS 0 0 116 ERG 12 PAR 3 VEC 0 0 -1 DIR=1
c
c Tally cards
*F8:E 1 2 3 4 5 6 7 8 9 10 11 12 13 14 15 16 17 18 19 20 21 22 23 24 25
     26 27 28 29 30 31 32 33 34 35 36 37 38 39 40 41 42 43 44 45 46
NPS 100000
print
```

APPENDIX B

Appendix B-1 MCNP geometry of water simulation

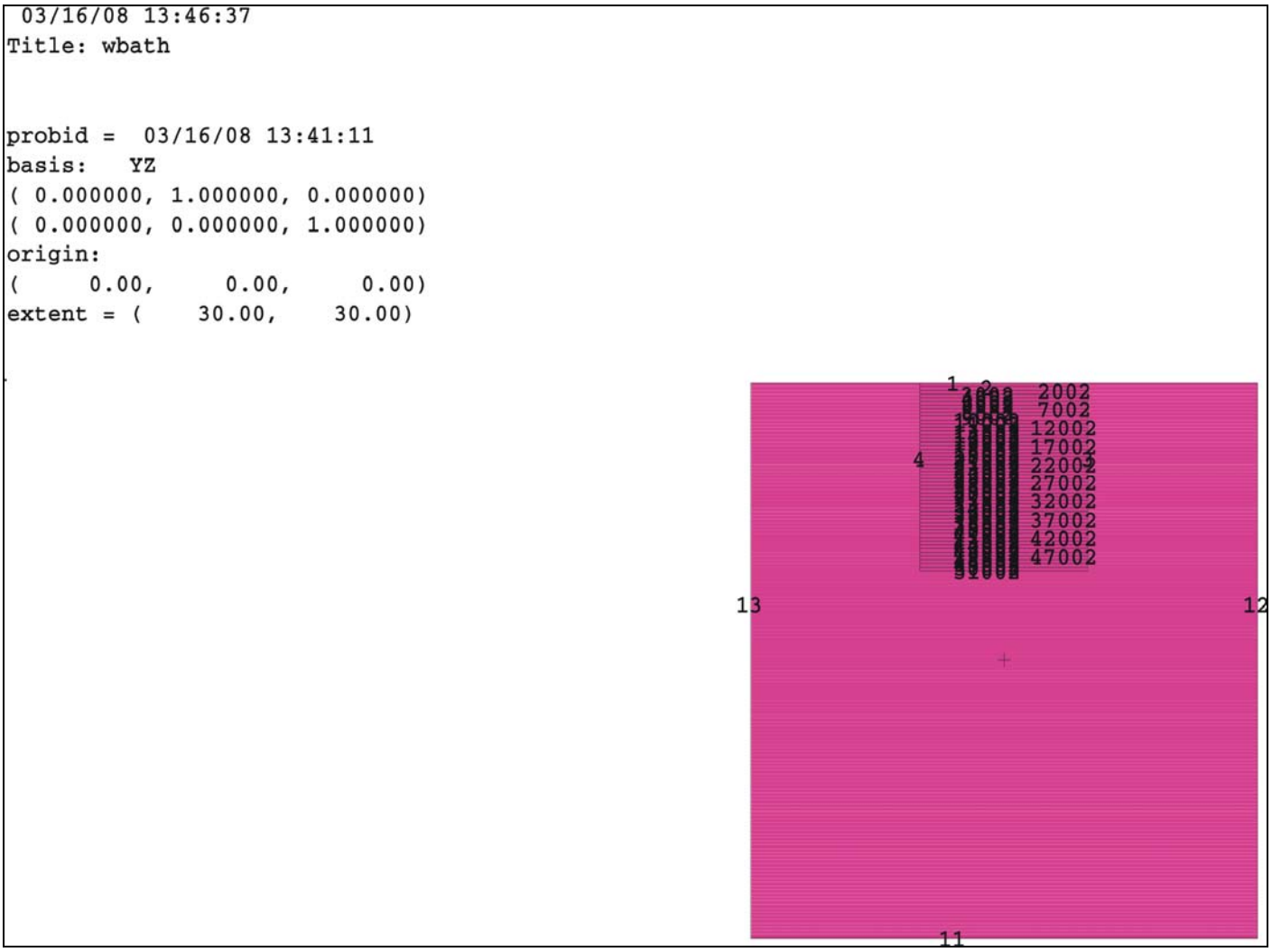

Appendix B-2 MCNP geometry of silicone prosthesis immersed in a water phantom

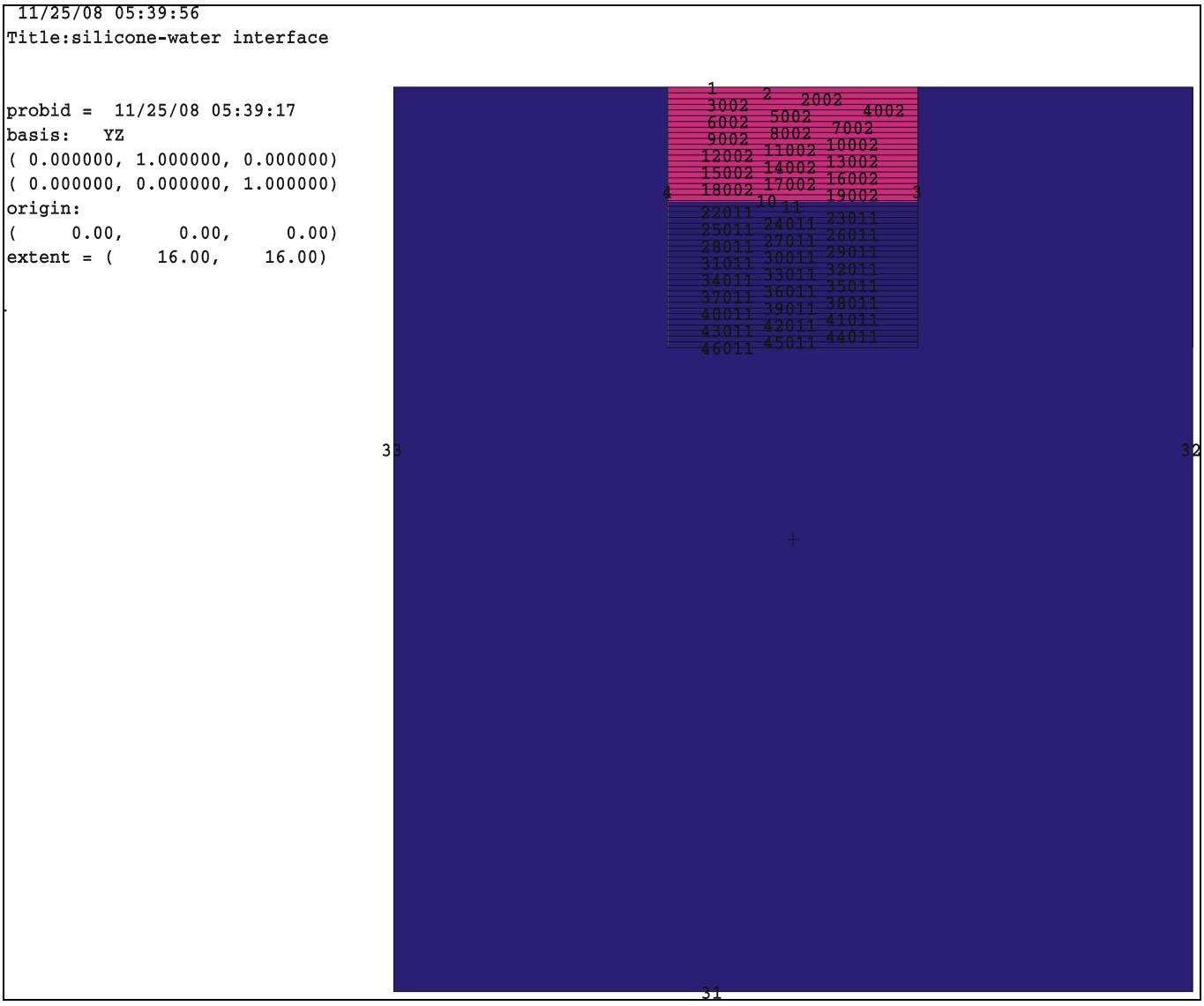

Appendix C

Appendix C-1: Example output file for electron beams in a water phantom

```
    Thread Name & Version = MCNP5_RSICC, 1.20

                        _
        ._ _    _  ._   ._   |_
        | | |  (_  | |  |_)  _)
                       |
+--------------------------------------------------------------------+
|   This program was prepared by the Regents of the University of    |
|California at Los Alamos National Laboratory (the University) under |
|  contract number W-7405-ENG-36 with the U.S. Department of Energy  |
|(DoE).  The University has certain rights in the program pursuant to|
|  the contract and the program should not be copied or distributed  |
| outside your organization.  All rights in the program are reserved |
|by the DoE and the University.  Neither the U.S. Government nor the |
| University makes any warranty, express or implied, or assumes any  |
|     liability or responsibility for the use of this software.      |
+--------------------------------------------------------------------+

1mcnp     version 5     ld=11052003                  03/01/08 17:09:33
 ******************************************************************************
probid =  04/04/09 19:11:40
 i=wbath3

    1-       Title: wbath
    2-       c cell cards
    3-       1  1 -1.0 -1 2 -3 4 -5 6                        imp:e=1
    4-       2     like 1 but trcl=(0 0 -0.2)
    5-       3     like 1 but trcl=(0 0 -0.4)
    6-       4     like 1 but trcl=(0 0 -0.6)
    7-       5     like 1 but trcl=(0 0 -0.8)
    8-       6     like 1 but trcl=(0 0 -1.0)
    9-       7     like 1 but trcl=(0 0 -1.2)
   10-       8     like 1 but trcl=(0 0 -1.4)
   11-       9     like 1 but trcl=(0 0 -1.6)
   12-       10    like 1 but trcl=(0 0 -1.8)
   13-       11    like 1 but trcl=(0 0 -2.0)
   14-       12    like 1 but trcl=(0 0 -2.2)
   15-       13    like 1 but trcl=(0 0 -2.4)
   16-       14    like 1 but trcl=(0 0 -2.6)
   17-       15    like 1 but trcl=(0 0 -2.8)
   18-       16    like 1 but trcl=(0 0 -3.0)
   19-       17    like 1 but trcl=(0 0 -3.2)
   20-       18    like 1 but trcl=(0 0 -3.4)
   21-       19    like 1 but trcl=(0 0 -3.6)
   22-       20    like 1 but trcl=(0 0 -3.8)
   23-       21    like 1 but trcl=(0 0 -4.0)
   24-       22    like 1 but trcl=(0 0 -4.2)
   25-       23    like 1 but trcl=(0 0 -4.4)
   26-       24    like 1 but trcl=(0 0 -4.6)
   27-       25    like 1 but trcl=(0 0 -4.8)
   28-       26    like 1 but trcl=(0 0 -5.0)
   29-       27    like 1 but trcl=(0 0 -5.2)
   30-       28    like 1 but trcl=(0 0 -5.4)
```

```
31-      29    like 1 but trcl=(0 0 -5.6)
32-      30    like 1 but trcl=(0 0 -5.8)
33-      31    like 1 but trcl=(0 0 -6.0)
34-      32    like 1 but trcl=(0 0 -6.2)
35-      33    like 1 but trcl=(0 0 -6.4)
36-      34    like 1 but trcl=(0 0 -6.6)
37-      35    like 1 but trcl=(0 0 -6.8)
38-      36    like 1 but trcl=(0 0 -7.0)
39-      37    like 1 but trcl=(0 0 -7.2)
40-      38    like 1 but trcl=(0 0 -7.4)
41-      39    like 1 but trcl=(0 0 -7.6)
42-      40    like 1 but trcl=(0 0 -7.8)
43-      41    like 1 but trcl=(0 0 -8.0)
44-      42    like 1 but trcl=(0 0 -8.2)
45-      43    like 1 but trcl=(0 0 -8.4)
46-      44    like 1 but trcl=(0 0 -8.6)
47-      45    like 1 but trcl=(0 0 -8.8)
48-      46    like 1 but trcl=(0 0 -9.0)
49-      47    like 1 but trcl=(0 0 -9.2)
50-      48    like 1 but trcl=(0 0 -9.4)
51-      49    like 1 but trcl=(0 0 -9.6)
52-      50    like 1 but trcl=(0 0 -9.8)
53-      51    like 1 but trcl=(0 0 -10.0)
54-      52  1 -1.0 #1 #2 #3 #4 #5 #6 #7 #8 #9 #10 #11 #12 #13 #14 #15 #16 #17 #18 #19
55-                #20 #21 #22 #23 #24 #25 #26 #27 #28 #29 #30 #31 #32 #33 #34 #35 #36
56-                #37 #38 #39 #40 #41 #42 #43 #44 #45 #46 #47 #48 #49 #50 #51 -10 11
57-                -12 13 -14 15                          imp:e=1
58-      53   0  (10:-11:12:-13:14:-15) -20                    imp:e=1
59-      55   0     20                                  imp:e=0
60-
61-      c surface cards
62-      c water blocks
63-      1 pz 15
64-      2 pz 14.8
65-      3 py 5
66-      4 py -5
67-      5 px 5
68-      6 px -5
69-      c inner wbath
70-      10 pz 15
71-      11 pz -15
72-      12 py 15
73-      13 py -15
74-      14 px 15
75-      15 px -15
76-      c sphere surface
77-      20 so 116
78-
79-      c Data card
80-      mode e
81-      c material card
82-      m1 1000 2  8000 1         $ water
83-      c source card
84-      SDEF POS 0 0 115 ERG 9 PAR 3 VEC 0 0 -1 DIR=1
85-      c
86-      c Tally cards
87-      *F8:E 1 2 3 4 5 6 7 8 9 10 11 12 13 14 15 16 17 18 19 20 21 22 23 24 25 26 27
```

```
 88-          28 29 30 31 32 33 34 35 36 37 38 39 40 41 42 43 44 45 46 47 48 49 50 51
 89-      c
 90-      NPS 100000
 91-      print


1tally  8       nps =   100000
        tally type 8*   energy deposition                       units   mev
        tally for  electrons

 cell  1
            3.94726E-01 0.0034

 cell  2
            3.98672E-01 0.0034

 cell  3
            4.08130E-01 0.0033

 cell  4
            4.17432E-01 0.0032

 cell  5
            4.27191E-01 0.0030

 cell  6
            4.31008E-01 0.0030

 cell  7
            4.41469E-01 0.0028

 cell  8
            4.52089E-01 0.0028

 cell  9
            4.65789E-01 0.0027

 cell  10
            4.80097E-01 0.0027

 cell  11
            4.96076E-01 0.0027

 cell  12
            5.09077E-01 0.0027

 cell  13
            5.14893E-01 0.0027

 cell  14
            5.13154E-01 0.0028

 cell  15
            5.01766E-01 0.0028

 cell  16
            4.78927E-01 0.0030
```

cell 17
4.38168E-01 0.0032

cell 18
3.83077E-01 0.0036

cell 19
3.13948E-01 0.0041

cell 20
2.35322E-01 0.0049

cell 21
1.57040E-01 0.0062

cell 22
8.76543E-02 0.0085

cell 23
3.72422E-02 0.0130

cell 24
1.06523E-02 0.0235

cell 25
1.72417E-03 0.0548

cell 26
1.33557E-04 0.1788

cell 27
1.24879E-06 1.0000

cell 28
0.00000E+00 0.0000

cell 29
0.00000E+00 0.0000

cell 30
0.00000E+00 0.0000

cell 31
0.00000E+00 0.0000

cell 32
0.00000E+00 0.0000

cell 33
0.00000E+00 0.0000

cell 34
0.00000E+00 0.0000

cell 35
0.00000E+00 0.0000

cell 36
0.00000E+00 0.0000

cell 37
0.00000E+00 0.0000

cell 38
0.00000E+00 0.0000

cell 39
0.00000E+00 0.0000

cell 40
0.00000E+00 0.0000

cell 41
0.00000E+00 0.0000

cell 42
0.00000E+00 0.0000

cell 43
0.00000E+00 0.0000

cell 44
0.00000E+00 0.0000

cell 45
0.00000E+00 0.0000

cell 46
0.00000E+00 0.0000

cell 47
0.00000E+00 0.0000

cell 48
0.00000E+00 0.0000

cell 49
0.00000E+00 0.0000

cell 50
0.00000E+00 0.0000

cell 51
0.00000E+00 0.0000

==========

results of 10 statistical checks for the estimated answer for the tally fluctuation chart (tfc) bin of tally 8

tfc bin behavior	--mean-- behavior	value	---------relative error--------- decrease	decrease rate	value	----variance of the variance---- decrease	decrease rate	value	--figure of merit-- behavior	-pdf- slope
desired	random	<0.10	yes	1/sqrt(nps)	<0.10	yes	1/nps	constant	random	>3.00
observed	random	0.00	yes	yes	0.00	yes	yes	constant	random	10.00
passed?	yes	yes	yes	yes	yes	yes	yes	yes	yes	yes

==========

this tally meets the statistical criteria used to form confidence intervals: check the tally fluctuation chart to verify.
the results in other bins associated with this tally may not meet these statistical criteria.

----- estimated confidence intervals: -----

estimated asymmetric confidence interval(1,2,3 sigma): 3.9338E-01 to 3.9609E-01; 3.9202E-01 to 3.9745E-01; 3.9066E-01 to 3.9881E-01
estimated symmetric confidence interval(1,2,3 sigma): 3.9337E-01 to 3.9608E-01; 3.9201E-01 to 3.9744E-01; 3.9065E-01 to 3.9880E-01

1analysis of the results in the tally fluctuation chart bin (tfc) for tally 8 with nps = 100000 print table 160

normed average tally per history = 3.94726E-01	unnormed average tally per history = 3.94726E-01
estimated tally relative error = 0.0034	estimated variance of the variance = 0.0009
relative error from zero tallies = 0.0000	relative error from nonzero scores = 0.0034
number of nonzero history tallies = 100000	efficiency for the nonzero tallies = 1.0000
number of positive history tallies= 97940	unnormed avg positive history tally = 4.14114E-01
number of negative history tallies= 2060	unnormed avg negative history tally =-1.93888E-02
history number of largest tally = 18752	largest unnormalized history tally = 9.00000E+00
(largest tally)/(average tally) = 2.28007E+01	(largest tally)/(avg nonzero tally)= 2.28007E+01
(confidence interval shift)/mean = 0.0000	shifted confidence interval center = 3.94735E-01

if the largest history score sampled so far were to occur on the next history, the tfc bin quantities would change as follows:

estimated quantities	value at nps	value at nps+1	value(nps+1)/value(nps)-1.
mean	3.94726E-01	3.94812E-01	0.000218
relative error	3.44145E-03	3.44756E-03	0.001776
variance of the variance	8.92254E-04	9.00997E-04	0.009798
shifted center	3.94735E-01	3.94735E-01	0.000000
figure of merit	8.26700E+02	8.23771E+02	-0.003543

the estimated slope of the 200 largest tallies starting at 4.20631E+00 appears to be decreasing at least exponentially.

the large score tail of the empirical history score probability density function appears to have no unsampled regions.

fom = (histories/minute)*(f(x) signal-to-noise ratio)**2 = (9.791E+02)*(9.189E-01)**2 = (9.791E+02)*(8.443E-01) = 8.267E+02

1unnormed tally density for tally 8 nonzero tally mean(m) = 3.947E-01 nps = 100000 print table 161

Appendix C-2: Example output file for electron beams in silicone phantom

Thread Name & Version = MCNP5_RSICC, 1.20

```
                    _
      ._ _   _  ._   ._   |_
      | | | (_  | |  |_)  _)
                |
+--------------------------------------------------------------------+
|   This program was prepared by the Regents of the University of    |
|California at Los Alamos National Laboratory (the University) under |
|  contract number W-7405-ENG-36 with the U.S. Department of Energy  |
|(DoE).  The University has certain rights in the program pursuant to|
|  the contract and the program should not be copied or distributed  |
| outside your organization.  All rights in the program are reserved |
|by the DoE and the University.  Neither the U.S. Government nor the |
| University makes any warranty, express or implied, or assumes any  |
|    liability or responsibility for the use of this software.       |
+--------------------------------------------------------------------+

1mcnp     version 5     ld=11052003                  03/10/08 21:03:50
 ******************************************************************************
probid =  03/10/08 21:03:50
 i=wbath9MeV

   1-       Title: wbath
   2-       c cell cards
   3-       1  1 -1.16 -1 2 -3 4 -5 6                        imp:e=1
   4-       2     like 1 but trcl=(0 0 -0.2)
   5-       3     like 1 but trcl=(0 0 -0.4)
   6-       4     like 1 but trcl=(0 0 -0.6)
   7-       5     like 1 but trcl=(0 0 -0.8)
   8-       6     like 1 but trcl=(0 0 -1.0)
   9-       7     like 1 but trcl=(0 0 -1.2)
  10-       8     like 1 but trcl=(0 0 -1.4)
  11-       9     like 1 but trcl=(0 0 -1.6)
  12-       10    like 1 but trcl=(0 0 -1.8)
  13-       11    like 1 but trcl=(0 0 -2.0)
  14-       12    like 1 but trcl=(0 0 -2.2)
  15-       13    like 1 but trcl=(0 0 -2.4)
  16-       14    like 1 but trcl=(0 0 -2.6)
  17-       15    like 1 but trcl=(0 0 -2.8)
  18-       16    like 1 but trcl=(0 0 -3.0)
  19-       17    like 1 but trcl=(0 0 -3.2)
  20-       18    like 1 but trcl=(0 0 -3.4)
  21-       19    like 1 but trcl=(0 0 -3.6)
  22-       20    like 1 but trcl=(0 0 -3.8)
```

```
23-     21    like 1 but trcl=(0 0 -4.0)
24-     22    like 1 but trcl=(0 0 -4.2)
25-     23    like 1 but trcl=(0 0 -4.4)
26-     24    like 1 but trcl=(0 0 -4.6)
27-     25    like 1 but trcl=(0 0 -4.8)
28-     26    like 1 but trcl=(0 0 -5.0)
29-     27    like 1 but trcl=(0 0 -5.2)
30-     28    like 1 but trcl=(0 0 -5.4)
31-     29    like 1 but trcl=(0 0 -5.6)
32-     30    like 1 but trcl=(0 0 -5.8)
33-     31    like 1 but trcl=(0 0 -6.0)
34-     32    like 1 but trcl=(0 0 -6.2)
35-     33    like 1 but trcl=(0 0 -6.4)
36-     34    like 1 but trcl=(0 0 -6.6)
37-     35    like 1 but trcl=(0 0 -6.8)
38-     36    like 1 but trcl=(0 0 -7.0)
39-     37    like 1 but trcl=(0 0 -7.2)
40-     38    like 1 but trcl=(0 0 -7.4)
41-     39    like 1 but trcl=(0 0 -7.6)
42-     40    like 1 but trcl=(0 0 -7.8)
43-     41    like 1 but trcl=(0 0 -8.0)
44-     42    like 1 but trcl=(0 0 -8.2)
45-     43    like 1 but trcl=(0 0 -8.4)
46-     44    like 1 but trcl=(0 0 -8.6)
47-     45    like 1 but trcl=(0 0 -8.8)
48-     46    like 1 but trcl=(0 0 -9.0)
49-     47    like 1 but trcl=(0 0 -9.2)
50-     48    like 1 but trcl=(0 0 -9.4)
51-     49    like 1 but trcl=(0 0 -9.6)
52-     50    like 1 but trcl=(0 0 -9.8)
53-     51    like 1 but trcl=(0 0 -10.0)
54-     52  1 -1.16 #1 #2 #3 #4 #5 #6 #7 #8 #9 #10 #11 #12 #13 #14 #15 #16 #17 #18 #19
55-               #20 #21 #22 #23 #24 #25 #26 #27 #28 #29 #30 #31 #32 #33 #34 #35 #36
56-               #37 #38 #39 #40 #41 #42 #43 #44 #45 #46 #47 #48 #49 #50 #51 -10 11
57-               -12 13 -14 15                          imp:e=1
58-     53   0  (10:-11:12:-13:14:-15) -20                    imp:e=1
59-     55   0     20                                  imp:e=0
60-
61-     c surface cards
62-     c water blocks
63-     1 pz 15
64-     2 pz 14.8
65-     3 py 5
66-     4 py -5
67-     5 px 5
68-     6 px -5
69-     c inner wbath
70-     10 pz 15
71-     11 pz -15
72-     12 py 15
73-     13 py -15
74-     14 px 15
75-     15 px -15
76-     c sphere surface
77-     20 so 116
78-
79-     c Data card
```

```
 80-      mode e
 81-      c material card
 82-      m1 1000 2  8000 1        $ water
 83-      c source card
 84-      SDEF POS 0 0 115 ERG 9 PAR 3 VEC 0 0 -1 DIR=1
 85-      c
 86-      c Tally cards
 87-      *F8:E 1 2 3 4 5 6 7 8 9 10 11 12 13 14 15 16 17 18 19 20 21 22 23 24 25 26 27
 88-           28 29 30 31 32 33 34 35 36 37 38 39 40 41 42 43 44 45 46 47 48 49 50 51
 89-      c
 90-      NPS 100000
 91-      print

1tally   8       nps =   100000
         tally type 8*   energy deposition                    units   mev
         tally for  electrons

 cell  1
            4.56897E-01 0.0032

 cell  2
            4.58624E-01 0.0031

 cell  3
            4.81230E-01 0.0030

 cell  4
            4.80161E-01 0.0029

 cell  5
            4.97459E-01 0.0028

 cell  6
            5.07591E-01 0.0027

 cell  7
            5.22112E-01 0.0026

 cell  8
            5.38804E-01 0.0026

 cell  9
            5.62367E-01 0.0026

 cell  10
            5.81020E-01 0.0026

 cell  11
            5.93224E-01 0.0026

 cell  12
            5.95063E-01 0.0026

 cell  13
            5.80088E-01 0.0027

 cell  14
```

5.44926E-01 0.0029

cell 15
4.89975E-01 0.0031

cell 16
4.12316E-01 0.0036

cell 17
3.15416E-01 0.0043

cell 18
2.09141E-01 0.0056

cell 19
1.13721E-01 0.0077

cell 20
4.37461E-02 0.0124

cell 21
1.02100E-02 0.0247

cell 22
9.58060E-04 0.0741

cell 23
2.38537E-05 0.3944

cell 24
0.00000E+00 0.0000

cell 25
0.00000E+00 0.0000

cell 26
0.00000E+00 0.0000

cell 27
0.00000E+00 0.0000

cell 28
0.00000E+00 0.0000

cell 29
0.00000E+00 0.0000

cell 30
0.00000E+00 0.0000

cell 31
0.00000E+00 0.0000

cell 32
0.00000E+00 0.0000

cell 33

0.00000E+00 0.0000

cell 34
0.00000E+00 0.0000

cell 35
0.00000E+00 0.0000

cell 36
0.00000E+00 0.0000

cell 37
0.00000E+00 0.0000

cell 38
0.00000E+00 0.0000

cell 39
0.00000E+00 0.0000

cell 40
0.00000E+00 0.0000

cell 41
0.00000E+00 0.0000

cell 42
0.00000E+00 0.0000

cell 43
0.00000E+00 0.0000

cell 44
0.00000E+00 0.0000

cell 45
0.00000E+00 0.0000

cell 46
0.00000E+00 0.0000

cell 47
0.00000E+00 0.0000

cell 48
0.00000E+00 0.0000

cell 49
0.00000E+00 0.0000

cell 50
0.00000E+00 0.0000

cell 51
0.00000E+00 0.0000

==========
==========

results of 10 statistical checks for the estimated answer for the tally fluctuation chart (tfc) bin of tally 8

tfc bin	--mean--	---------relative error---------			----variance of the variance----			--figure of merit--	-pdf-
behavior	behavior	value	decrease	decrease rate	value	decrease	decrease rate	value	behavior slope
desired	random	<0.10	yes	1/sqrt(nps)	<0.10	yes	1/nps	constant	random >3.00
observed	random	0.00	yes	yes	0.00	yes	yes	constant	random 10.00
passed?	yes	yes	yes	yes	yes	yes	yes	yes	yes yes

==========
==========

this tally meets the statistical criteria used to form confidence intervals: check the tally fluctuation chart to verify.
the results in other bins associated with this tally may not meet these statistical criteria.

----- estimated confidence intervals: -----

estimated asymmetric confidence interval(1,2,3 sigma): 4.5544E-01 to 4.5837E-01; 4.5397E-01 to 4.5984E-01; 4.5251E-01 to 4.6131E-01
estimated symmetric confidence interval(1,2,3 sigma): 4.5543E-01 to 4.5836E-01; 4.5396E-01 to 4.5983E-01; 4.5250E-01 to 4.6130E-01

1analysis of the results in the tally fluctuation chart bin (tfc) for tally 8 with nps = 100000 print table 160

normed average tally per history = 4.56897E-01	unnormed average tally per history = 4.56897E-01
estimated tally relative error = 0.0032	estimated variance of the variance = 0.0008
relative error from zero tallies = 0.0000	relative error from nonzero scores = 0.0032
number of nonzero history tallies = 100000	efficiency for the nonzero tallies = 1.0000
number of positive history tallies= 97919	unnormed avg positive history tally = 4.77108E-01
number of negative history tallies= 2081	unnormed avg negative history tally =-2.02105E-02
history number of largest tally = 18752	largest unnormalized history tally = 9.00000E+00
(largest tally)/(average tally) = 1.96981E+01	(largest tally)/(avg nonzero tally)= 1.96981E+01
(confidence interval shift)/mean = 0.0000	shifted confidence interval center = 4.56907E-01

if the largest history score sampled so far were to occur on the next history, the tfc bin quantities would change as follows:

estimated quantities	value at nps	value at nps+1	value(nps+1)/value(nps)-1.
mean	4.56897E-01	4.56983E-01	0.000187

```
     relative error               3.20958E-03          3.21439E-03              0.001498
     variance of the variance     7.80651E-04          7.86721E-04              0.007776
     shifted center               4.56907E-01          4.56907E-01              0.000000
     figure of merit              9.42827E+02          9.40008E+02              -0.002990

 the estimated slope of the 200 largest  tallies starting at  4.53507E+00 appears to be decreasing at least
exponentially.
 the large score tail of the empirical history score probability density function appears to have no
unsampled regions.

 fom = (histories/minute)*(f(x) signal-to-noise ratio)**2 = (9.712E+02)*( 9.853E-01)**2 =
(9.712E+02)*(9.707E-01) = 9.428E+02

1unnormed tally density for tally   8          nonzero tally mean(m) = 4.569E-01   nps =    100000    print
table 161
```

Appendix C-3: Example output file for electron beams with silicone prosthesis immersed in water.

```
Thread Name & Version = MCNP5_RSICC, 1.20

                    _
       ._ _   _  ._   ._  |_
       | | | (_  | |  |_)  _)
                 |

 +---------------------------------------------------------------------+
 |   This program was prepared by the Regents of the University of    |
 |California at Los Alamos National Laboratory (the University) under |
 |  contract number W-7405-ENG-36 with the U.S. Department of Energy  |
 |(DoE).  The University has certain rights in the program pursuant to|
 |  the contract and the program should not be copied or distributed  |
 | outside your organization.  All rights in the program are reserved |
 |by the DoE and the University.  Neither the U.S. Government nor the |
 | University makes any warranty, express or implied, or assumes any  |
 |     liability or responsibility for the use of this software.      |
 +---------------------------------------------------------------------+

1mcnp     version 5     ld=11052003                  11/15/08 22:48:56
 ******************************************************************************
probid =  11/15/08 22:48:56
 i=siwa4a

    1-       Title:silicone-water interface
    2-       c cell card
    3-       1  1 -0.98 -1 2 -3 4 -5 6                  imp:e=1
    4-       2    like 1 but trcl=(0 0 -0.2)
    5-       3    like 1 but trcl=(0 0 -0.4)
    6-       4    like 1 but trcl=(0 0 -0.6)
    7-       5    like 1 but trcl=(0 0 -0.8)
    8-       6    like 1 but trcl=(0 0 -1.0)
    9-       7    like 1 but trcl=(0 0 -1.2)
   10-       8    like 1 but trcl=(0 0 -1.4)
   11-       9    like 1 but trcl=(0 0 -1.6)
```

```
12-      10   like 1 but trcl=(0 0 -1.8)
13-      11   like 1 but trcl=(0 0 -2.0)
14-      12   like 1 but trcl=(0 0 -2.2)
15-      13   like 1 but trcl=(0 0 -2.4)
16-      14   like 1 but trcl=(0 0 -2.6)
17-      15   like 1 but trcl=(0 0 -2.8)
18-      16   like 1 but trcl=(0 0 -3.0)
19-      17   like 1 but trcl=(0 0 -3.2)
20-      18   like 1 but trcl=(0 0 -3.4)
21-      19   like 1 but trcl=(0 0 -3.6)
22-      20   like 1 but trcl=(0 0 -3.8)
23-      21 2 -1.0 -10 11 -12 13 -14 15                imp:e=1
24-      22   like 21 but trcl=(0 0 -0.2)
25-      23   like 21 but trcl=(0 0 -0.4)
26-      24   like 21 but trcl=(0 0 -0.6)
27-      25   like 21 but trcl=(0 0 -0.8)
28-      26   like 21 but trcl=(0 0 -1.0)
29-      27   like 21 but trcl=(0 0 -1.2)
30-      28   like 21 but trcl=(0 0 -1.4)
31-      29   like 21 but trcl=(0 0 -1.6)
32-      30   like 21 but trcl=(0 0 -1.8)
33-      31   like 21 but trcl=(0 0 -2.0)
34-      32   like 21 but trcl=(0 0 -2.2)
35-      33   like 21 but trcl=(0 0 -2.4)
36-      34   like 21 but trcl=(0 0 -2.6)
37-      35   like 21 but trcl=(0 0 -2.8)
38-      36   like 21 but trcl=(0 0 -3.0)
39-      37   like 21 but trcl=(0 0 -3.2)
40-      38   like 21 but trcl=(0 0 -3.4)
41-      39   like 21 but trcl=(0 0 -3.6)
42-      40   like 21 but trcl=(0 0 -3.8)
43-      41   like 21 but trcl=(0 0 -4.0)
44-      42   like 21 but trcl=(0 0 -4.2)
45-      43   like 21 but trcl=(0 0 -4.4)
46-      44   like 21 but trcl=(0 0 -4.6)
47-      45   like 21 but trcl=(0 0 -4.8)
48-      46   like 21 but trcl=(0 0 -5.0)
49-      47  2 -1.0 #1 #2 #3 #4 #5 #6 #7 #8 #9 #10 #11 #12 #13 #14 #15 #16 #17
50-           #18 #19 #20 #21 #22 #23 #24 #25 #26 #27 #28 #29 #30
51-           #31 #32 #33 #34 #35 #36 #37 #38 #39 #40 #41 #42 #43 #44 #45 #46
52-            -30 31 -32 33 -34 35                  imp:e=1
53-      48 0   (30:-31:32:-33:34:-35) -40                  imp:e=1
54-      49 0  40                                  imp:e=0
55-
56-      c surface card
57-      c 1st silicone cell
58-      1 pz 16
59-      2 pz 15.8
60-      3 py 5
61-      4 py -5
62-      5 px 5
63-      6 px -5
64-      c water cells
65-      10 pz 12.0
66-      11 pz 11.8
67-      12 py 5
68-      13 py -5
```

```
 69-      14 px 5
 70-      15 px -5
 71-      c wbath
 72-      30 pz 16
 73-      31 pz -16
 74-      32 py 16
 75-      33 py -16
 76-      34 px 16
 77-      35 px -16
 78-      c sphere surface
 79-      40 so 117
 80-
 81-      c data card
 82-      mode e
 83-      c material cards
 84-      m1 1000 6 6000 2 8000 1 14000 1 $ silicone prosthesis
 85-      m2 1000 2 8000 1   $ water
 86-      c source card
 87-      SDEF POS 0 0 116 ERG 6 PAR 3 VEC 0 0 -1 DIR=1
 88-      c
 89-      c Tally cards
 90-      *F8:E 1 2 3 4 5 6 7 8 9 10 11 12 13 14 15 16 17 18 19 20 21 22 23 24 25
 91-           26 27 28 29 30 31 32 33 34 35 36 37 38 39 40 41 42 43 44 45 46
 92-      NPS 100000
1tally   8       nps =   100000
       tally type 8*   energy deposition                    units   mev
       tally for  electrons

cell  1
          3.45140E-01 0.0028

cell  2
          3.79669E-01 0.0027

cell  3
          4.03314E-01 0.0026

cell  4
          4.24100E-01 0.0026

cell  5
          4.55104E-01 0.0027

cell  6
          4.88036E-01 0.0027

cell  7
          5.16848E-01 0.0027

cell  8
          5.30394E-01 0.0027

cell  9
          5.24029E-01 0.0028

cell  10
          4.97208E-01 0.0029
```

cell 11
4.46072E-01 0.0031

cell 12
3.70858E-01 0.0036

cell 13
2.87609E-01 0.0043

cell 14
1.85432E-01 0.0055

cell 15
9.56504E-02 0.0079

cell 16
3.29621E-02 0.0133

cell 17
6.37907E-03 0.0289

cell 18
4.82483E-04 0.0978

cell 19
9.94179E-06 0.5735

cell 20
0.00000E+00 0.0000

cell 21
0.00000E+00 0.0000

cell 22
0.00000E+00 0.0000

cell 23
0.00000E+00 0.0000

cell 24
0.00000E+00 0.0000

cell 25
0.00000E+00 0.0000

cell 26
0.00000E+00 0.0000

cell 27
0.00000E+00 0.0000

cell 28
0.00000E+00 0.0000

cell 29
0.00000E+00 0.0000

cell 30
0.00000E+00 0.0000

cell 31
0.00000E+00 0.0000

cell 32
0.00000E+00 0.0000

cell 33
0.00000E+00 0.0000

cell 34
0.00000E+00 0.0000

cell 35
0.00000E+00 0.0000

cell 36
0.00000E+00 0.0000

cell 37
0.00000E+00 0.0000

cell 38
0.00000E+00 0.0000

cell 39
0.00000E+00 0.0000

cell 40
0.00000E+00 0.0000

cell 41
0.00000E+00 0.0000

cell 42
0.00000E+00 0.0000

cell 43
0.00000E+00 0.0000

cell 44
0.00000E+00 0.0000

cell 45
0.00000E+00 0.0000

cell 46
0.00000E+00 0.0000

==========
==========

results of 10 statistical checks for the estimated answer for the tally fluctuation chart (tfc) bin of tally 8

tfc bin	--mean--	---------relative error---------			----variance of the variance----			--figure of merit--	-pdf-
behavior	behavior	value	decrease	decrease rate	value	decrease	decrease rate	value	behavior slope
desired	random	<0.10	yes	1/sqrt(nps)	<0.10	yes	1/nps	constant	random >3.00
observed	random	0.00	yes	yes	0.00	yes	yes	constant	random 10.00
passed?	yes	yes	yes	yes	yes	yes	yes	yes	yes yes

==========

this tally meets the statistical criteria used to form confidence intervals: check the tally fluctuation chart to verify.
the results in other bins associated with this tally may not meet these statistical criteria.

----- estimated confidence intervals: -----

estimated asymmetric confidence interval(1,2,3 sigma): 3.4419E-01 to 3.4610E-01; 3.4324E-01 to 3.4705E-01; 3.4229E-01 to 3.4800E-01
estimated symmetric confidence interval(1,2,3 sigma): 3.4419E-01 to 3.4609E-01; 3.4324E-01 to 3.4704E-01; 3.4228E-01 to 3.4800E-01

1analysis of the results in the tally fluctuation chart bin (tfc) for tally 8 with nps = 100000 print table 160

normed average tally per history = 3.45140E-01 unnormed average tally per history = 3.45140E-01
estimated tally relative error = 0.0028 estimated variance of the variance = 0.0008
relative error from zero tallies = 0.0000 relative error from nonzero scores = 0.0028

number of nonzero history tallies = 100000 efficiency for the nonzero tallies = 1.0000
number of positive history tallies= 98096 unnormed avg positive history tally = 3.58563E-01
number of negative history tallies= 1904 unnormed avg negative history tally =-1.34225E-02
history number of largest tally = 14801 largest unnormalized history tally = 6.00000E+00
(largest tally)/(average tally) = 1.73842E+01 (largest tally)/(avg nonzero tally)= 1.73842E+01

(confidence interval shift)/mean = 0.0000 shifted confidence interval center = 3.45146E-01

if the largest history score sampled so far were to occur on the next history, the tfc bin quantities would change as follows:

estimated quantities	value at nps	value at nps+1	value(nps+1)/value(nps)-1.
mean	3.45140E-01	3.45197E-01	0.000164
relative error	2.75882E-03	2.76320E-03	0.001588
variance of the variance	7.67952E-04	7.74819E-04	0.008942
shifted center	3.45146E-01	3.45146E-01	0.000000
figure of merit	1.36330E+03	1.35898E+03	-0.003168

the estimated slope of the 200 largest tallies starting at 3.04626E+00 appears to be decreasing at least exponentially.
the large score tail of the empirical history score probability density function appears to have no unsampled regions.

fom = (histories/minute)*(f(x) signal-to-noise ratio)**2 = (1.038E+03)*(1.146E+00)**2 = (1.038E+03)*(1.314E+00) = 1.363E+03

1status of the statistical checks used to form confidence intervals for the mean for each tally bin

tally result of statistical checks for the tfc bin (the first check not passed is listed) and error magnitude check for all bins

8 passed the 10 statistical checks for the tally fluctuation chart bin result
missed all bin error check: 46 tally bins had 27 bins with zeros and 1 bins with relative errors exceeding 0.10

the 10 statistical checks are only for the tally fluctuation chart bin and do not apply to other tally bins.

the tally bins with zeros may or may not be correct: compare the source, cutoffs, multipliers, et cetera with the tally bins.

warning. 1 of the 1 tallies had bins with relative errors greater than recommended.
1tally fluctuation charts

tally 8

nps	mean	error	vov	slope	fom
8000	3.4812E-01	0.0095	0.0102	3.2	1446
16000	3.4603E-01	0.0069	0.0048	6.4	1350
24000	3.4338E-01	0.0055	0.0031	10.0	1412
32000	3.4425E-01	0.0049	0.0024	10.0	1363
40000	3.4452E-01	0.0044	0.0020	10.0	1358
48000	3.4501E-01	0.0040	0.0017	10.0	1372
56000	3.4560E-01	0.0037	0.0014	10.0	1355
64000	3.4532E-01	0.0035	0.0012	10.0	1355
72000	3.4535E-01	0.0033	0.0011	10.0	1353
80000	3.4563E-01	0.0031	0.0010	10.0	1378
88000	3.4522E-01	0.0029	0.0009	10.0	1373
96000	3.4511E-01	0.0028	0.0008	10.0	1373
100000	3.4514E-01	0.0028	0.0008	10.0	1363

****
dump no. 3 on file runtpi nps = 100000 coll = 2213784824 ctm = 96.37 nrn = 12720056633

3 warning messages so far.

run terminated when 100000 particle histories were done.

computer time = 96.41 minutes

Appendix D

D-1: PDD values for electron beams simulation in a water phantom

cell no	depth	%6 MeV	%9MeV	%12 MeV	%15 MeV
1	0.0	67.6	75.5	79.6	87.7
2	0.2	73.0	79.3	84.5	88.2
3	0.4	77.1	81.8	84.0	91.9
4	0.6	79.9	83.3	85.7	92.6
5	0.8	84.5	86.0	86.9	94.4
6	1.0	90.4	87.8	88.6	94.8
7	1.2	95.9	90.4	90.1	95.2
8	1.4	100.0	92.9	92.1	95.7
9	1.6	99.9	95.1	93.6	96.3
10	1.8	95.8	95.4	95.5	97.3
11	2.0	86.3	98.9	95.8	97.9
12	2.2	71.6	99.6	96.3	98.1
13	2.4	52.7	100.0	97.0	98.4
14	2.6	31.0	99.1	97.8	99.2
15	2.8	12.8	93.2	98.1	99.4
16	3.0	3.0	85.4	98.9	99.6
17	3.2	0.3	77.4	100.0	99.7
18	3.4	0.0	66.8	99.4	99.9
19	3.6	0.0	56.2	97.9	100.0
20	3.8	0.0	43.8	95.0	98.8
21	4.0	0.0	30.5	92.1	98.7
22	4.2	0.0	17.0	87.1	98.5
23	4.4		7.2	82.0	98.2
24	4.6		2.1	73.8	95.7
25	4.8		0.3	64.2	93.9
26	5.0		0.0	53.3	91.6
27	5.2		0.0	41.3	88.4
28	5.4		0.0	29.4	83.9
29	5.6		0.0	18.5	81.2
30	5.7		0.0	9.9	75.9
31	5.8			4.4	67.6
32	6.0			1.5	58.4
33	6.2			0.3	54.1
34	6.4			0.0	43.7
35	6.6			0.0	31.9
36	6.8			0.0	18.6
37	7.0			0.0	11.3
38	7.2				6.0
39	7.4				2.6
40	7.6				0.9

41	7.8				0.2
42	8.0				0.0
43	8.2				0.0
44	8.4				0.0
45	8.6				0.0
46	8.8				0.0
47	9.0				0.0
48	9.2				0.0

D-2: PDD values for electron beams simulation in a silicone (0.98g/cm^3) phantom

Cell no	depth	%6 MeV	%9 MeV	%12 MeV	%15 MeV
1.0	0.0	65.1	70.5	78.5	87.3
2.0	0.2	71.3	76.0	80.9	88.6
3.0	0.4	75.6	76.9	83.4	90.0
4.0	0.6	80.1	79.7	83.4	90.0
5.0	0.8	85.8	80.9	85.3	92.4
6.0	1.0	92.2	83.3	86.4	92.7
7.0	1.2	97.6	85.5	86.7	92.1
8.0	1.4	100.0	88.1	87.9	94.0
9.0	1.6	98.5	91.5	88.9	93.3
10.0	1.8	93.9	94.1	90.5	94.0
11.0	2.0	85.2	97.3	92.2	95.2
12.0	2.2	72.6	99.4	92.8	95.1
13.0	2.4	56.0	100.0	94.4	94.9
14.0	2.6	37.6	98.8	96.9	96.5
15.0	2.8	20.3	96.5	98.2	96.5
16.0	3.0	7.6	91.6	99.0	97.4
17.0	3.2	1.6	84.8	100.0	98.7
18.0	3.4	0.1	75.8	99.6	100.0
19.0	3.6	0.0	65.1	98.7	100.0
20.0	3.8		52.7	97.2	100.0
21.0	4.0		39.1	94.2	99.8
22.0	4.2		25.9	89.8	99.7
23.0	4.4		14.5	84.2	99.3
24.0	4.6		6.6	76.8	99.3
25.0	4.8		2.2	69.0	99.4
26.0	5.0		0.5	58.8	96.9
27.0	5.2		0.1	48.7	93.5
28.0	5.4		0.0	38.0	89.5
29.0	5.6			27.8	84.3
30.0	5.7			18.3	78.3
31.0	5.8			10.9	71.1
32.0	6.0			5.3	63.3
33.0	6.2			2.1	54.9
34.0	6.4			0.7	46.3
35.0	6.6			0.2	37.0
36.0	6.8			0.0	27.9

37.0	7.0			0.0	19.4
38.0	7.2			0.0	12.9
39.0	7.4				7.8
40.0	7.6				4.1
40.1	7.8				1.8
40.2	8.0				0.6
40.3	8.2				0.2
40.4	8.4				0.0
40.5	8.6				0.0

D-3: PDD values for electron beams simulation in a silicone (0.96g/cm^3) Phantom

Cell no	depth	%6MeV	%9MeV	%12MeV	%15MeV
1.0	0.0	67.1	72.5	80.5	89.3
2.0	0.2	73.3	78.0	82.9	90.6
3.0	0.4	77.6	78.9	85.4	92.0
4.0	0.6	82.1	81.7	85.4	92.0
5.0	0.8	87.8	82.9	87.3	94.4
6.0	1.0	94.2	85.3	88.4	94.7
7.0	1.2	98.6	87.5	88.7	94.1
8.0	1.4	99.3	90.1	89.9	96.0
9.0	1.6	100.0	93.5	90.9	95.3
10.0	1.8	95.9	96.1	92.5	96.0
11.0	2.0	87.2	97.4	94.2	97.2
12.0	2.2	74.6	98.8	94.8	97.1
13.0	2.4	58.0	99.2	96.4	96.9
14.0	2.6	39.6	100.0	97.4	97.7
15.0	2.8	22.3	98.5	98.2	98.5
16.0	3.0	9.6	93.6	98.9	99.1
17.0	3.2	3.6	86.8	99.5	99.8
18.0	3.4	2.1	77.8	100.0	99.9
19.0	3.6	0.0	67.1	99.2	100.0
20.0	3.8	0	54.7	97.5	99.2
21.0	4.0	0	41.1	96.2	98.9
22.0	4.2		27.9	91.8	98.5
23.0	4.4		16.5	86.2	98.2
24.0	4.6		8.6	78.8	97.9
25.0	4.8		4.2	71.0	97.2
26.0	5.0		2.5	60.8	96.3
27.0	5.2		2.1	50.7	95.5
28.0	5.4		0.0	40.0	91.5
29.0	5.6		0.0	29.8	86.3
30.0	5.7		0.0	20.3	80.3
31.0	5.8			12.9	73.1
32.0	6.0			7.3	65.3
33.0	6.2			4.1	56.9

34.0	6.4			2.7	48.3
35.0	6.6			2.2	39.0
36.0	6.8			0.0	29.9
37.0	7.0			0.0	21.4
38.0	7.2			0.0	14.9
39.0	7.4			0.0	9.8
40.0	7.6				6.1
41.0	7.8				3.8
42.0	8.0				2.6
43.0	8.2				2.2
44.0	8.4				0.0
	8.6				0.0

D-4: PDD values for electron beams simulation with silicone prosthesis (0.96g/cm^3) immersed in water phantom

cell no	depth	%6 MeV	%9 MeV	%12 MeV	%15 MeV
1	0.0	65.1	71.0	78.5	82.1
2	0.2	71.2	76.4	81.2	83.0
3	0.4	75.7	77.7	83.5	84.4
4	0.6	79.4	80.4	83.5	86.0
5	0.8	85.3	81.9	85.5	86.6
6	1.0	91.8	84.0	86.3	87.5
7	1.2	96.7	85.9	87.0	87.7
8	1.4	100.0	89.1	88.3	87.9
9	1.6	99.7	92.0	88.3	88.9
10	1.8	95.1	94.6	90.3	89.3
11	2.0	86.2	97.6	91.5	89.5
12	2.2	73.8	99.5	93.0	89.7
13	2.4	58.3	100.0	95.0	90.0
14	2.6	40.2	100.0	96.1	91.9
15	2.8	22.4	98.0	98.0	92.2
16	3.0	9.2	93.4	99.3	93.3
17	3.2	2.1	87.2	100.0	94.9
18	3.4	0.2	78.4	99.0	95.0
19	3.6	0.0	67.7	98.7	96.2
20	3.8	0.0	53.8	95.0	96.9
21	4.0	0.0	43.5	89.8	100.0
22	4.2	0.0	29.1	86.8	98.7
23	4.4	0.0	16.9	78.2	97.5
24	4.6		7.6	71.3	97.1
25	4.8		2.5	63.3	95.2
26	5.0		0.5	52.2	93.7
27	5.2		0.0	40.2	90.9
28	5.4		0.0	29.0	83.0
29	5.6		0.0	18.4	77.6
30	5.7		0.0	10.0	74.2

31	5.8		0.0	4.6	70.1
32	6.0		0.0	1.6	62.1
33	6.2			0.4	53.6
34	6.4			0.1	44.6
35	6.6			0.0	35.0
36	6.8			0.0	25.6
37	7.0			0.0	17.5
38	7.2			0.0	10.8
39	7.4			0.0	5.7
40	7.6			0.0	2.6
41	7.8				1.0
42	8.0				0.3
43	8.2				0.0
44	8.4				0.0
45	8.6				0.0
46	8.8				0.0
47	9.0				0.0
48	9.2				0.0

D-5: PDD values for electron beams simulation with silicone prosthesis (0.98g/cm^3) immersed in water phantom

cell no	depth	%6mev	%9mev	%12mev	%15mev
1	0.0	65.1	70.9	78.7	83.6
2	0.2	71.6	76.1	81.1	85.6
3	0.4	76.0	77.4	83.3	85.8
4	0.6	80.0	80.1	83.6	86.4
5	0.8	85.8	81.4	85.2	88.1
6	1.0	92.0	83.7	85.9	88.5
7	1.2	97.4	86.2	87.4	88.9
8	1.4	100.0	89.0	88.7	89.3
9	1.6	98.8	92.1	88.7	89.4
10	1.8	93.7	94.9	90.0	89.8
11	2.0	84.1	98.0	91.6	89.8
12	2.2	69.9	100.0	93.2	91.0
13	2.4	54.2	99.6	94.7	91.9
14	2.6	35.0	99.6	96.8	92.0
15	2.8	18.0	95.9	97.9	92.9
16	3.0	6.2	91.5	99.3	94.3
17	3.2	1.2	83.4	100.0	94.5
18	3.4	0.1	74.3	99.3	94.8
19	3.6	0.0	62.9	97.3	95.4
20	3.8	0.0	49.0	93.5	97.4
21	4.0	0.0	37.4	89.9	100.0

22	4.2	0.0	23.8	86.3	99.5
23	4.4	0.0	12.6	76.8	98.7
24	4.6		5.2	67.8	97.2
25	4.8		1.3	63.1	95.2
26	5.0		0.2	52.0	89.9
27	5.2		0.0	41.0	85.5
28	5.4		0.0	35.1	81.0
29	5.6		0.0	20.6	76.5
30	5.7		0.0	13.6	71.8
31	5.8		0.0	7.6	66.8
32	6.0		0.0	3.2	58.7
33	6.2			1.0	51.3
34	6.4			0.2	40.2
35	6.6			0.0	33.3
36	6.8			0.0	24.4
37	7.0			0.0	17.6
38	7.2			0.0	10.9
39	7.4			0.0	6.5
40	7.6			0.0	1.7
41	7.8				0.6
42	8.0				0.1
43	8.2				0.0
44	8.4				0.0
45	8.6				0.0
46	8.8				0.0
47	9.0				0.0
48	9.2				0.0

Appendix E

E-1: Measured Electron beam data in water

depth in water	%6 MeV	%9MeV	%12 MeV	%15 MeV
0.0	73	78.1	83.7	88.7
0.2	76.4	81.7	86.2	88.3
0.4	80.1	83.6	88.8	92.3
0.6	84.6	86.4	89.8	93.9
0.8	89.4	87.8	91.9	95.3
1.0	94.2	90.3	92.9	95.9
1.2	97.8	91.8	93.7	96.7
1.4	100	93.9	94.7	96.8
1.6	98.3	96.5	95.6	97.6
1.8	92.8	98.3	96.1	98.0
2.0	82.6	99.6	97.6	98.1
2.2	67.2	99.8	98.2	98.5
2.4	49.7	99.5	98.6	99.0
2.6	31.4	96.3	99.2	99.7
2.8	18.2	91.3	99.9	99.5

3.0	7.4	84	100	99.4
3.2	2.8	74.8	99.8	99.9
3.4	1.2	64.4	98.4	100.0
3.6	0.8	51.8	96.4	99.7
3.8	0.8	39.5	93.6	99.3
4.0	0.8	27.2	90	99.1
4.2	0.8	16.9	84.7	98.6
4.4	0.7	9	78.4	97.2
4.6	0.7	4.3	69.7	95.4
4.8	0.7	2.2	61	93.2
5.0	0.7	1.6	51.6	90.5
5.2	0.6	1.4	41.8	86.7
5.4	0.6	1.4	32.1	82.5
5.6	0.7	1.4	23.8	78.1
5.8	0.6	1.3	16.3	72.4
6.0	0.6	1.3	10.9	66.4
6.2	0.7	1.3	6.8	59.4
6.4	0.6	1.3	4.3	52.5
6.6	0.6	1.2	3	45.0
6.8	0.6	1.2	2.4	36.9
7.0	0.6	1.1	2.2	29.6
7.2	0.6	1.2	2.2	22.8
7.4	0.5	1.1	2.1	17.1
7.6	0.6	1.1	2.1	12.4
7.8	0.5	1.1	2.1	9.0
8.0	0.5	1.1	2.1	6.7
8.2	0.5	1.1	2	5.1
8.4	0.5	1	2	4.3
8.6	0.5	1	1.9	3.8
8.8	0.5	1	2	3.49
9	0.4	1	1.9	3.49
9.2	0.4	1	1.9	3.49
9.4	0.4	1	1.9	3.29
9.6	0.4	0.8	1.8	3.29
9.8	0.4	1	1.8	3.19
10	0.4	0.8	1.8	3.29
10.2	0.4	0.8	1.8	3.091
10.4	0.4	0.8	1.8	3.091
10.6	0.4	0.8	1.7	3.091
10.8	0.4	0.8	1.7	3.091
11	0.4	0.7	1.7	2.991
11.2	0.4	0.8	1.7	2.991
11.4	0.3	0.7	1.6	2.792
11.6	0.3	0.8	1.6	88.7
11.8	0.3	0.7	1.6	88.3
12	0.3	0.7	1.6	92.3
12.2	0.3	0.7	1.6	93.9
12.4	0.4	0.7	1.4	95.3
12.6	0.3	0.6	1.4	95.9
12.8	0.3	0.7	1.4	96.7

13	0.3	0.6	1.3	96.8
13.2	0.3	0.7	1.4	97.6
13.4	0.3	0.6	1.3	98.0
13.6	0.3	0.6	1.4	98.1
13.8	0.3	0.6	1.3	98.5
14	0.3	0.6	1.3	99.0
14.2	0.3	0.6	1.3	99.7
14.4	0.3	0.6	1.3	99.5
14.6	0.3	0.5	1.3	99.4
14.8	0.3	0.6	1.2	99.9
15	0.3	0.6	1.2	100.0

E-2: Measured PDD values for electron beams with silicone (0.96g/cm^3) prosthesis immersed in water phantom

depth in water	% 9 MeV	% 12 MeV	% 15 MeV
4	28.1	89.5	100
4.2	18.7	83.2	98.7
4.4	10.9	76.3	96.8
4.6	5.7	68.7	94.1
4.8	3	59.6	91.4
5	1.9	50.6	87.9
5.2	1.6	41.5	82.8
5.4	1.4	32.5	78.5
5.6	1.4	24.4	73.3
5.8	1.4	17.6	67.5
6	1.4	12.2	60.7
6.2	1.3	7.9	54.4
6.4	1.3	5.2	47.4
6.6	1.3	3.5	40.2
6.8	1.3	2.8	32.6
7	1.2	2.5	26.1
7.2	1.3	2.5	19.7
7.4	1.2	2.3	14.9
7.6	1.1	2.3	11
7.8	1.1	2.3	8.1
8	1.1	2.2	6.3
8.2	1.1	2.1	4.9
8.4	1.1	2.2	4.2
8.6	1.1	2.1	3.8
8.8	1.1	2.1	3.5
9	1	2.1	3.5
9.2	1	2	3.5
9.4	1	2	3.4
9.6	1	1.9	3.4
9.8	1	1.9	3.3
10	1	2	3.2
10.2	0.9	1.9	3.3
10.4	1	1.9	3.2
10.6	0.9	1.8	3.1

10.8	0.9	1.8	3.1
11	0.9	1.8	3
11.2	0.9	1.7	3
11.4	0.9	1.7	2.9
11.6	0.8	1.7	2.8
11.8	0.8	1.7	2.9
12	0.8	1.6	2.8
12.2	0.8	1.6	2.9
12.4	0.8	1.6	2.8
12.6	0.8	1.6	2.7
12.8	0.8	1.5	2.7
13	0.8	1.6	2.7
13.2	0.8	1.5	2.6
13.4	0.7	1.5	2.6
13.6	0.8	1.5	2.6
13.8	0.7	1.4	2.5
14	0.7	1.4	2.5
14.2	0.7	1.4	2.5
14.4	0.7	1.4	2.4
14.6	0.7	1.4	2.4
14.8	0.7	1.4	2.4
15	0.7	1.3	2.3

E-3: Measured PDD values for electron beams in a silicone ($0.98 g/cm^3$) prosthesis immersed in water phantom

depth cm	% 6 MeV	% 9 MeV	% 12 MeV
4	26	89.4	100.0
4.2	17.4	83.7	98.6
4.4	9.7	76.5	96.6
4.6	5.2	68.6	93.2
4.8	2.7	60.2	90.4
5	1.8	51	87.1
5.2	1.6	41.7	82.8
5.4	1.4	32.7	77.9
5.6	1.5	24.7	72.9
5.8	1.5	17.6	67.0
6	1.4	11.9	61.2
6.2	1.4	7.8	54.3
6.4	1.4	5.2	47.5
6.6	1.3	3.5	39.9
6.8	1.3	2.8	33.0
7	1.3	2.6	26.3
7.2	1.3	2.4	20.2
7.4	1.2	2.3	15.0
7.6	1.3	2.3	11.1
7.8	1.2	2.3	8.0
8	1.2	2.3	6.0
8.2	1.2	2.2	4.8

8.4	1.2	2.1	4.0
8.6	1.1	2.1	3.8
8.8	1.1	2.1	3.5
9	1.1	2	3.4
9.2	1.1	2	3.4
9.4	1	2	3.3
9.6	1.1	2	3.3
9.8	1	2	3.3
10	1.1	1.9	3.1
10.2	1	1.9	3.2
10.4	1	1.8	3.1
10.6	1	1.8	3.1
10.8	1	1.7	3.0
11	1	1.8	2.9
11.2	0.9	1.7	2.9
11.4	0.9	1.7	2.8
11.6	0.9	1.7	2.9
11.8	0.9	1.7	2.8
12	0.9	1.6	2.7
12.2	0.9	1.6	2.7
12.4	0.9	1.6	2.6
12.6	0.8	1.5	2.7
12.8	0.8	1.6	2.6
13	0.8	1.5	2.6
13.2	0.8	1.5	2.5
13.4	0.8	1.5	2.5
13.6	0.8	1.5	2.6
13.8	0.8	1.5	2.5
14	0.8	1.4	2.5
14.2	0.8	1.4	2.5
14.4	0.8	1.3	2.4
14.6	0.8	1.4	2.4
14.8	0.7	1.3	2.4
15	0.7	1.4	2.4